Designed, Fabricated and Constructed Tissue Engineering Scaffolds Based on Mimic and Bio-inspiration Approach for Maxillofacial Defect Treatment and Disease Evaluation

Supaporn Sangkert

A Thesis Submitted in Fulfillment of the Requirements for the Degree of Doctor of Philosophy in Biomedical Engineering

Prince of Songkla University

2019

Thesis Title	Designed, Fabricated and Constructed Tissue Engineering Scaffolds Based on Mimic and Bio-inspiration Approach for Maxillofacial Defect Treatment and Disease Evaluation
Author	Miss Supaporn Sangkert
Major Program	Biomedical Engineering

Major Advisor :

……

(Assoc. Prof. Dr .Jirut Meesane)

Co-advisor :

……

(Assoc. Prof. Dr. Suttatip Kamonmattayakul)

……

(Prof. Dr. Michael Gelinsky)

Examining Committee :

…….……Chairperson

(Assoc. Prof. Dr. Kawee Srikulkit)

…….....Committee

(Assoc. Prof. Dr. Jirut Meesane)

…….....Committee

(Assoc. Prof.Dr. Suttatip Kamonmattayakul)

…….....Committee

(Assoc. Prof. Dr. Thongchai Nuntanaranont)

The Graduate School, Prince of Songkla University, has approved this thesis as fulfillment of the requirements for the Doctor of Philosophy in Biomedical Engineering

..……

(Prof. Dr. Damrongsak Faroongsarng)

Dean of Graduate School

This is to certify that the work here submitted is the result of the candidate's own investigations. Due acknowledgement has been made of any assistance received.

……..Signature

(Assoc. Prof. Dr. Jirut Meesane)

Major Advisor

……..Signature

(Miss Supaporn Sangkert)

Candidate

I hereby certify that this work has not been accepted in substance for any degree, and is not being currently submitted in candidature for any degree.

……..Signature

(Miss Supaporn Sangkert)

Candidate

ชื่อวิทยานิพนธ์ การออกแบบ ประดิษฐ์ และสร้างโครงร่างวิศวกรรมเนื้อเยื่อบนพื้นฐานของการเลียนแบบและแรงบันดาลใจทางชีวภาพสำหรับการรักษาและประเมินการเกิดโรคบริเวณข้อบกพร่องของขากรรไกร

ผู้เขียน นางสาวสุภาพร แสงเกิด

สาขาวิชา วิศวกรรมชีวการแพทย์

ปีการศึกษา 2561

บทคัดย่อ

ปัจจุบันปัญหาการเกิดรอยวิกรานบริเวณใบหน้าและขากรรไกรอันเนื่องมาจากการบาดเจ็บและโรคเป็นปัญหาสำคัญสำหรับผู้ป่วยจำนวนมาก โดยบางกรณีจำเป็นต้องใช้วัสดุที่มีประสิทธิภาพสำหรับการรักษาและการประเมินผลของโรค ซึ่งโครงร่างวิศวกรรมเนื้อเยื่อเป็นวัสดุชีวภาพที่น่าสนใจและนำมาใช้เพื่อขึ้นรูปและออกแบบเพื่อใช้ในการวิจัยนี้ สำหรับโครงร่างวิศวกรรมเนื้อเยื่อได้ออกแบบโดยอาศัยพื้นฐานของการเลียนแบบและการสร้างตามลักษณะทางกายภาพของกระเนื้อเยื่อเพื่อใช้ในการปลูกถ่ายและการประเมินโรค อันดับแรกโครงร่างสองมิติที่ออกแบบเพื่อใช้ในเนื้อเยื่ออ่อนในบริเวณใบหน้า อันดับที่สองคือโครงสร้างสามมิติแบบจำลองเพื่อการประเมินความเสี่ยงของโรคกระดูกพรุน โครงร่างที่สามคือการออกแบบโครงร่างให้มีความคล้ายคลึงกับลักษณะทางชีวภาพสำหรับใช้งานทางด้านวิศวกรรมเนื้อเยื่อกระดูก โครงร่างที่สี่คือการรวมโครงสร้างกับไทเทเนียมคาร์ไบด์ที่เคลือบด้วยคาร์บอนเพื่อช่วยในการสะสมแร่ธาตุในกระบวนการสมานกระดูก ผลการทดลองแสดงให้เห็นว่าโครงสร้างแรกมีคุณสมบัติที่เหมาะสมทางชีวภาพกับงานด้านเนื้อเยื่ออ่อนบริเวณใบหน้าและกระดูกขากรรไกร โครงร่างที่สองแสดงโครงสร้างที่เหมาะสมและฟังก์ชันการทำงานที่เหมาะสมในการประเมินโรคกระดูกพรุน โครงร่างที่สามแสดงให้เห็นถึงโครงสร้างที่คล้ายโครงสร้างระหว่างการสร้างกระดูก ซึ่งพบว่ามีประสิทธิภาพและใช้ในงานวิศวกรรมเนื้อเยื่อกระดูกได้ โครงร่างที่สี่แสดงให้เห็นถึงลักษณะเฉพาะในกระบวนการสมานกระดูก จากผลการศึกษาพบว่าการประดิษฐ์โครงร่างจากการลอกเลียนแบบลักษณะทางชีวภาพมีแนวโน้มที่สามารถนำมาใช้ในการปลูกถ่ายทางการแพทย์ในบริเวณใบหน้าและขากรรไกรและใช้ในการประเมินโรค

Thesis Title Designed, Fabricated and Constructed Tissue Engineering Scaffolds Based on Mimic and Bio-inspiration Approach for Maxillofacial Defect Treatment and Disease Evaluation.

Author Miss Supaporn Sangkert

Major Program Biomedical Engineering

Academic Year 2018

Abstract

Maxillofacial defect from trauma and diseases is the critical problems for many patients. Some defects need performance biomaterials for treatment and evaluation. Tissue engineering scaffolds is the attractive performance biomaterials which were selected to create, fabricate, and construct in this research. Four tissue engineering scaffolds based on mimic and bio-inspiration design were proposed for using in tissue defect treatment and disease evaluation. The first mimicked scaffold was created for using in soft tissue engineering in maxillofacial defect. The second mimicked pathogenic scaffold was used as ex-vivo biomaterials for osteoporosis evaluation. The third scaffold was created with the bio-inspiration for bone tissue engineering. The fourth scaffold incorporated with TiC coated carbon particles was designed to use for mineralization in bone healing. The results demonstrated that the first scaffold showed the suitable structure and biological performance which is fit for soft tissue engineering at maxillofacial defect. The second scaffold displayed the suitable structure and functionality which relate and fit to ex-vivo biomaterial for osteoporosis. The third scaffold showed the structural formation similar to structural organization during bone formation. This scaffold had the performance which could promote bone tissue engineering. The fourth scaffolds showed unique performance to enhance mineralization in bone healing. This research indicated that those scaffolds based on mimic and bio-

inspiration design is promising to be the performance biomaterials for maxillofacial defect treatment and disease evaluation.

Acknowledgements

This thesis would not have been successful unless I had got supported guided and assisted. I'm cordially thankful to my supervisors Associate Professor Jirut Meesane, Associate Professor Suttatip Kamonmattayakul and Professor Michael Gelinsky, whose encouragement, supervision and support from preliminary to the concluding level enabled me to develop an understanding all of the subject and raise me up more than I can be.

Special thanks and regards to Associate Professor Thongchai Nuntanaranont and Associate Professor Kawee Srikulkit for being my examining committee

Next, I would like to thank Miss Khanitta Panjapheree, Miss Jutakarn Thonglam for lab technician in this study. And I would like to thank to personnel of institute of BME for document procedure.

I would like to sincerely thank to the research center of faculty of Dentistry and institute of BME, faculty of Medicine, Prince of Songkla University for their help and support through the thesis.

Sincere acknowledgement is also expressed to faculty of Medicine, PSU graduate school for their financial support of this study

Supaporn Sangkert

Contents

Content	Page
List of table	X
List of figures	XI
List of Abbreviations and Symbols	XV
Chapter 1	1
Chapter 2	16
Chapter 3	28
Chapter 4	54
Chapter 5	83
Chapter 6	100
Chapter 7	137
Appendix	139
Vitae	140

List of tables

Table	Page
Table 1 Experiment groups	17
Table 2 Experiment groups	29
Table 3 The experimental group of silk fibroin/gelatin scaffold	56
Table 4 The experimental groups	84
Table 5 The experiment group	101

List of Figures

Figure **Page**

Figure 1. The tissue engineering concept 5

Figure 2. The schematic of Silk fibroin structure 6

Figure 3. The chemical structure of chitosan 8

Figure 4. Coated SF fabrics from different SF solution concentrations 20

Figure 5. Thicknesses of the SF Fabrics 20

Figure 6. Surface morphologies of silk fabrics by scanning electron microscope 21

Figure 7. Swelling properties of SF fabrics 22

Figure 8. Amount of BCA release in 15-120 min in PBS solution 23

Figure 9. Cell proliferation in the SF fabrics at days 1, 3, and 5 24

Figure 10. Cell viability on the SF fabric after staining with FDA 25

Figure 11. Non-coated side of silk fabric 33

Figure 12. The surface morphology of coated silk fabric 34

Figure 13. XRD spectra of constructed laminate composite 35

Figure 14. DSC thermograms of constructed laminate composite 36

Figure 15. The swelling properties of silk fabric in all groups 37

Figure 16. Degradation of constructed biphasic sheet by lysozyme 39

Figure 17. The stress-percentage strain curve of silk fibroin fabric 40

Figure 18. Showed fibroblast cell proliferation in the silk fibroin fabric 42

Figure 19. Cell viability staining with FDA on the silk fibroin fabric 43

List of Figures (Continued)

Figure **Page**

Figure 20. Cell morphology on the silk fabric scaffold on day 3 and 5 44

Figure 21. Masson trichrome staining on day 14 and 28 46

Figure 22. Showed keratinocyte cell proliferation in the silk fibroin fabric 47

Figure 23. Keratinocyte cell viability staining with FDA on the silk fibroin fabric 48

Figure 24. Cell morphology on the silk fabric scaffold on day 3 and 7 49

Figure 25. Silk fibroin and gelatin scaffold 60

Figure 26. Morphology of SF/GT 61

Figure 27. The pore size diameter along with distribution percentage of scaffold 63

Figure 28. The interconnect pore size as well as distribution of scaffold 63

Figure 29. Swelling behavior of scaffolds SF/GT 64

Figure 30. The degradation of scaffolds with lysozyme at days 7, 14 and 21 65

Figure 31. Cell proliferation of osteoblast cell in the scaffold 66

Figure 32. Alkaline phosphatase activity, from osteoblast cell in the scaffold 67

Figure 33. Calcium content, on the scaffolds in each group 68

Figure 34. Calcium deposition on scaffolds at days 7, and 21 69

Figure 35. The histology of cell mophology on porous of scaffolds 70

Figure 36. The chitosan/BiCP solution adjused with NaOH 87

Figure 37. The morphological structure of the scaffold in all groups 88

Figure 38. Morphology from SEM image of scaffolds 89

List of Figures (Continued)

Figure **Page**

Figure 39. The swelling properties of the scaffolds in the PBS solution 90

Figure 40. The degradation of scaffold in all groups after incubating with lysozyme 91

Figure 41. The protein synthesis of osteoblasts after culture in the scaffold 92

Figure 42. The cell viability of osteoblast in the scaffolds after staining with FDA 93

Figure 43. Cell proliferation of osteoblast cell on the scaffold in all groups 94

Figure 44. The ALP activity of osteoblasts in scaffolds 95

Figure 45. The calcium analysis of osteoblasts in scaffolds 96

Figure 46. Histology of cultured osteoblast cell in scaffolds at difference time 97

Figure 47. SEM image and TEM image of TiC-coated carbon nanoparticles 105

Figure 48. Agarose solutions at different concentrations of TiC-coated nanoparticles 106

Figure 49. Hydrogel stages in agarose at different of TiC-coated nanoparticles 106

Figure 50. Agarose hydrogel membranes at different of TiC-coated nanoparticles 107

Figure 51. LM images of agarose hydrogel 108

Figure 52. SEM surface images of agarose hydrogels 109

Figure 53. SEM cross-sectional images of agarose hydrogels 110

Figure 54. FT-IR spectroscopy analysis of the hydrogels in all groups 111

Figure 55. The DSC thermogram of the hydrogels in all groups 112

Figure 56. DSC thermograms: each hydrogel of all groups 113

Figure 57. DMA spectrum of hydrogels of all groups 114

List of Figures (Continued)

Figure **Page**

Figure 58. Water contact angles of the hydrogels in all groups 115

Figure 59. Fluorescence microscopy images of the cells in agarose hydrogels 117

Figure 60. SEM images of cell adhesion on agarose hydrogel 118

Figure 61. Cell proliferation of the agarose hydrogels 119

Figure 62. ALP activity of agarose hydrogels 120

Figure 63. Calcium nodules on agarose hydrogels 122

Figure 64. Protein synthesis of cells on agarose hydrogels 123

Figure 65. Osteocalcin synthesis on days 7, 14, and 21 124

List of Abbreviations and Symbols

SF	=	Silk fibroin
GT	=	Gelatin
LiBr	=	Lithium bromide
CS	=	Chitosan
BiCP	=	Bicomponent calciumphospate
TiC	=	Titanium carbonate
SEM	=	Scanning Electron Microscope
ECM	=	Extracellular matrix
M	=	Molar
h	=	Hour
V	=	Volume
mm	=	Millimeter
cm	=	Centimeter
mg	=	Miligram
ml	=	Milliliter
SEM	=	Scanning electron microscope
FT-IR	=	Fourier transform infrared
XRD	=	X-ray diffraction
AFM	=	Atomic Force Microscopy
FDA	=	Fluorescein diacetate
ANOVA	=	One-way analysis of variance
min	=	Minute
µm	=	Micrometer
et al	=	And others
H&E	=	Hematoxylin and eosin
OD	=	Optical density
SD	=	Standard deviation

CHAPTER 1

Introduction

Currently, there are often many cases of maxillofacial defects from disease and trauma that have been increasing around the globe [1]. To treat and evaluate those defects need the potential approach. Interestingly, to use potential biomaterials is presently an attractive choice for those treatments and evaluation [2]. Hence, to create those biomaterials is challenge for materials scientists and surgeons. Especially, tissue engineering scaffolds which show smart performance for tissue defect treatment to enhance maxillofacial regeneration. Furthermore, scaffolds can act as the clues for cell regulation into order and disorder tissue formation which is the cause of some diseases [3]. These scaffolds demonstrate their performance for evaluation of tissue disease [4]. Therefore, to create the performance scaffolds for tissue defect treatment and disease evaluation were emphasized on this research.

Mimicking and bio-inspiration is an attractive approach, which has often been used to create performance scaffolds for bone tissue engineering. Especially because, mimicking and bio-inspiration has been applied to construct the porous structures of scaffolds, with these being similar to the extracellular matrix within native tissue [5]. Those scaffolds often demonstrate the suitable biomaterials which have distinguish performances for tissue engineering [6]. According to those performances, mimicked and bio-inspirated scaffolds was therefore emphasized in this research.

Silk fibroin is the biopolymer obtained from the silk worm and it consists of glycine (43%), alanine (30%) and serine (12%) [7]. Importantly, the silk fibroin has the excellent property, for example biocompatibility with various cells, degradation in the body, non-toxicity and good mechanical property that suitable for new tissue formation [8]. Now a day silk fibroin has been used in part of skeletal tissue like a cartilage, bone, ligament and connective tissue. Therefore, silk fibroin is the efficacy choice and has the

stability tissue engineering. Hence, silk fibroin was selected as based materials to fabricate performance scaffolds in this research.

Gelatin is hydrolyzed collagen which has been often used for biomedical application [9]. Gelatin has unique biological functionality to induce cell adhesion and proliferation which lead to enhancing of tissue regeneration [10]. Due to that unique biological functionality, gelatins have been fabricated into porous scaffolds for tissue regeneration [11]. Therefore, gelatin was chosen for this research.

Chitosan is biopolymers which have the unique properties to enhance new tissue formation [12]. Hence, chitosan is often fabricated into tissue engineering scaffolds [13]. Furthermore, chitosan showed attractive function to induce cell behavior which leads to promote tissue regeneration [14]. As that functionality, chitosan was selected to use in this research.

Tri-calcium phosphate (TCP) and hydroxyapatite (HA) is bioactive inorganic molecules which show the performance as soluble and insoluble components, respectively. Those components show the roles which can induce bone formation [15]. Hence, tri-calcium phosphate and hydroxyapatite was used as based materials to create tissue engineering scaffolds in this research.

TiC-coated carbon particles (TCBs) are another bioactive inorganic compound and show unique biological functionality which can stimulate the bone formation [16]. Therefore, TCBs were used to incorporate with scaffolds for enhancement of their performance in this research.

In this research, the performance scaffolds based on silk fibroin, chitosan, gelatin, and TiC coated carbon particles were fabricated with mimicking design. Those scaffolds were proposed for using in maxillofacial defect treatment and disease evaluation which was focused on creating of ex-vivo biomaterials.

Reference

[1] Kim JH, Shin SY, Paek J, Lee JH, Kwon HB. Analysis of maxillofacial prosthetics at university dental hospitals in the capital region of Korea. J Adv Prosthodont 2016:8;229–234.

[2] Zavaglia CAC, Prado da MS. Feature Article: Biomaterials. 2016 Reference Module in Materials Science and Materials Engineering 2016:1-5.

[3] Chan, BP, Leong, KW. Scaffolding in tissue engineering: general approaches and tissue-specific considerations. Eur Spine J 2008;17:467–479.

[4] Brahatheeswaran D, Yasuhiko Y, Toru M, Sakthi DK. Polymeric Scaffolds in Tissue Engineering Application: A Review. International Journal of Polymer Science. 2011;2011:1-19.

[5] Gong T, Xie J, Liao J, Zhang T, Lin S, Lin Y. Nanomaterials and bone regeneration. Bone Res 2015;3:1-7.

[6] Minardi S, Corradetti B, Taraballi F, Sandri M, Van Eps J, Cabrera FJ, Weiner BK, Tampieri A, Tasciotti E. Evaluation of the osteoinductive potential of a bio-inspired scaffold mimicking the osteogenic niche for bone augmentation. Biomaterials 2015;62:128–137.

[7] Vepari C, Kaplan DL. Silk as a Biomaterial. Prog Polym Sci 2007;32:991–1007.

[8] Thurber AE, Omenetto FG, Kaplan DL. In Vivo Bioresponses to Silk Proteins. Biomaterials 2015;71:145–157

[9] Khan R, Khan MH. Use of collagen as a biomaterial: An update. J Indian Soc Periodontol 2013;17:539–542.

[10] Wu SC, Chang WH, Dong GC, Chen KY, Chen YS, Yao CH. Cell adhesion and proliferation enhancement by gelatin nanofiber scaffolds. Journal of Bioactive and Compatible Polymers 2011;26:565–577.

[11] Poursamar SA, Hatami J, Lehner AN, da Silva CL, Ferreira FC, Antunes APM. Gelatin porous scaffolds fabricated using a modified gas foaming technique: Characterisation and cytotoxicity assessment. Materials Science and Engineering: C 2015;48:63–70.

[12] Croisier F, Jerome C. Chitosan-based biomaterials for tissue engineering. European Polymer Journal, Biobased Polymers and Related Materials 2013;49: 780–792.

[13] Levengood SL, Zhang M. Chitosan-based scaffolds for bone tissue engineering. J Mater Chem B Mater Biol Med 2014;2:3161–3184.

[14] Rodriguez-Vázquez M, Vega-Ruiz B, Ramos-Zuniga R, Saldana-Koppel DA, Quinones-Olvera LF. Chitosan and Its Potential Use as a Scaffold for Tissue Engineering in Regenerative Medicine. Biomed Res Int 2015;2015:1-15.

[15] Barrere F, van Blitterswijk CA, de Groot K. Bone regeneration: molecular and cellular interactions with calcium phosphate ceramics. Int J Nanomedicine 2006;1:317–332.

[16] NandarSoe H, Khangkhamano M, Sangkert S, Meesane J, Kokoo R. TiC-coated carbon particles as bioactive substrates for inducing of mineralization in bone healing. Materials Letters 2018;229:118-21.

Review of Literature

1. Tissue engineering

Tissue engineering is the multidisciplinary field that combines the knowledge and technology in clinical medicine and materials science that can generate the new tissue formation by combining the cell, scaffold and growth factor, that can perform as the tissue regeneration template.

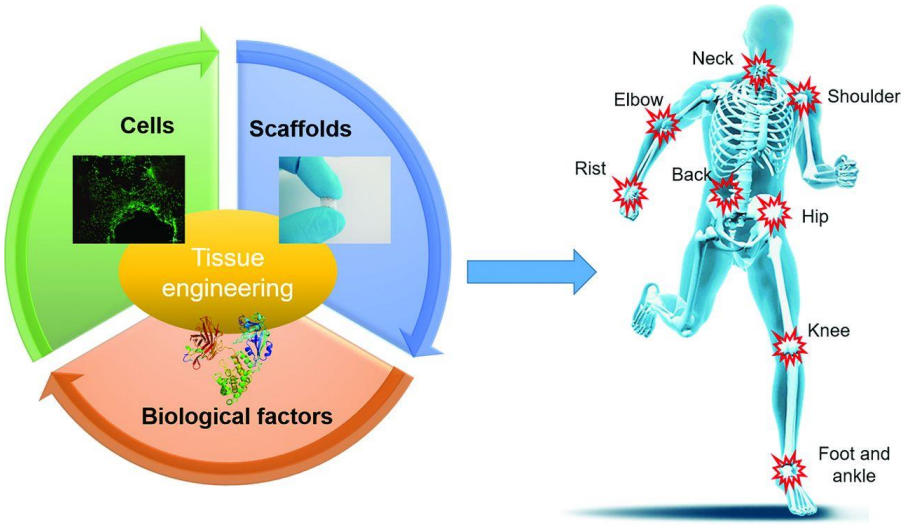

Figure 1. The tissue engineering concept [1]

The scaffolds have been produced from variety materials including the natural and synthesis materials. The first property of those materials is the biocompatibility and non-rejection from immune system. In addition, the scaffolds can degrade match with the new tissue formation and the by-product of scaffold after degradation process should nontoxic with cell. In the bone cartilage and cardiovascular tissue engineering, the mechanical property is the important function that scaffold must sturdy enough for defect handing during the new tissue formation. Moreover, the architecture of scaffold is the critical importance in tissue engineering. In the bone tissue engineering, the scaffold must have the interconnective pore size with high porosity that suitable for nutrients diffusion and the waste product easy in transport

process. In addition, the cells can migration and synthesis the extracellular matrix for new tissue formation [2].

2. The materials used as scaffold in bone tissue engineering

In the tissue engineering scaffolds, the natural, synthetic and hybrid material were offered and tested as scaffold in tissue engineering [3]. There are many types of materials that use for scaffold fabrication that use in bone tissue engineering process. The material for bone tissue engineering must show the good mechanical property, bioactive for osteoblast cell and stable during defect healing.

Silk fibroin in the protein polymer gets from the *Bombyx mori* (silkworm, the silk fibroin including the main 3 type of protein Glycine (43%), Alanine (30%) and Serine (12%). Silk fibroin is the excellent biopolymer and promising for bone tissue substitution with the biocompatibility, good mechanical property, morphological cues and safe by-product during degradation process. The structure of Silk fibroin has 3 types including random coil, α-helices and β-sheets structure. The β-sheets is the stable structure and support for cell proliferation.

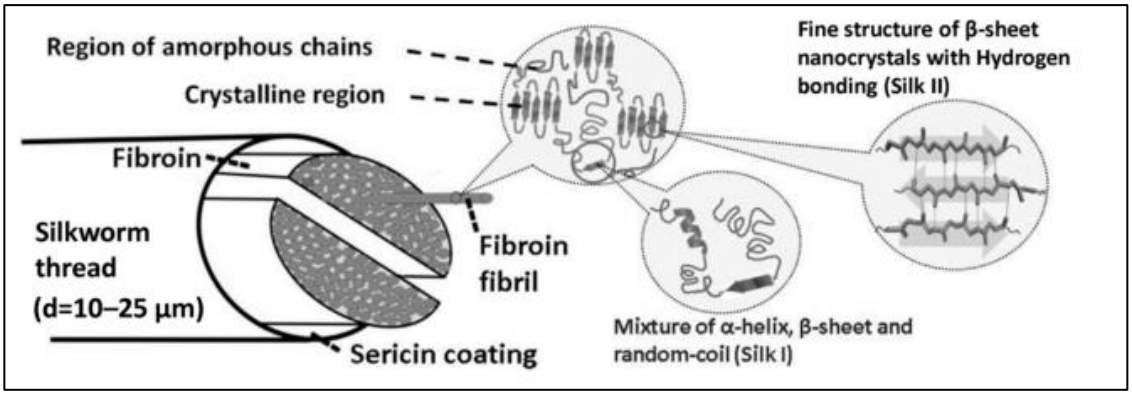

Figure 2. The schematic of Silk fibroin structure [4]

Moreover the Silk fibroin can fabricate into various form such as porous scaffold, hydrogel, fabric, film and nanoparticle. The RDG amino acid sequence in the Silk fibroin is the specific protein binding for cell attachment [5].

Gelatin is the hydrolysis of collagen that composes of amino acid like collagen including glycine, proline, alanine and hydroxyproline. Gelatin is obtained from animal tendon, skin and tendon [6]. Gelatin is the popular material that has the bioactive molecules that can stimulate cell attachment and proliferation, osteocompatible and suitable to combine with other materials [7]. Moreover, gelatin is fabricated in many form including hydrogel, porous scaffold, membrane and particle. Mostly, gelatin is always combined with other materials for biofunctional improvement. Gelatin normally has high swelling value and easy to degradation, the combining gelatin with the other materials that have good mechanical property is the alternative way to improve the physical property of gelatin [8]

Chitosan is the polysaccharide that is derived from the chitin, it mostly found in the crustacean shells. Chitosan is the only positive charged, normally in the polysaccharide group. The -OH and -NH_2 groups in the chitosan structure can from the strong covalent bonding with other materials. The antifungal and exhibits antibacterial was found in the chitosan property. Moreover, chitosan shows the excellent function for tissue engineering such as for scaffold fabrication. Chitosan is fabricated into various form including 3D porous, film, microsphere and particle. Chitosan has biocompatibility, degradation and good mechanical. Chitosan has the biological function to the cell attachment because the positive charge of chitosan was interacted with the negative charge of cell membrane. Furthermore, chitosan is the biodegradation material, it is degraded during the new tissue formation and the by-product nontoxic with cell [9].

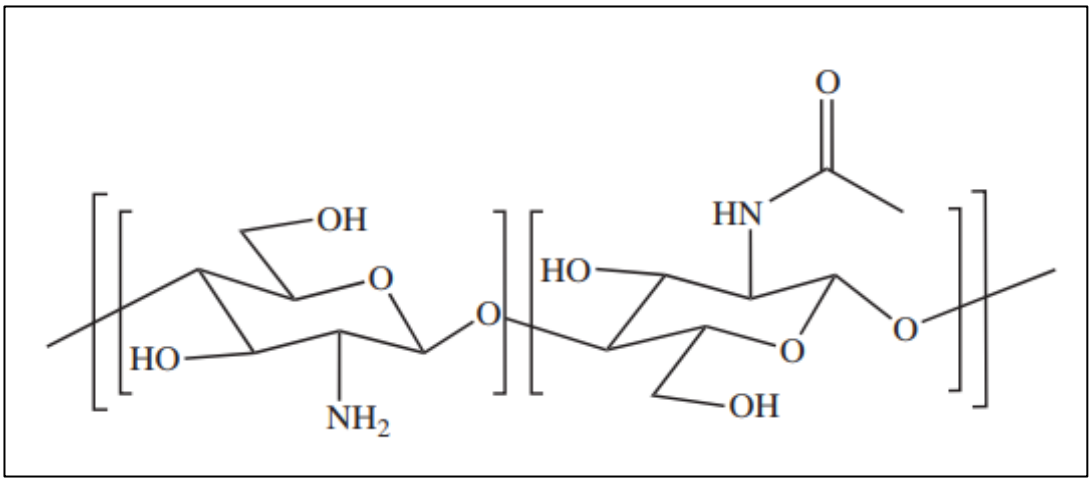

Figure 3. The chemical structure of chitosan

Calcium phosphate is the bioactive material that has the property like bone in body. Generally, the ratio of Ca/P and crystalline crystallinity phase of CaP have effect on the new bone formation by phosphate and calcium ion releasing in the bone mineralization. CaP is normally degraded in human body. Its degradation is important function to support the new tissue formation by slowly weaker during the completely of new bone replacement. CaP has been fabricated into two and three dimensional scaffolds. The CaP scaffolds showed the good mechanical property when compare with other materials [10].

Agarose is the polysaccharide from the natural, it always use in food or medical engineering. The molecule structure of the agarose including the monomer D-Galactose link with 3,6-Anhydro-L-galactose. Agarose is high on swelling property, this reason agarose excellent for hydrogel fabrication. Agarose hydrogel is suitable to adjust the cell signaling and growth factor adding in bone or cartilage tissue engineering.

3. The composite scaffold

The composite scaffold is referring to the combination of two or more of material that have the different properties. Composite scaffolds always show the specific on the mechanical, morphology structure, chemical and functional. After fabrication, the

composite scaffold shows the excellent and interesting function in each material [11]. For example, the poly(ε-caprolactone) (PCL) and PLA are non-bioactive material, to make the better function by combine with tricalcium phosphate (TCP) or hydroxyapatite (HA) that improve the osteoconductivity of scaffold and reinforcement the scaffold as composite polymer-bioceramic scaffold [12]. The combination of gelatin with silk fibroin and conjugate with HA can enhance the new bone formation in rat. The gelatin can promote the cell attachment and the silk fibroin and HA were support for reinforcement of scaffold and also in bioactive function [13]. The improvement of mechanical properties and bioactive function of chitosan by mix with hydroxyapatite and fabricate with 3D printing, the scaffold showed the osteoinductivity after culture with mouse bone marrow stem cell after compare with chitosan-silica hybrid scaffold [14]. The study showed incorporation of silk fibroin with chitosan for antibacterial activity. Furthermore, the incorporated silk fibroin had the function to enhance cell proliferation and attachment. For this study, silk fibroin was fabricated into nanofibrous membrane by electrospining with layer by layer method. The result showed that increasing of fiber diameter and layer of membrane has an effect on increasing of mechanical property. The suitable layer was 15 layers that can stimulate the cell function during good mechanical property [15].

4. The method for scaffold fabrication

In the present day, it has many methods to fabricate the scaffold for tissue engineering including the freeze drying, electrospining, phase separate, film casting, and self- assembly. Each method can generate the different architecture structure both nano and micro to mimic the extracellular matrix of native tissue, the porous structure that similar with bone structure and has the space for new tissue formation. Generally, the scaffolds are designed into the structure which is similar to the tissue defect such as the 2D membrane always use for wound healing and soft tissue because the thin layer of soft tissue fits with the thickness of membrane. The 3D porous

structure is designed into the interconnected pore size which can support migration of osteoblasts and mineral deposition for new bone formation. In the cartilage tissue engineering, the scaffolds are always designed into the hydrogel or porous structure that have the flexible and good mechanical property and the lacunar structure need for chondrocyte proliferation and matrix synthesis.

Freeze drying is the popular method that has been used for scaffolds fabrication. Principally, scaffold fabrication with freeze drying has two steps; 1) the first step is frozen the solution in low temperature (-20, -80) and 2) the second step is that the frozen solution is put into chamber before drying with the evaporation ice crystals. Then, the porous structure from evaporation of ice crystal remains in scaffold. The freeze drying methods usually generate the 3D porous scaffold.

Mimicking and bio-inspiration is the approach that has been used to create scaffolds for tissue engineering. Such scaffolds often have the attractive structure and function that is similar to natural tissue. For the structural mimicking, the scaffolds have been constructed into similar porous or fibers to extracellular matrix in natural tissue. Those scaffolds showed good performance to induce new tissue formation that is similar to natural tissue [16]. In the case of functional mimicking, scaffolds are often fabricated with materials which have similar physical, mechanical and biological function to the natural tissue [17]. For instance, for bone tissue engineering, CaP and collagen are selected as based materials for scaffold [18]. This scaffold has the unique biological function to promote new bone formation from the based materials of CaP and collagen.

Reference

[1] Joao BC, Helder P, Joao EM, Gilson K, Joaquim MO, Rui LR. Tissue engineering in orthopaedic sports medicine: current concepts. Journal of ISAKOS: Joint Disorders & Orthopaedic Sports Medicine 2017;2:60-66.

[2] Fergal JO. Biomaterials & scaffolds for tissue engineering. Materialstoday 14; 2011:1-8.

[3] Antonio G, Roberto DS, Luigi A. Polymer-based composite scaffolds for tissue engineering. Journal of Applied Biomaterials & Biomechanics 2010;8:57-67.

[4] Volkov, V.; Ferreira, A.V.; Cavaco-Paulo, A. On the Routines of Wild-Type Silk Fibroin Processing Toward Silk-Inspired Materials: A Review. Macromol. Mater. Eng. 2015, 300, 1199–1216.

[5] Yu Q, Hui W, Kai W, Ya Y, Ru-YZ, Ick SK, Ke-Qin Z. A Review of Structure Construction of Silk Fibroin Biomaterials from Single Structures to Multi-Level Structures. International Journal of Molecular Sciences. 2017;18:1-21.

[6] Md EH, Kim YT, Tamrin N, Norshariza N. Gelatin Based Scaffolds For Tissue Engineering – A review. Polymers Research Journal 2015;9:1-19.

[7] James BR, Settimio P, Alicia JH, Harminder SD, Andrew H, Lisa JW, Felicity R. AJR. Gelatin-Based Materials in Ocular Tissue Engineering. Materials 2014;7: 3106-3135.

[8] Julie G, Shuichi M. Collagen Scaffolds for Tissue Engineering. Biopolymers 2008; 89:338-44.

[9] Florence C, Christine J. Chitosan-based biomaterials for tissue engineering. European Polymer Journal 2013;49:780–792.

[10] Isabelle D, Liisa TK. Design and characterization of calcium phosphate ceramic scaffolds for bone tissue engineering. Dental materials 2016;32:43–53.

[11] Antonio G, Roberto DS, Luigi A. Polymer-based composite scaffolds for tissue engineering. Journal of Applied Biomaterials & Biomechanics 2010;8:57-67.

[12] Min W. Composite Scaffolds for Bone Tissue Engineering. American Journal of Biochemistry and Biotechnology 2006;2:80-84.

[13] Tonporn L, Kumpanart S, Sawang K, Sorada K, Siriporn D. In Vivo Bone Regeneration of Thai Silk Fibroin Scaffolds with Gelatin, Hydroxyapatite and Hyaluronic Acid. Thai J Vet Med. 2017;47:165-172.

[14] Yifan D, Jinning L, Yihang C, Shan X, Naru Z. Fabrication of novel bioactive hydroxyapatite-chitosan-silica hybridscaffolds: Combined the sol-gel method with 3D plotting technique. Carbohydrate Polymers 2018;197:183–193.

[15] Liangbin X, Youmei L, Dan L, Li H, Yanqing W, Fangfang D, Fenghua T, Yanxiang C, Hongbing D. LBL deposition of chitosan and silkfibroin on nanofibers for improvingphysical and biological performance of patches. International Journal of Biological Macromolecules 2019;130:348–356.

[16] Yunfan H, Feng L. Development of Synthetic and Natural Materials for Tissue Engineering Applications Using Adipose Stem Cells. Stem Cells Int. 2016; 2016: 5786257.

[17] Tingli L, Yuhui L, Tao C. Techniques for fabrication and construction of three-dimensional scaffolds for tissue engineering. International Journal of Nanomedicine 2013:8:337–350.

[18] Dawei Z, Xiaowei W, Jingdi C, Kaili L. The development of collagen based composite scaffolds for bone regeneration. Bioact Mater 2018;3:129-138.

Objective of this study

1. To create and construct silk fibroin scaffolds based on mimicking design for tissue engineering of soft tissue defect in maxillofacial area.
2. To design and fabricate mimicked pathogenic scaffolds of the silk fibroin/gelatin as ex-vivo biomaterials for osteoporosis evaluation.
3. To create and fabricate calcium phosphate/chitosan scaffolds base on bio-inspiration design for bone tissue engineering.
4. To evaluate the scaffolds incorporated with TiC coated carbon particles for bone healing

Hypothesis:

1) A constructed silk fibroin scaffolds based on mimicking design will provide a better cellular response, barrier membrane and improve quality of fabric in terms of cell adhesion, proliferation and ECM synthesis.
2) A mimicked pathogenic scaffolds based on the silk fibroin/gelatin can be used as ex-vivo biomaterials for osteoporosis evaluation.
3) A fabricated calcium phosphate/chitosan scaffolds base on bio-inspiration design can promote the bone formation.
4) A scaffolds incorporated with TCBs nanoparticle will stimulate the mineralization in bone healing.

Expected Benefits:

We expect that the created scaffolds in this research can use as biomaterials for treatment of tissue defect and evaluation of tissue diseases. The expected benefits is classified in to 4 clusters; Firstly, constructed silk fibroin scaffolds based on mimicking design can support and promote both cell fibroblast and

keratinocyte in part of cell proliferation and ECM synthesis. Furthermore, a modified silk fibroin fabric is promising for mucosa defect. Secondly, the combining between silk fibroin and gelatin will be suitable for ex-vivo biomaterials for osteoporosis evaluation. Thirdly, the chitosan construct with calcium phosphate base on design of bio-inspiration can be used in bone tissue engineering. Finally, the TCBs can be used as substrate for induce the mineralization in bone healing.

Overall of study

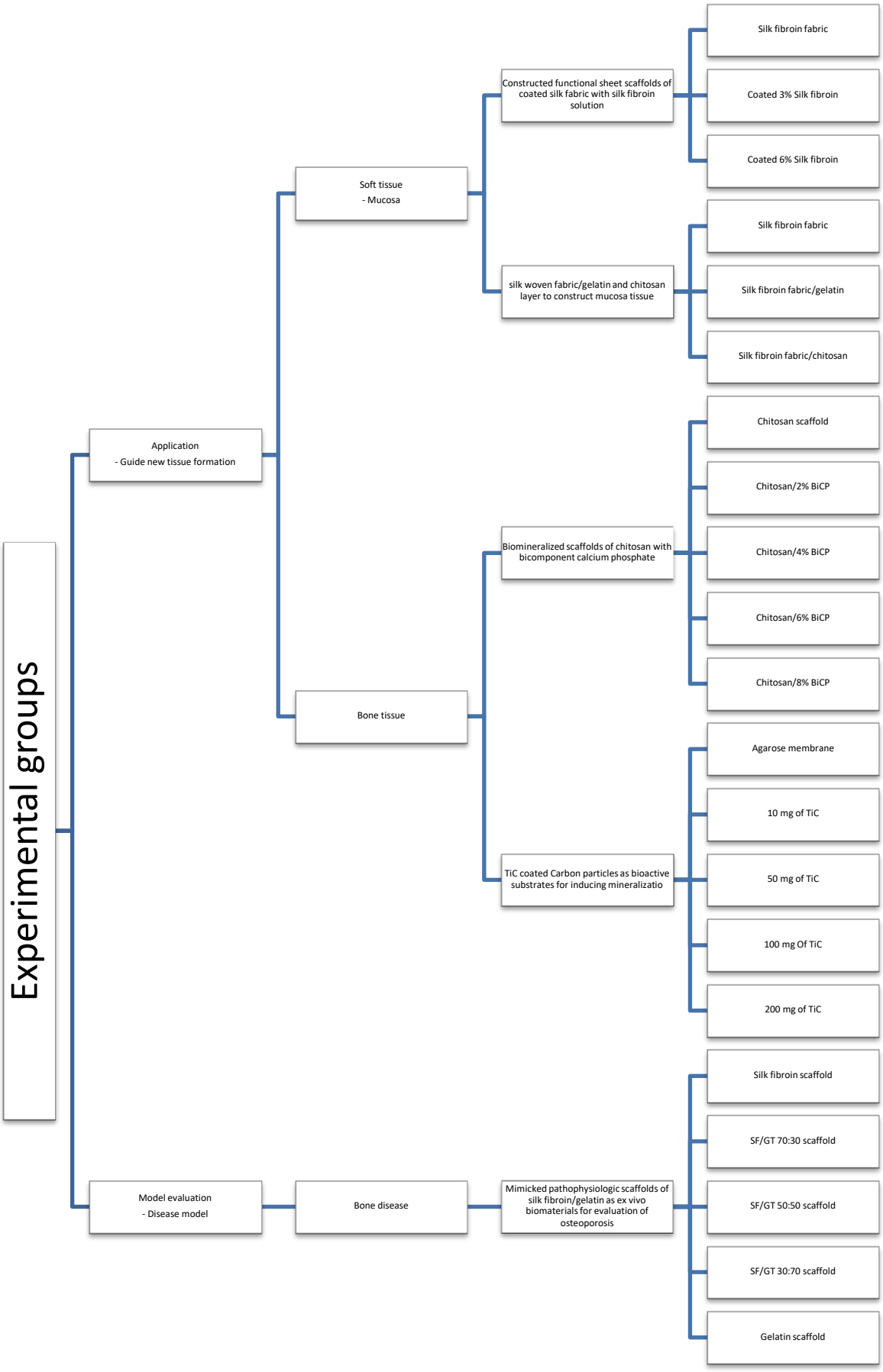

CHAPTER 2

Constructed functional sheet scaffolds of coated silk fabric with silk fibroin solution for soft tissue regeneration in cleft palate surgery

Abstract

Cleft palate is a congenital malformation of the soft and hard tissue at the oral cavity. An attractive treatment is an operation by substitution of scaffolds to induce tissue regeneration at the defect area. This research proposes constructed silk fabric coated in silk fibroin solutions for soft tissue regeneration of cleft palate. In this research, silk fabrics were coated with 3% and 6% silk fibroin solutions. The morphological structure of the silk fibroin fabric was observed by scanning electron microscopy. The swelling behavior and protein release of the coated silk fabric was used for evaluation of physical performance. L929 fibroblast cells were cultured on the coated silk fabrics. Cell proliferation and viability were used to evaluate the biological performance. The morphological structure of the coated silk fabric showed fibers that were covered and glued with silk fibroin. The coated silk fabric had lower swelling behavior than the non-coated silk fibroin fabric. Protein release and cell proliferation of the coated silk fabric was higher than the non-coated silk fabric. The results indicated that the coated silk fabric from silk fibroin solutions had good performance for soft tissue regeneration for cleft palate surgery.

Materials and methods

Coating silk fibroin fabric

The SF fabric was provided by the Research Unit and Queen Sirikit Seri Culture Centre, Narathiwat, Thailand. The SF fabric was cut into 1×1 cm pieces and then coated with 3% and 6% SF solutions. The SF solutions were prepared by

dissolving the degummed SF fiber in 9.3 M LiBr in dH_2O for 4 h at 70 C. After that, the SF solution was dialyzed for 72 h and the water was changed every 30 min during the first 4 h [1]. The SF solution was centrifuged to separate the protein precipitate. The precipitate was weighed to calculate the SF concentration. After coating with the 3% and 6% SF solutions, the SF fabric was kept at room temperature for 24 h for water evaporation. Finally, all groups of the SF fabric were soaked in 80% methanol to induce the beta-sheet structure [2].

Modification of silk fibroin fabric scaffolds

The SF fabric was modified by the 3%and 6% SF solutions. The silk fabric scaffolds were dipped in the silk solutions and left at room temperature for 24 h. There were 3 groups of different SF solutions (Table 1).

Group	Detail
A	Non coated SF fabric
B	Coated 3% SF fabric
C	Coated 6% SF fabric

Table 1. Experiment groups.

Measurement of silk fabric thickness

The thicknesses of the SF fabrics in each group were measured at 3 random points by a micrometer (Mitutoyo, USA).

Scanning electron microscopy (SEM) observation

The morphological structure of the SF fabric in all groups was observed by an SEM machine (Quanta400, FEI, Czech Republic). The SF fabric was coated with gold using a gold sputter coater machine (SPI Supplies, Division of STRUCTURE PROBE Inc., Westchester, PA, USA) before the investigation.

Swelling property

The SF fabric was immersed in a phosphate-buffered saline (PBS) solution at 37 °C and evaluated at 0.5, 1, 2, and 4 h. The weights of the SF fabrics were measured before and after immersion. The swelling ratio was calculated from this equation. Swelling ratio = (Ws – Wd)/Wd × 100 where Ws and Wd are the weight of the swollen scaffold and weight of the dry scaffold, respectively [3].

Protein release

Protein release from the fabric was evaluated in all SF fabric groups by the BCA Protein Assay Kit (Pierce BCA Protein Assay Kit, Thermo Scientific, USA). The SF fabric in all groups was soaked in a PBS solution for different time durations: 15, 30, 60, 120 and 240 min. According to the instructions of the BCA Protein Assay kit, 20 µL of solution was used for the assay.

Cell Culturing

The L929 fibroblast cell line was used in this study. The L929 cells were cultured in alpha-MEM medium (α-MEM, GibcoTM, Invitrogen, Carlsbad, CA, USA) with the addition of 1% penicillin/streptomycin, 0.1% Fungizone and 10% fetal bovine serum at 37 °C in a humidified 5% CO2/95% air incubator. The L929 cells were seeded in the SF fabric with 2×104 cells and the media was changed every 3-4 days [4, 5].

Cell proliferation assay (PrestoBlueTM on days 1, 3 and 5)

Cell proliferation of the L929 cells was evaluated at days 1, 3, 5, and 7 using the PrestoBlue (PrestoBlue® Cell Viability Reagent, Invitrogen, USA) assay. The media was removed and 1/10th volume of PrestoBlue reagent was added directly into the complete media and incubated for 1 h at 37 °C. The proliferation rate of the cells was measured by monitoring the wavelength absorbance at 600 nm emission.

Cell viability (fluorescence microscope on days 3 and 5)

The cell viability and cell morphology of the L929 cells in the SF fabric was observed by staining with fluorescein diacetate (FDA). The FDA compound embeds into the cellular cluster and extracellular matrix. Acetone was used to dissolve the FDA at a ratio of 5 mg/ml. In the staining process, the media was removed and 1 mL of fresh media was added. Next, 5 μL of the FDA solution was added and kept at 37 °C for 5 min and protected from the light. The SF fabric was rinsed with 1X PBS and cell viability was observed by fluorescence microscope [6].

Statistical analysis

The samples were measured and statistically compared by one-way ANOVA and Tukey's HSD test (SPSS 16.0 software package). Statistical significance was defined at $p < 0.05$ and all data are shown as mean ± standard deviation.

Results and discussion

Morphological structure of the silk fibroin fabric scaffolds

The non-coated SF fabric was whiter than the coated SF fabric. Moreover, a looser arrangement of the fiber structure was found in the non-coated SF fabric compared to the coated SF fabric. In addition, the SF fibers in the non-coated SF fabric were facile to unbound with other fibers. The coated SF fabric had more compact and tight features, particularly the coated 6% SF fabric, compared to the noncoated SF fabric.

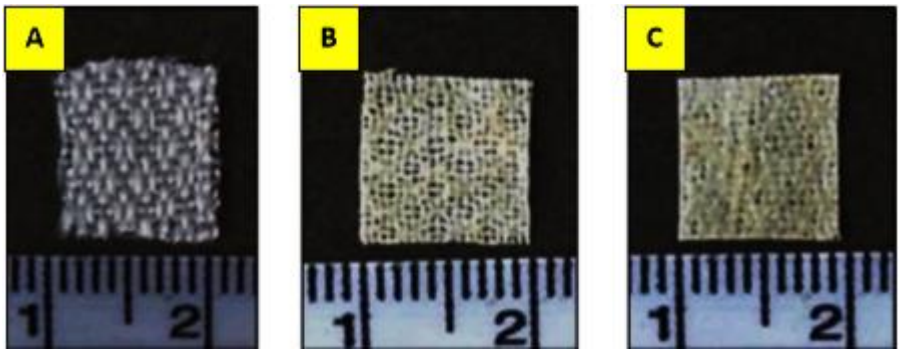

Figure 4. Coated SF fabrics from different SF solution concentrations: (A) non-coated SF fabric; (B) coated 3% SF fabric; (C) coated 6% SF fabric.

The thickness of the non-coated SF fabric was thinner than the coated 3% and 6% SF fabrics. The coated SF fabrics increased in thickness as the percentage of SF solution increased. However, there was little difference between the 3% and 6% SF fabrics (Figure 2).

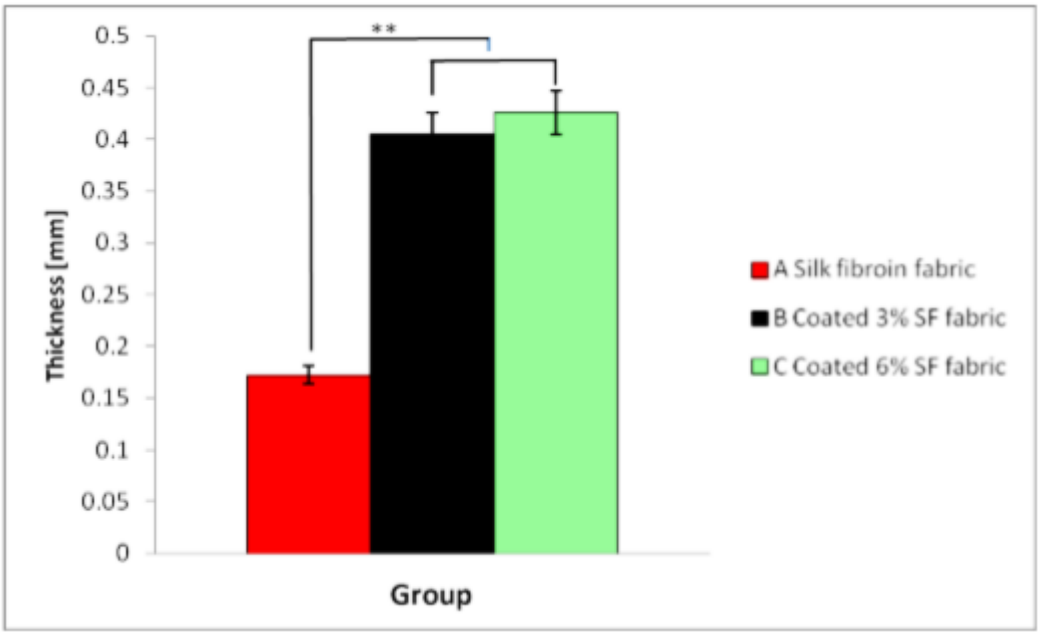

Figure 5. Thicknesses of the SF Fabrics: (A) non-coated SF fabric; (B) coated 3% SF fabric; (C) coated 6% SF fabric.

The morphological structures of the SF fabrics are shown in Figure 3. The patterns of silk fiber arrangement were similar in all groups of the non-coated SF and coated SF fabrics. In the case of the coated SF fabric, the fibers in bundles showed denser spaces than the non-coated SF fabric. The 6% SF fabric had the densest space.

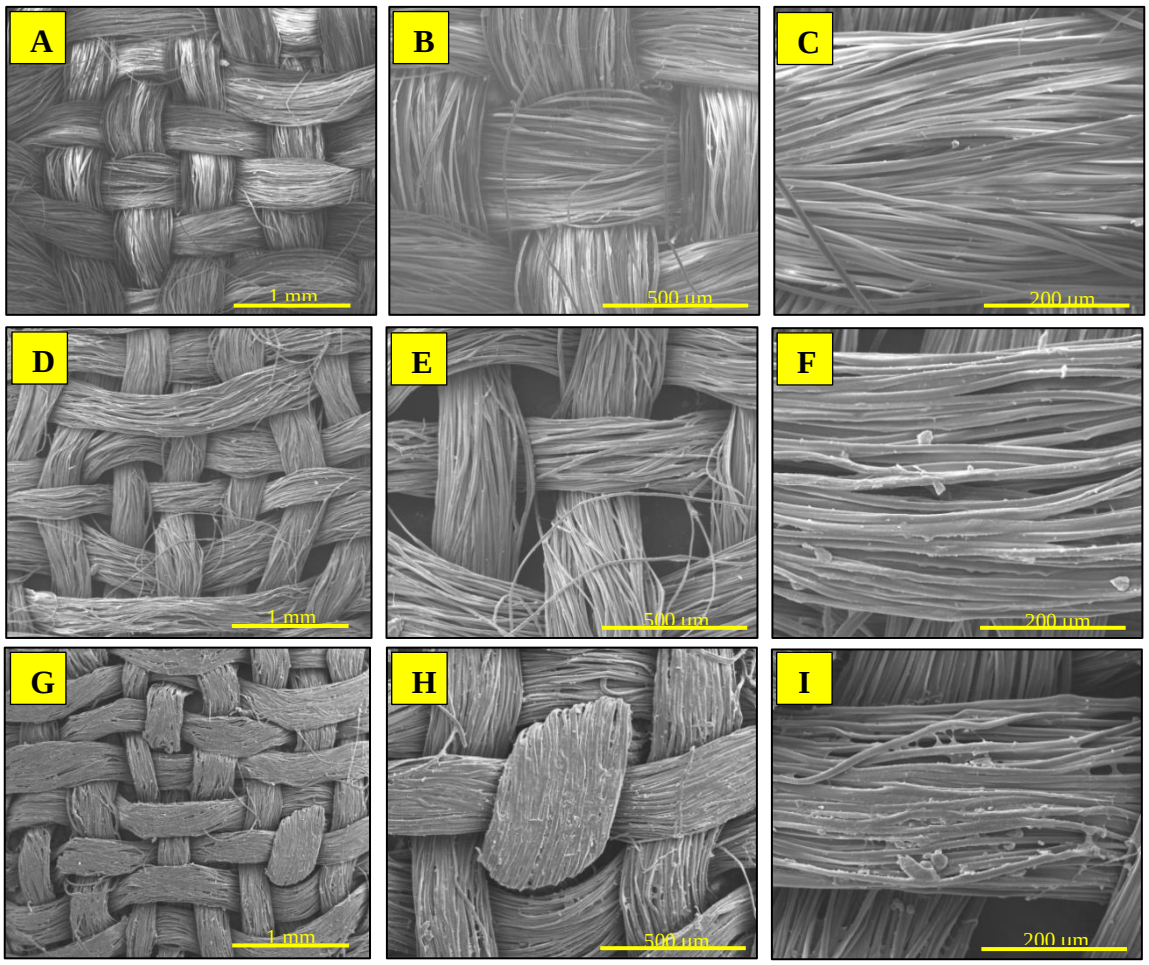

Figure 6. Surface morphologies of silk fabrics by scanning electron microscope(SEM) with different magnifications: non-coated SF fabric (A-C); coated 3% SF fabric (DF); coated 6% SF fabric (G-I).

Swelling property

The percentage of swelling was tested at different time points from 30 min to 240 min. The results showed that the percentage of swelling increased as time

increased. The non-coated SF fabric had the highest swelling percentage in the first 30 min and continued to increase in 60, 120, and 240 min. After coating, the percentage of swelling decreased. The coated 3% SF fabric had a higher swelling percentage than the coated 6% SF fabric in all time points. As the percentage of SF solution increased, the swelling percentage of the coated fabric decreased. The results indicated that the SF coating solution had the effect of decreasing the swelling behavior. These results imply physical stability and the barrier function of coated SF fabrics that make the scaffolds suitable as soft tissue layers in cleft palate.

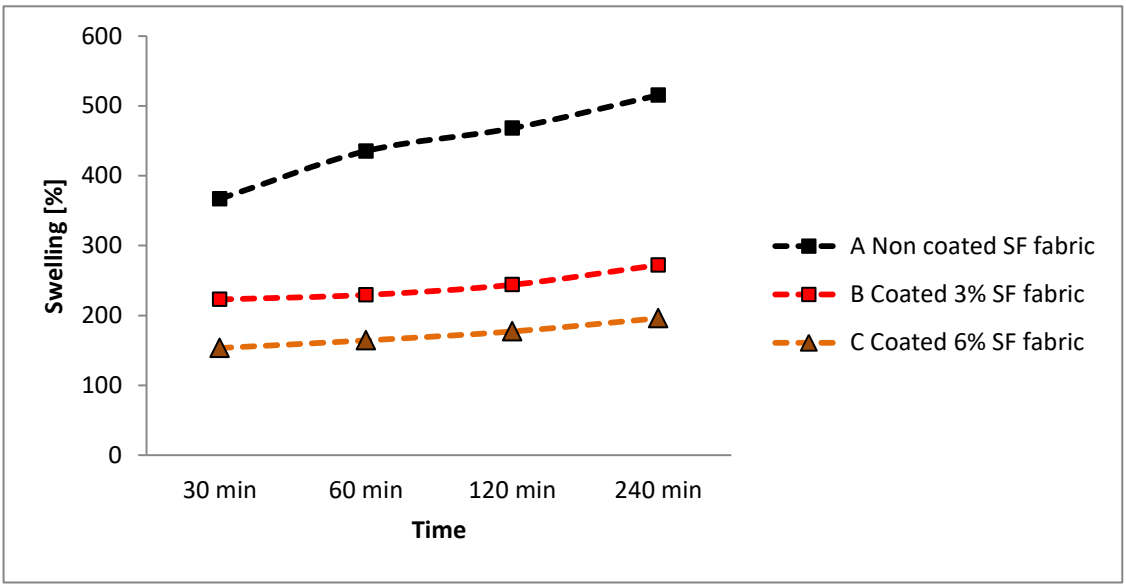

Figure 7. Swelling properties of SF fabrics: non-coated SF fabric (black line); coated SF fabrics (red [3%]/orange [6%] lines).

Protein release

Within the first 15-30 min of soaking the SF fabrics in the PBS solution, protein release was not found. However, at 60 min protein release was observed in the coated SF fabrics but decreased at 120 min. The non-coated SF fabric did not show any protein activity at any of the time points. The SF protein that coated the SF fiber

surface easily released into PBS solution. The 6% SF fabric showed the highest protein release.

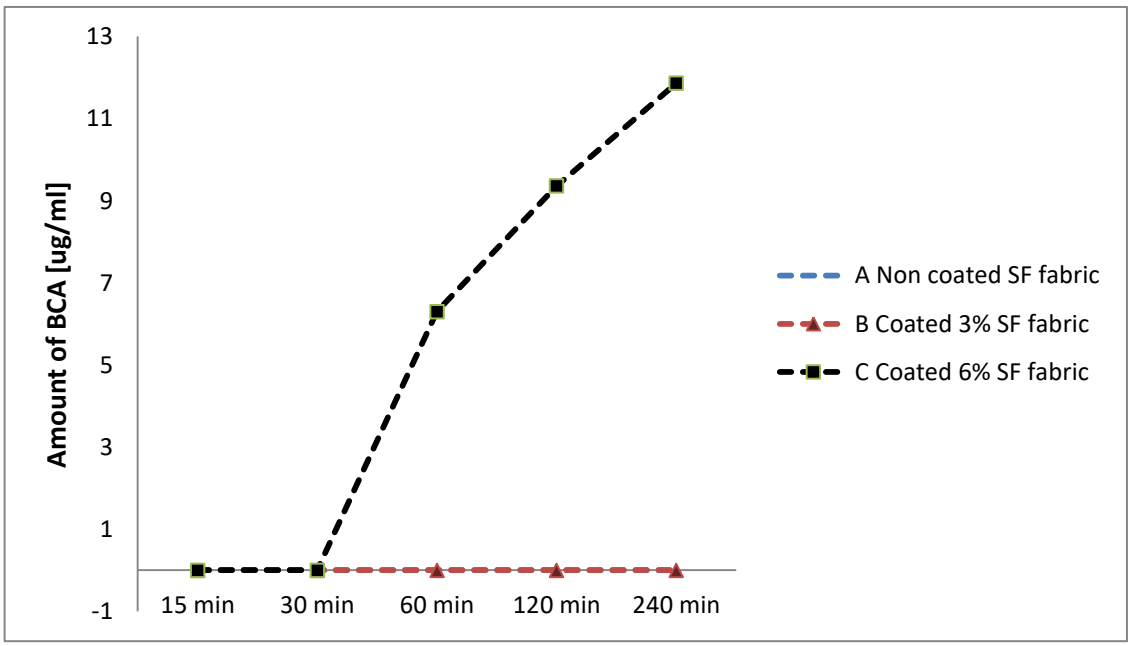

Figure 8. Amount of BCA release in 15-120 min in PBS solution.

Cell proliferation

Cell proliferation in all groups showed an increasing trend from day 1 through day 5. On days 1 and 3, the results were not significantly different between the noncoated SF fabric and the coated 3% SF fabric. The coated 6% SF fabric had significantly higher cell proliferation than the non-coated SF fabric on days 3 and 5. An increased percentage of SF solution on the SF fabric can promote cell proliferation.

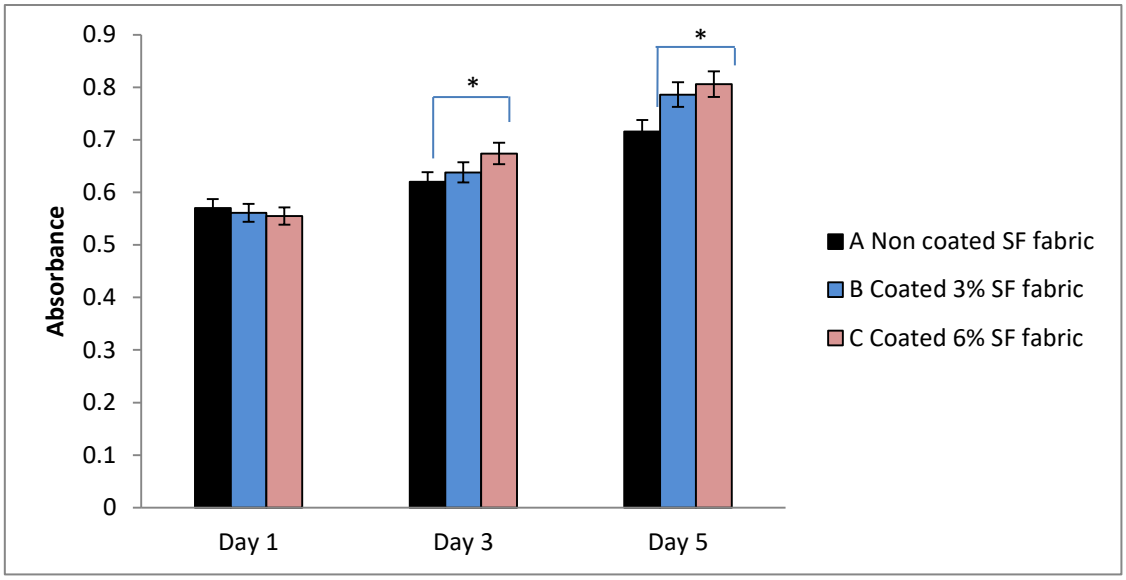

Figure 9. Cell proliferation in the SF fabrics at days 1, 3, and 5: non-coated SF fabric (A); coated 3% SF fabric (B); coated 6% SF fabric (C).

Cell viability

Cell viability was observed on days 3 and 5. Cell attachment in the non-coated SF and coated SF fabric was considerable. On day 1, the non-coated and coated SF fabric showed slight cell attachment but increased on day 3. On day 5, the coated SF fabrics revealed a greater amount of cell attachment compared to the non-coated SF fabric. The results showed that the coated SF fabric was biologically suitable for cell viability.

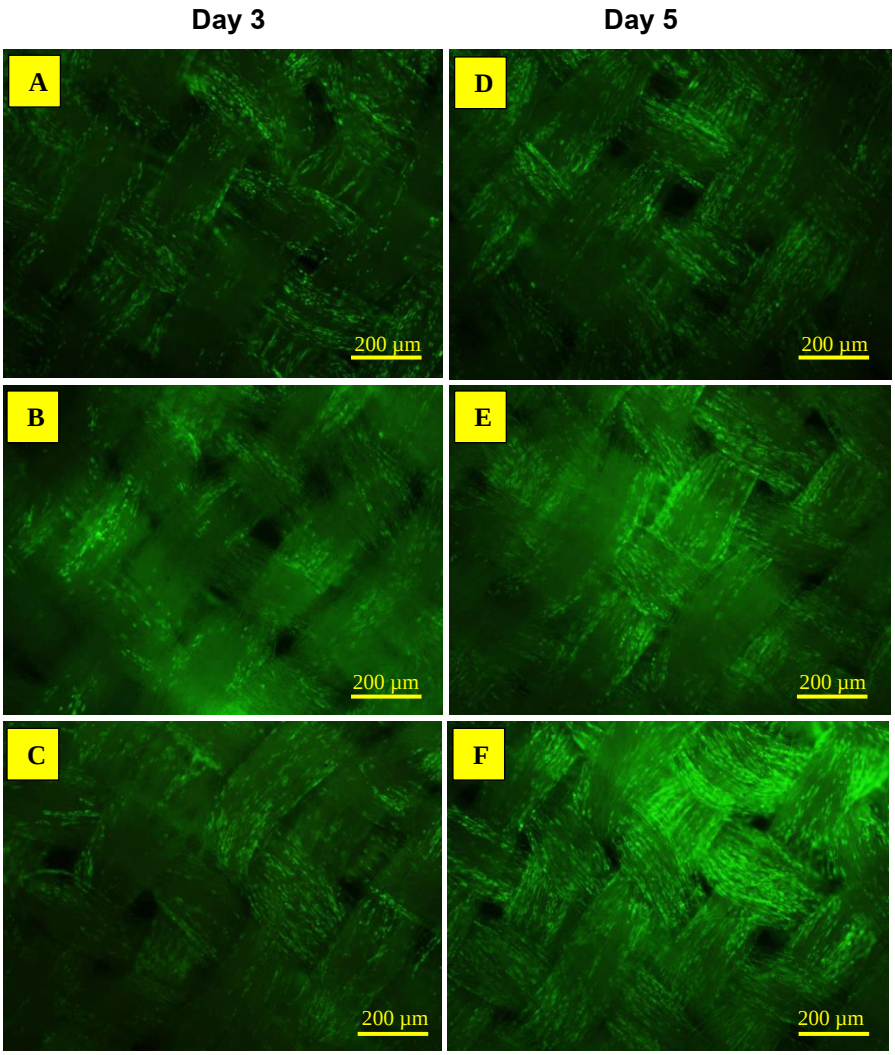

Figure 10. Cell viability on the SF fabric after staining with FDA: non-coated SF fabric at day 3 (A); coated 3% SF fabric at day 3 (B); coated 6% SF fabric at day 3 (C); noncoated SF fabric at day 5 (D); coated 3% SF fabric at day 5 (E); coated 6% SF fabric at day 5 (F).

Conclusion

In this study, SF fabric was modified by coating in SF solutions. Coating SF fabric with 3% and 6% SF solutions resulted in physical and biological properties that are suitable for soft tissue regeneration. The morphological assessment of the coated SF fabric indicated that the SF solution could diffuse and penetrate into the

spaces. The SF solution fulfilled the role as a welding glue. The glue could bind the fibers into bundles. An evaluation of the physical performance by observing the swelling behavior indicated that the SF solutions decreased the extent of swelling of the SF fabrics which implied sufficient physical stability and barrier function to serve as scaffolds for soft tissue layer in cleft palate. The biological performance assessment of the coated SF fabric revealed higher cell proliferation than the non-coated SF fabric. This demonstrated that the coated SF fabric had the bioactive ability to induce cell proliferation. Some research reported that the SF particles could induce cell adhesion and proliferation [7]. Therefore, the high protein release of the coated SF was possibly due to the active particles which induced the cell proliferation. The results demonstrated that the coated SF fabric showed a suitable performance for use as scaffolds for soft tissue engineering in cleft palate.

Reference

[1] Mandal BB, Sonia K, Subhas CK. Silk fibroin/polyacrylamide semi-interpenetrating network hydrogels for controlled drug release. India : Biomaterials 2009;30:2826-2836.

[2] Qiang L, Xiao H, Xiaoqin W, Jonathan AK, Shenzhou L, Peggy C, David LK. Water-Insoluble Silk Films with Silk I Structure. USA : NIH Public Access 2010;6:1380-1387.

[3] Nicholas G, Annie B, Bernardo PR, David LK. Lyophilized silk fibroin hydrogels for the sustained local delivery of therapeutic monoclonal antibodies. United States of America : Biomaterials. 2011;32:2642-2650.

[4] Serrano MC, Pagani R, Vallet-RM, Pena J, Ramila A, Izquierdo I, Portoles MT. In vitro biocompatibility assessment of poly(ε caprolactone) films using L929 mouse fibroblasts. Spain : Biomaterials 2004;25:5603-5611.

[5] Thonemann B, Schmalz G, Hiller KA, Schweikl H. Responses of L929 mouse fibroblasts, primary and immortalized bovine dental papilladerived cell lines to dental resin components. Germany : Dental Materials 2002;18:318-323.

[6] John AM, Diane GK, Thomas JB. Role of Fibronectin in Collagen Deposition : Fab' to the Gelatin-binding Domain of Fibronectin Inhibits Both Fibronectin and Collagen Organization in Fibroblast Extracellular Matrix. United States : Cell Biology 1982;92:485-495.

[7] Jing Q, Lu W, Yongpei H, Lingshuang W, Renchuan Y, Mingzhong L. Preparation of Silk Fibroin Microspheres and Its Cytocompatibility. China : Journal of Biomaterials and Nanobiotechnology 2013;4:84-90.

CHAPTER 3

Mimicked anatomical biphasic scaffolds based on silk woven fabric/gelatin and chitosan layer to construct mucosa tissue for maxillofacial surgery

Abstract

Mucosa tissue defect in maxillofacial area is a critical problem for many patients. For some case, those patients have to get operation with performance scaffold substitution. In this research, mimicked anatomical biphasic scaffolds were constructed by coated silk woven fabric with gelatin and chitosan. Then, the morphology, crystal, and structure were observed and characterized with Scanning Electron Microscopy, X-ray Diffraction, and Differential Scanning Calorometry, respectively. Physical performance was presented with swelling behavior , mechanical properties, and biodegradation. Biological performance tested with fibroblast and keratinocyte. Then, cell proliferation, viability, and histology was evaluated. The results showed that coated silk woven fabrics showed crystal structure of silk fibroin and amorphous of gelatin and chitosan layer. Coated fabrics had residual water in their structure. Physical performance of coated silk woven fabric with gelatin showed suitable swelling behavior, mechanical properties, biodegradation for insertation in defect site. The biological performance cell proliferation, viability, and histology for mucosa tissue construction at defect sites. Finally, the results showed that mimicked anatomical biphasic scaffolds based on silk woven fabric/gelatin layer was promising for mucosa tisse construction in maxillofacial surgery.

Materials and methods

Coating silk fibroin fabric

The silk fibroin fabric was supported by Research Unit and Queen Sirikit Seri Culture Centre, Narathiwat, Thailand. Silk fibroin fabric was cut into1.0×1.0 cm Then, cut silk fibroin fabric was coated with gelatin and chitosan solution. All coating solution was prepared at 3% w/v. The gelatin powder (Gelatin from porcine skin, Sigma-aldrich) was dissolved in distill water at 50 °C for 15 min [1]. The 0.1M acetic acid was used for chitosan (%DD ≥ 90 %, Marine Bio Resources Co.,Ltd) dissolving [16], the chitosan solution was filtered with cheesecloth. In the coating step, the silk fibroin fabric was soaked in each solution for 30 min at 37 °C and continue dry at room temperature for 24 hrs.

Groups	Detail
SF	Silk fibroin fabric
SF-GT	Silk fibroin fabric/gelatin
SF-CS	Silk fibroin fabric/chitosan

Table 2. Experimental group

Scanning electron microscope (SEM)

The surface and morphological structure of fabric in all groups was observed with a scanning electron microscope (Quanta400, FEI, Czech Republic). The samples were coated pre-coated with gold using a gold sputter coater machine (SPI Supplies, Division of STRUCTURE PROBE Inc., Westchester, PA USA).

Swelling property

All groups of fabric were soaked in PBS in different time point include 0.5, 1, 2, 4, 8, 12 and 24 hrs. The weight of fabric was collected before and after PBS

soaking. The swollen samples were weighed immediately, the swelling ratio was calculated using the following equation.

$$\text{Swelling (\%)} = (Ws - Wd)/Wd \times 100$$

Where the Ws and Wd are the weight of swollen scaffold and weight of dry scaffold, respectively [2].

Tensile Property Testing

The silk fabric was cut into 1×5 cm and fix with glue on the plastic plate. The sample was evaluated the tensile property by LLOYD INTRUMENT with condition 10N/min. The data were collected for stress and percentage strain analysis.

Fourier transform infrared (FT-IR) characterization

Molecular organization of silk fibroin fabric, and silk fibroin coated gelatin fabric and silk fibroin coated chitosan fabric were analyzed by FT-IR. The samples were analyzed as a KBr pellet in a FT-IR spectrophotometer using the EQUINOX 55 (Bruker Optics, Germany) in the range of 4000-400 cm-1.

X-ray diffraction (XRD) characterization

Crystal structure of silk fibroin fabric, and silk fibroin coated gelatin fabric and silk fibroin coated chitosan fabric were analyzed by XRD (X'Pert MPD (PHILIPS, Netherlands). Samples were put in XRD instrument and measured diffraction patterns over a 2θ range of 5-90 θ with a step size of 0.05 θ and time per step of 1 s.

Cell culture experiments

In this study, murine fibroblast L929 cells line was used for the biological function of fabric in all groups. The murine fibroblast L929 cells line was cultured in alpha-MEM medium (α-MEM, GibcoTM, Invitrogen, Carlsbad, CA) with the addition of 1% penicillin/streptomycin, 0.1% fungizone and 10% fetal bovine serum (FBS) at 37°C

in a humidified 5% of CO2 and 95% air incubator. The murine fibroblast L929 cell line was seeded with a 2 ×104/silk fabric and the medium was changed every 3-4 days [3] The H357 keratinocyte cell line was culture in the Dulbecco's modified Eagle's medium (DMEM) combined with Ham's F-12 nutrient mixture, supplemented with 10 % fetal calf serum, epidermal growth factor (10 ng/ml), hydrocortisone (0.5 g/ml), penicillin (100 U/ml), streptomycin (100 g/ml), and amphotericin B (2.5 g/ml) [4].

Cell proliferation assay (PrestoBlue; Day 1, 3, 5, and 7)

The cell proliferation of L929 and H357 cell line in silk fibroin fabric was observed by PrestoBlue [PrestoBlue® Cell Viability Reagent, Invitrogen, USA] assay. The measurement of cell proliferation was performed according to the manufacturer's instructions. After cell seeding at day 1, 3, 5 and 7, the media was removed, next washed twice with 1X PBS and then 1/10th volume of PrestoBlue reagent was added directly into the complete media and incubated for 1 hour at 37°C and the proliferation rate of the cells was measured by monitoring the wavelength absorbance at 600 nm emission.

Cell viability (Fluorescence Microscope on Day 3, 5 and 7)

To observe the cell migration and viability of L929 fibroblast cell and H357 keratinocyte in the silk fabric, the Fluorescein Diacetate (FDA) was used for fluorescence staining. The function of FDA was stained the extracellular matrix. The FDA powder was dissolved in acetone at 5 mg/ml. The 5 µl of FDA solution was added in silk fabric in 1 ml fresh media. After that, the1X PBS was washed for FDA excess, next put the fabric on the glass slide and observed under fluorescence microscope [5].

Histology

The L929 fibroblast cell and H357 keratinocyte in the silk fabric in all groups were stained with H&E at day 3 and 5 for morphology observation. Moreover,

the collagen deposition of L929 fibroblast was detected with masson trichrome staining on day 14 and 28. All groups of fabric were immersed in paraffin after fix with 4% formaldehyde at 4 °C for 24 h. The paraffin was cut into 5 micron and put on the glass slide. The slide was deparaffinized and hydrated for H&E and masson trichrome staining [6].

Statistical analysis

All data were shown as mean ± standard deviation. The samples were measured and statistically compared by one-way ANOVA and Tukey's HSD test (SPSS 16.0 software package). $P < 0.05$ was accepted as statistically significant.

Results and discussion

Morphological structure of mimicked anatomical biphasic scaffolds

After construction of silk fabric into mimicked anatomical biphasic scaffolds (Figure.8), morphological structure was observed by SEM. The result showed that for SF had the geometry as the woven structure (Figure. A-D). For the SF-GT and SF-CS, morphological structure showed the coated fiber bundle of silk woven fabric (Figure. 9E, F, I, and J). Some free space between bundles of fiber were filled by gelatin and chitosan. For the coating layer, the silk woven fabric was covered by gelatin and chitosan for the whole area (Figure 9G, H, K, and L). Notably, some areas of the covered surface show the cue pattern of bundle of fibers (Figure. 9H and L).

Importantly, the results from morphological observing indicated that gelatin and chitosan showed; 1) the thin layer covering on bundles of fibers, 2) the smooth layer covering on surface of woven structure. Interestingly, the covered thin film on bundles of fibers and smooth layer on woven might be the structural cue that has an effect on the biological performance of mimicked anatomical biphasic scaffolds. However, to prove this hypothesis, the evaluation on cell experiment was undertaken.

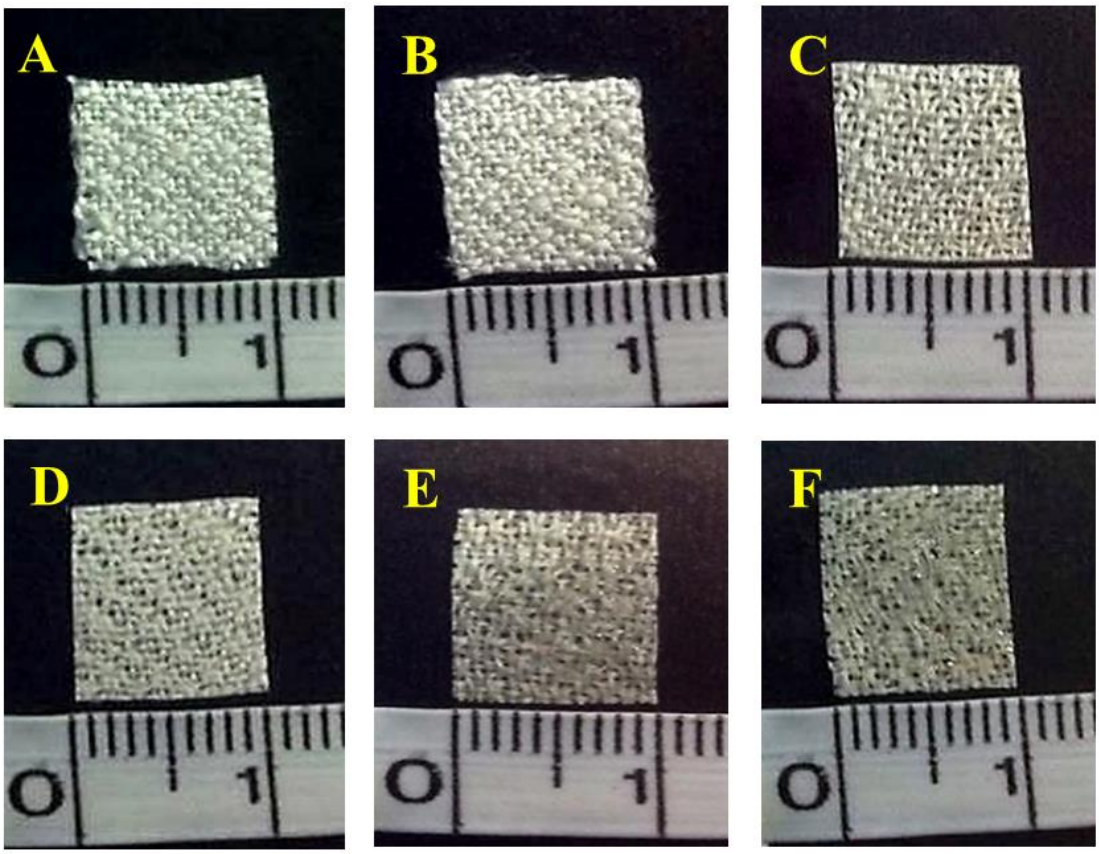

Figure 11. Non-coated side of silk fabric (A, D), Non-coated side of silk fabric with gelatin (B), Non-coated side of silk fabric with chitosan (C), Coated side of silk fabric with gelatin, (E), and Coated side of silk fabric with chitosan (F),

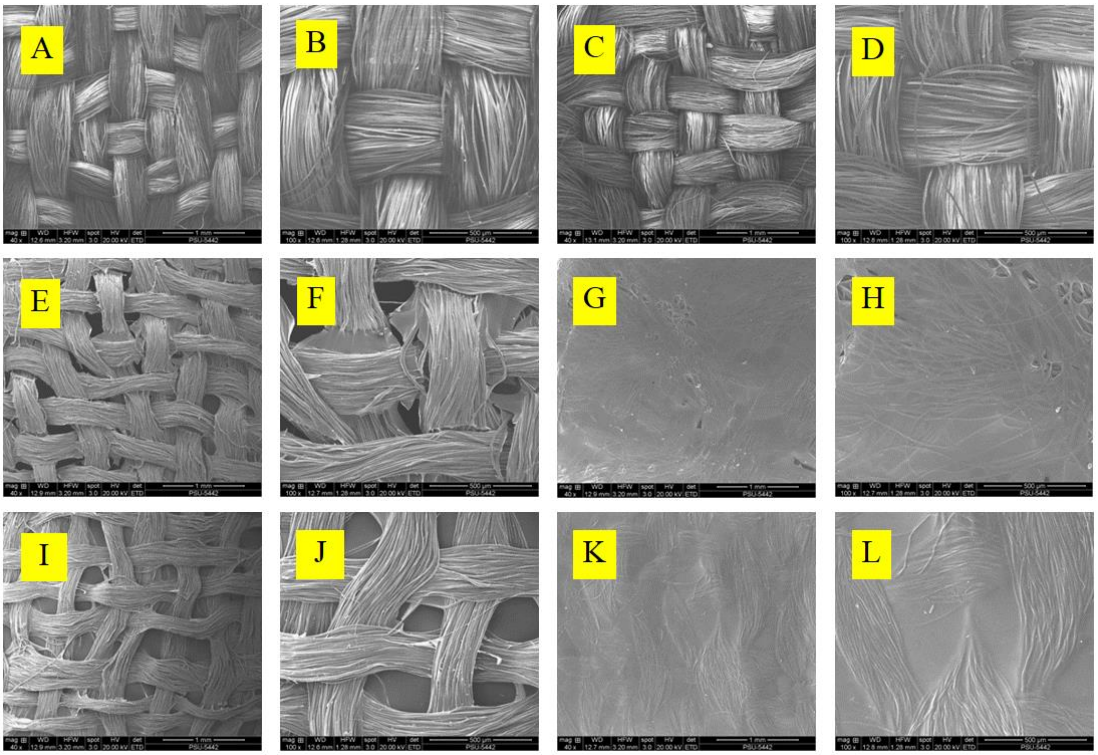

Figure 12. The surface morphology of coated silk fabric; Non-coated side of silk fabric (A, B, C, D), Non-coated side of silk fabric with gelatin (E,F), Non-coated side of silk fabric with chitosan (I,J), Coated side of silk fabric with gelatin, (G,H), and Coated side of silk fabric with chitosan (K,L),

Structural formation of mimicked anatomical biphasic scaffolds

The crystal structure of mimicked anatomical biphasic scaffolds were characterized by XRD (Figure 10). The crystal analysis was shown around the 20 degrees, this peak indicated that the beta-sheet conformation of silk fibroin was found in all groups [7]. Notably, for the SF-GT and SF-CS, there were the shoulder around 20 to 40 degree. This represented the amorphous structure of gelatin and chitosan [8]. Especially, SF-CS showed broader shoulder than SF-GT. This demonstrated that chitosan form more amorphous structure than gelatin.

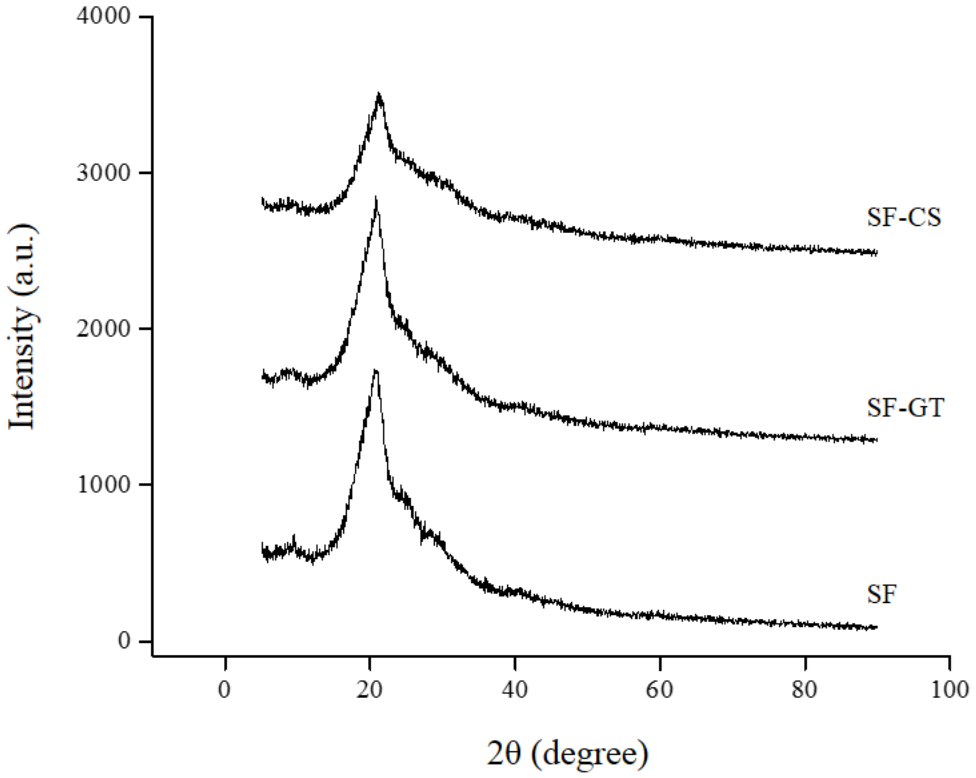

Figure 13. XRD spectra of constructed laminate composite: SF, SF-GT, and SF-CS

The structural formation on mimicked anatomical biphasic scaffolds were characterized by DSC (Figure 11). The DSC thermograms showed that all samples had the peaks at around 50 to 60 °C. Those peaks showed at 65.4, 63.6, and 59.4 °C that represented the hydration of SF, SF-GT, and SF-CS, respectively [9, 10,11]. This indicated that SF had more stability of water structure than SF-GT and SF-CS.

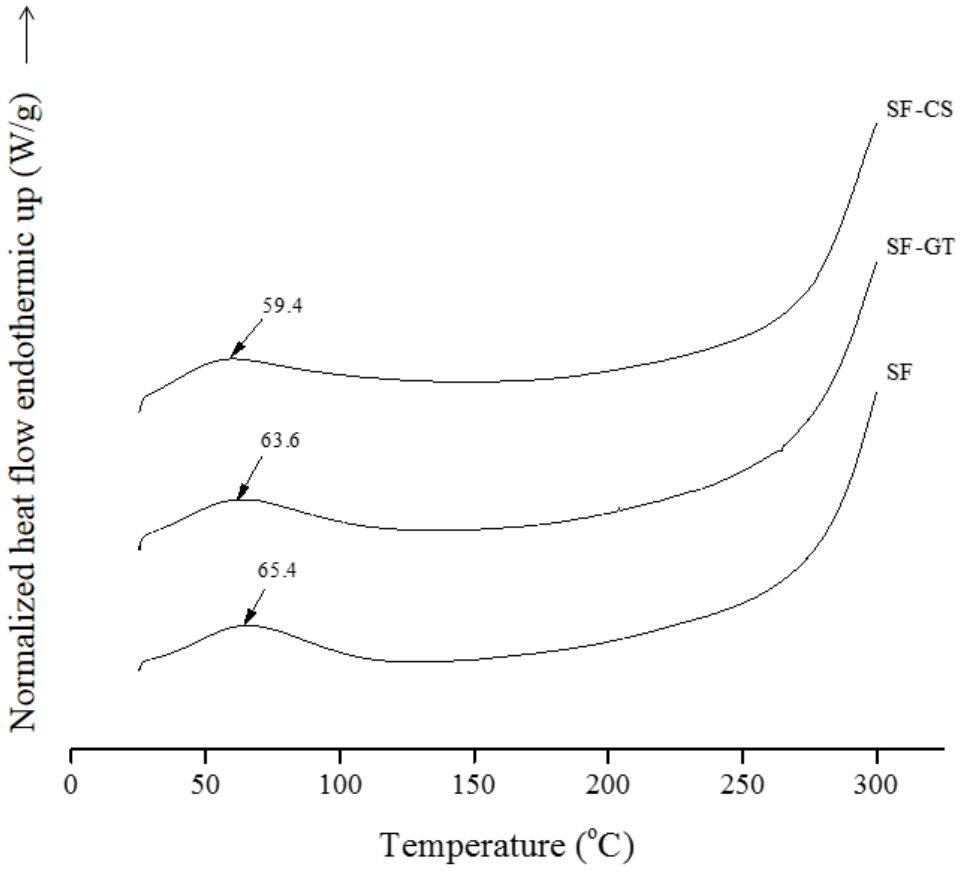

Figure 14. DSC thermograms of constructed laminate composite ; SF, SF-GT, and SF-CS

Physical performance of mimicked anatomical biphasic scaffolds

In this research, swelling behavior was chosen to evaluate physical performance of mimicked anatomical biphasic scaffolds. The swelling behavior was showed in Fig. 12, In the first 30 min, the SF revealed a higher value of water absorption than both SF-GT and SF-CS. This is because SF showed the free space between the bundles of woven. Furthermore, the loose structures in those bundles also support water absorption.

For coated silk fabric, SF-GT showed more swelling behavior than SF-CS. This demonstrated that gelatin coating had more water absorption than chitosan coating. Notably, SF-GT showed the rapid swelining behavior at around 30-60 min.

This might come from the unique hydrogel characteristic of gelatin that lead to the higher swelling behavior than SF-CS [12].

Interestingly, some reports demonstrated that the inserted membranes for mucosa tissue construction in maxillofacial area have to show barrier performance. Such performances have to shield mucosa cells invasion into the bone tissue during regeneration. Furthermore, those membranes have to show the physical performance which had the certain swelling behavior for tissue construction similar to native mucosa layer in maxillofacial area [13].

According to the results of swelling behavior, SF-GT might therefore have the optimized physical performance which is suitable for construction of mocosa tissue in maxillofacial area.

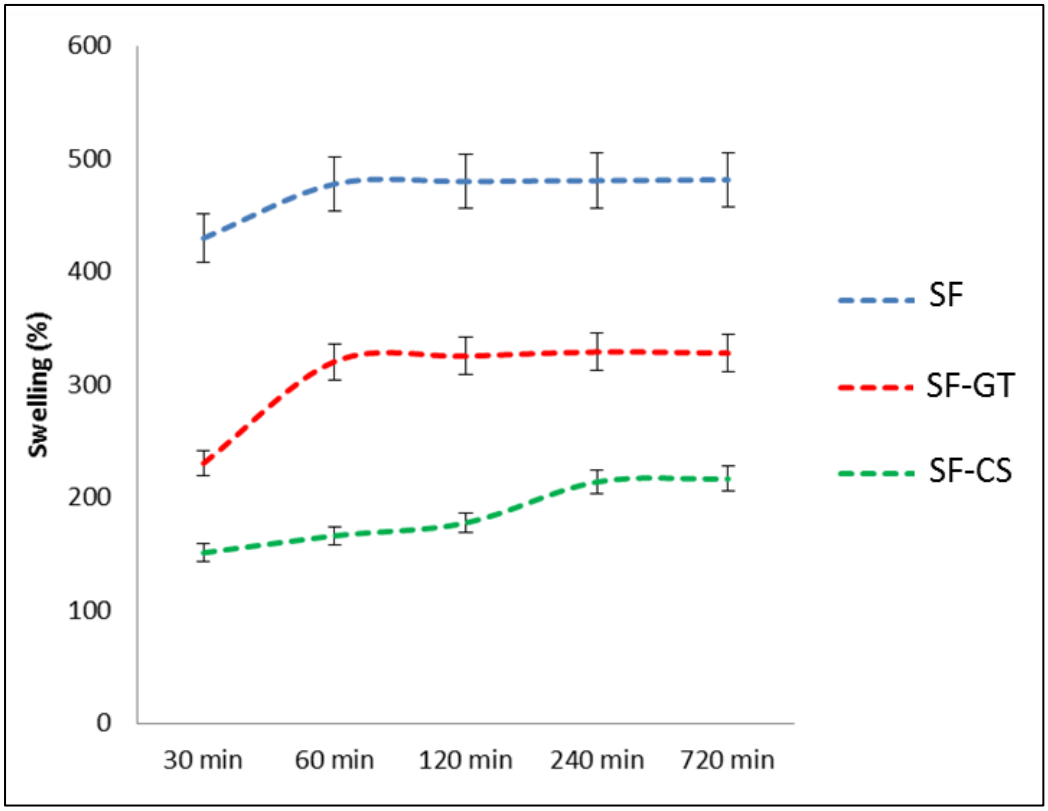

Figure 15. The swelling properties of silk fabric in all groups from 30 min to 720 min in PBS solution.

To evaluate degradation, lysozyme was used to test with biphasic sheet. After degradation with lysozyme, the result showed that silk fibroin fabric revealed a lower degradation with enzyme than the others (Figure. 13). On the other hand, the high degradation was found in groups of silk fibroin coated gelatin fabric and silk fibroin coated chitosan fabric. On day 7, the silk fibroin coated gelatin was significant higher than silk fibroin fabric coated chitosan and except day 14, 21 and 28. This results showed that gelatin was actively degradation with lysozyme at the early state. Then, the degradation of lysozyme on gelatin showed the similar rate as chitosan at the prolong state.

According to the degration of coated silk woven fabric, the results could related to structural tissue formation of native mucosa. The thin coating layer represented the layer which contact to keratinocyte. Notably, some research demonstrated that the certain degradation of scaffolds is important to promote keratinocyte proliferation [14]. Those scaffolds showed degraded structure which could hold physical stability until completed tissue regeneration [15]. The results indicated that SF-GT showed suitable degradation performance from gelatin and the physical stability from silk woven fabric. This is suitable performance for mucosa tissue construction.

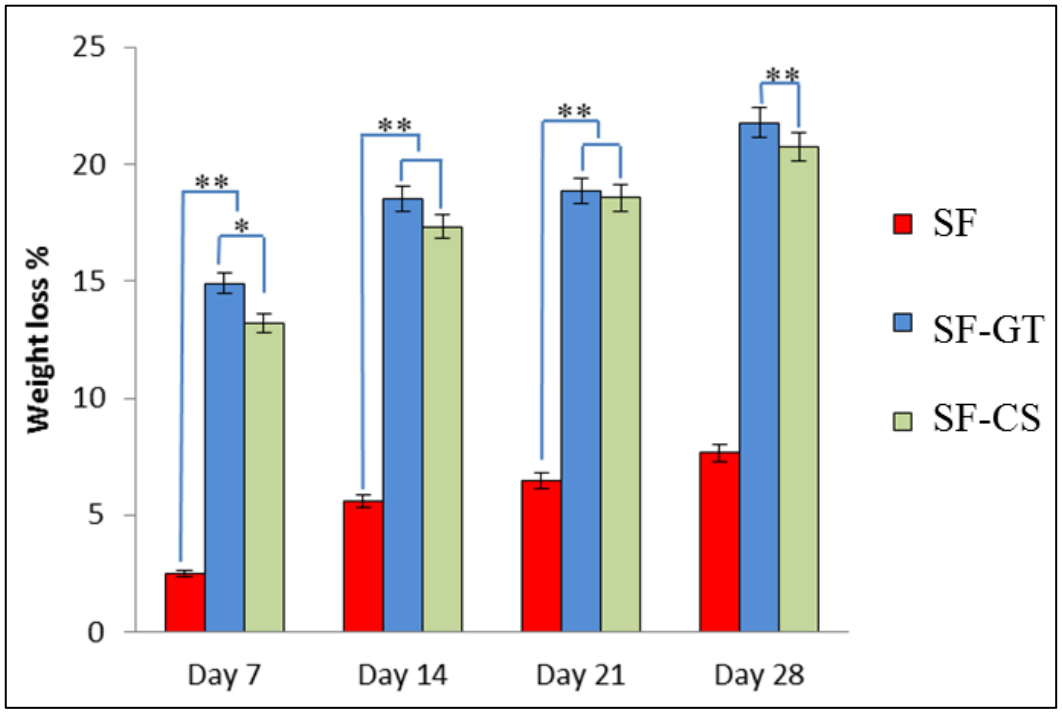

Figure 16. Degradation of constructed biphasic sheet by lysozyme at different time points; Day 7, 14, 21 and 28

In this research, tensile testing was selected to evaluate mechanical behavior of mimicked scaffolds. The results showed that SF showed more extension at the early stage than the others (Figure. 14). This might come from the loose structure between bundle of fibers that lead to the more extension of SF at the early stage. Then, SF show more difficult extenstion than the others. That extension started after around three percentage of strain. This might come from the loose structure of SF showed more alignment of fibers than the other.

Therefore, that alignment could induce the rapid stress increasing which lead to the difficult extention [16]. Afterward, SF start to break at the lower extension than the others. This migh come from that SF have non-coated fiber which show non shielding of coating. This might be the cause for breaking of SF at the lower extension.

On the other hand, SF-CS and SF-GT showed the hard extension at the early stage. Notably, SF-GT had the more difficult extension than SF-CS at the early

stage. This might come from the effect of gelatin coating on the surface. Generally, gelatin showed unique functionality of adhesion which can strickly bond with silk fabric [17]. This is the cause of the difficult extension at the early stage. Then, coated silk fabric of SF-CS and GT showed gradually increasing of stress which lead to the more extension than SF. This demonstrated that the chitosan and gelatin coating disturb the alignment of fibers during extension. Therefore, SF-GT and CS had no rapid stress inceasing. Finally, the results showed that the coated silk fabric showed the breaking at the more extension point than non-coated silk fabric. This indicated that chitosan and gelatin coating acted as the force shielding which can prolong the breaking to the more extension point.

According to the mechanical behavior, the results indicated that coated fabric had unique mechanical behavior. Especially, SF-GT showed high elongation at maximum stress. This showed the flexible behavior which is similar to mucosa tissue [18]. The results indicated that SF-GT showed the certain mechanical performance for insertion in the defect for mucosa tissue construction.

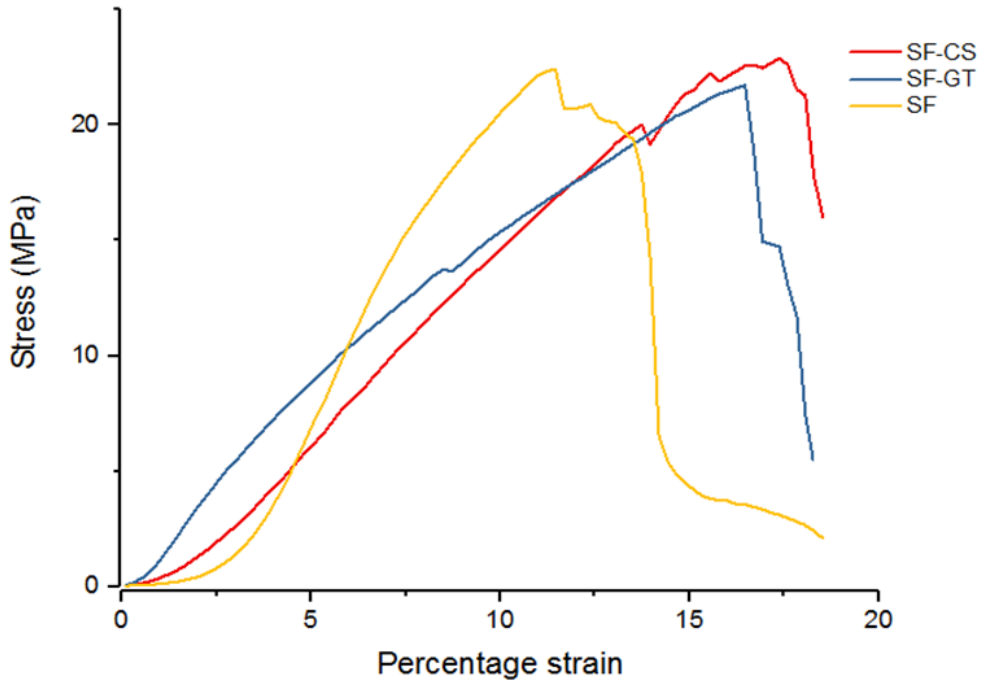

Figure 17. The stress-percentage strain curve of silk fibroin fabric in each group.

Biological performance of mimicked anatomical biphasic scaffolds

In this research, cell proliferation was selected to present biological performance of mimicked anatomical scaffolds. The coated silk fibroin fabric was mimicked similar to anatomy of native mucusa tissue . The thick woven fabric and thin coating layer presented similar to fibroblast and keratinocyte layer, respectively.

Biological performance of the silk woven fabric layer

For the proliferation of fibroblast on silk woven layer, the results showed that the trend of cell growth was continuously increased along with day 1 to day 5 and decreases on day 7 in group of SF-GT and SF-CS. On day 1, SF-GT was significant higher than SF and SF-CS (Fig.15). On day 3, all groups revealed a similar action of cell proliferation, except SF-CS. The SF-GT was indicated the significantly higher than other groups and representative of cell behavior on day 5. On day 7, the all groups became lower, except SF was significantly different than the other groups.

For the mimicked anatomical structure of fibroblast layer, coated showed more cell proliferation at early stage ; day 1 to 5 than the others. The results showed that SF and SF-GT had higher cell proliferation than SF-CS. This might come from bioactive functionality of gelatin and silk fibroin which can induce cell proliferation [19,20]. On the other hand, SF-CS showed lowest cell proliferation for all stages. Some reports demonstrated that released chitosan debris had an effect on decreasing of cell proliferation [21].

For the later stage; day 7, the result showed that cell proliferation of coated silk fabric decreased. This might come from the degraded gelatin and chitosan which leaded to the cell detachment. Such cell detachment had an effect on the decrease of cell proliferation [22].

Interstingly, the results indicated that fibroblasts rapidly adhered and proliferated at the early stage on silk woven fabric layer of SF-GT. The silk woven fabiric of SF-GT showed the suitable biological performance similar to process of

mucosa tissue regeneration. Such process firstly start with early stage of fibroblast proliferation. Then, keratinocyte begin to express proliferation. This indicated that the silk fibroin woven fabric of SF-GT regulated fibroblast proliferation similar to early stage of mucosa tissue formation

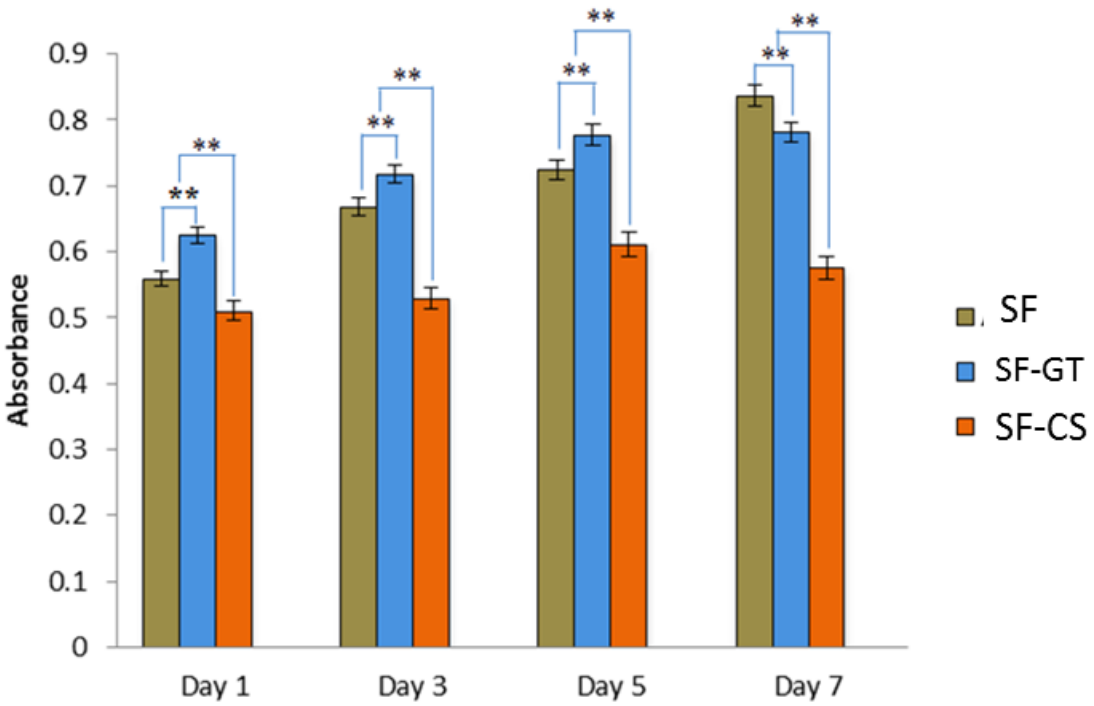

Figure 18. Showed fibroblast cell proliferation in the silk fibroin fabric on day 1, 3, 5 and 7.

For cell viability was selected to represent as biological performance of mimicked anatomical biphasic scaffolds. The results showed the fibroblast adhesion on the surface of non-coated and coated silk woven fabric. The result showed that SF and SF-GT showed the more unique fibroblast adhesion on the surface than SF-CS from the day 1 to 7. Notably, SF-GT had more fibroblast adhesion than SF for early stage; day 1. This might come from RGD groups of which can promote cell adhesion. Such cell adhesion lead to enhance cell viability [23].

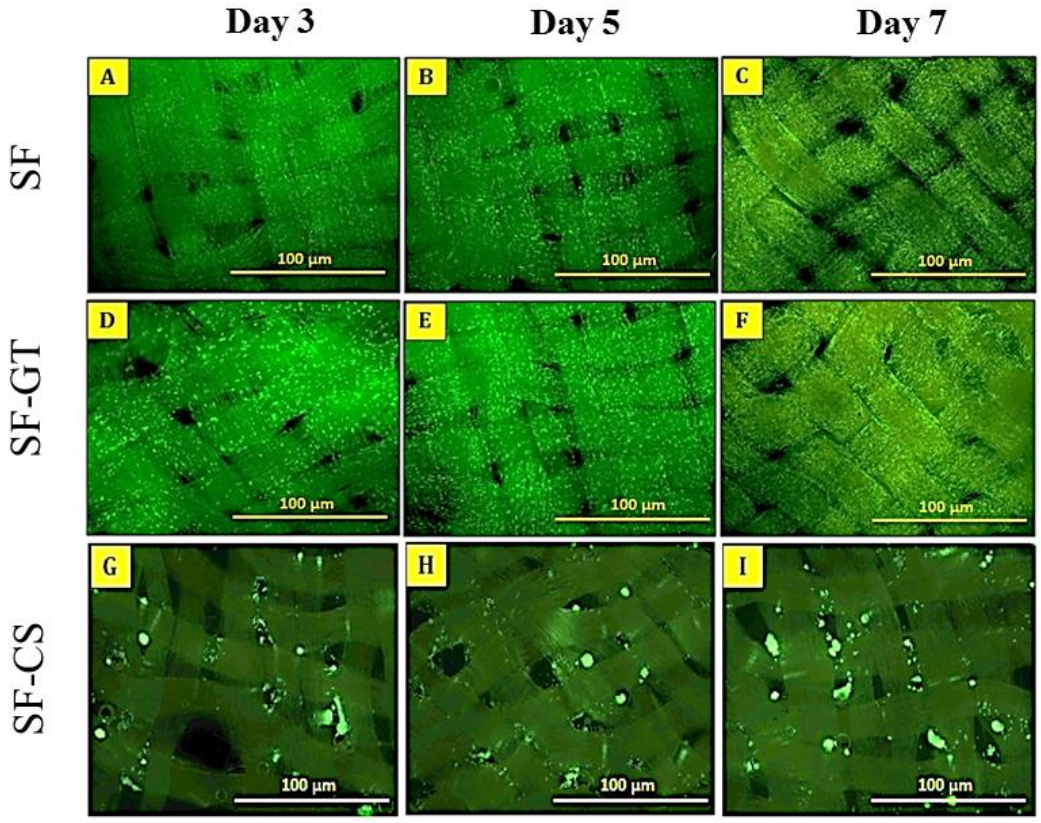

Figure 19. Cell viability staining with FDA on the silk fibroin fabric (A); silk fibroin coated gelatin fabric (B); silk fibroin coated chitosan fabric (C); at day 3, 5 and 7.

The cell morphology of the fibroblast was observed on non-coated side at day 3 and 5. On day 3, the results showed that the groups of SF and SF-GT clearly had cell adhesion and elongation on the surface. In the SF-CS showed clusters of cell aggregation which had non-elongation on the surface. This indicated that the surface of SF, SF-GT showed suitable structure and characteristic to promote adhesion and elongation of fibroblasts.

On day 5, the dense cell adhesion and elongation was found on the surface of SF and SF-GT. Notably, fibroblasts showed deeper migration inside the bundle of silk fiber of SF-GT than SF and SF-CS. This might come from the free spaces of dissolved and degraded gelatin during culture. Those free spaces could enhance cell migration. On the other hand, SF-CS had the dense cluster of cell aggregation on the surface and no cell migration inside bundle of fibers. This might

come from that SF-CS showed the low degradation. Such low degradation led to the few free space formation. This led to the non cell migration inside fiber bundle of SF-CS.

Importantly, the results demonstrated that the morphological formation of SF-GT could induce cell adhesion. The fiber bundle structure promoted the cell migration [24]. Those cell adhesion and migration lead to enhance mucosa tissue regeneration [25].

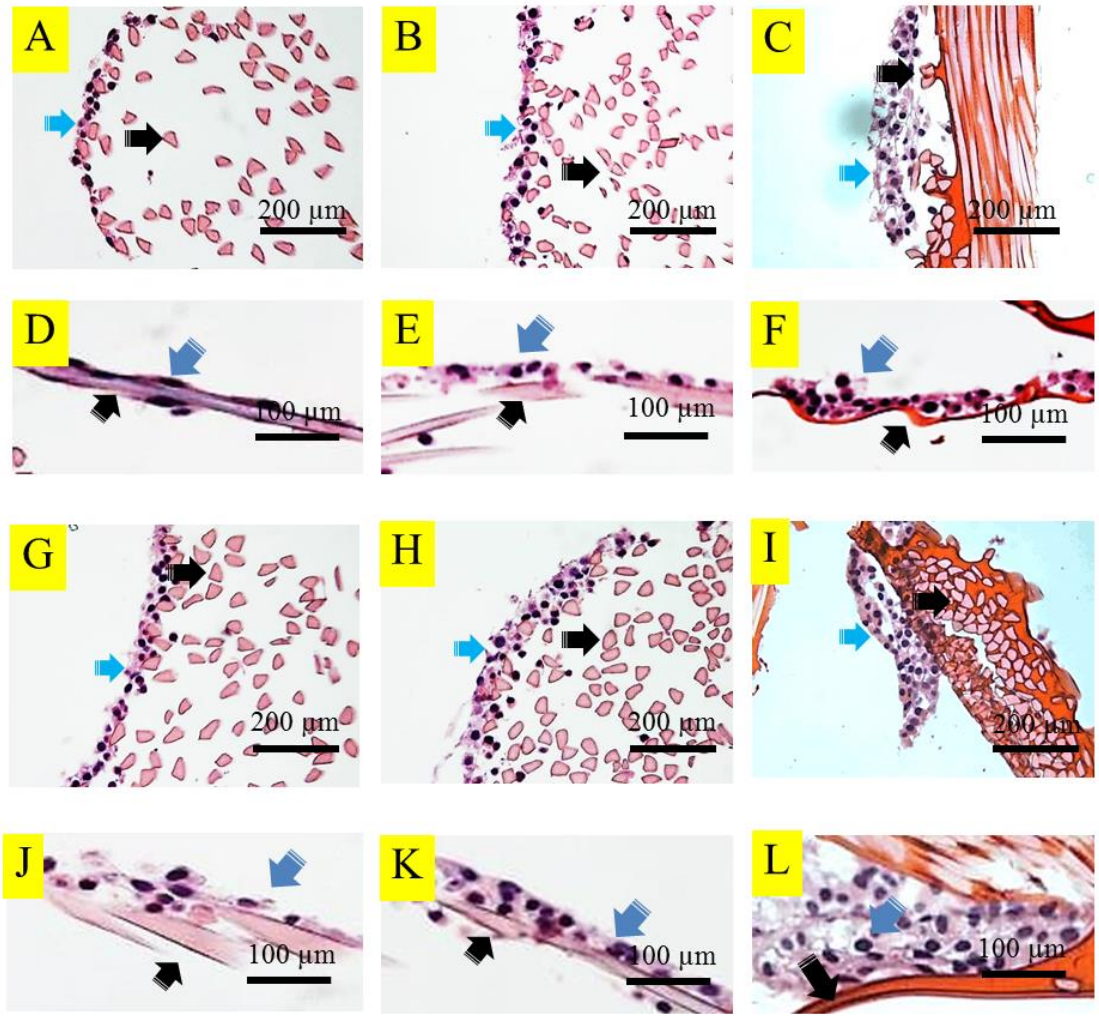

Figure 20. Cell morphology on the silk fabric scaffold on day 3 and 5 by H&E staining. Blue arrow; Fibroblast, Black arrow; Scaffold

Masson trichrome staining was used to evaluate the deposited collagen which was systhesized by fibroblast on the silk fabric in all groups [26]. The silk fabric in all groups was performed on day 14 and 28.

On day 14, it was clear that SF-GT revealed more collagen deposition than the others. SF-CS had non-collagen deposition on the surface. Notably, cells expressed distribution on the whole surface of SF and SF-GT. On the other hand, SF-CS had the clusters of cell aggregation on the surface.

On day 28, SF-GT clearly showed the collagen deposition on he surface of silk woven fabric. The fiber bundles were adhered with collagen deposition. Furthemore, collagen could diffuse and deposite in the free space of fiber bundles. SF had the collagen matrix nodule which was adhered and spread on the fiber bundles. A few of collagen deposition was found in SF-CS.

Interestingly, the SF-GT induced the collagen deposition which synthesized from fibroblasts. The studies reported that gelatin could stimulate the collagen deposition from fibroblast cell by the RGD sequence and promoted the wound healing during mucosa tissue regeneration [27].

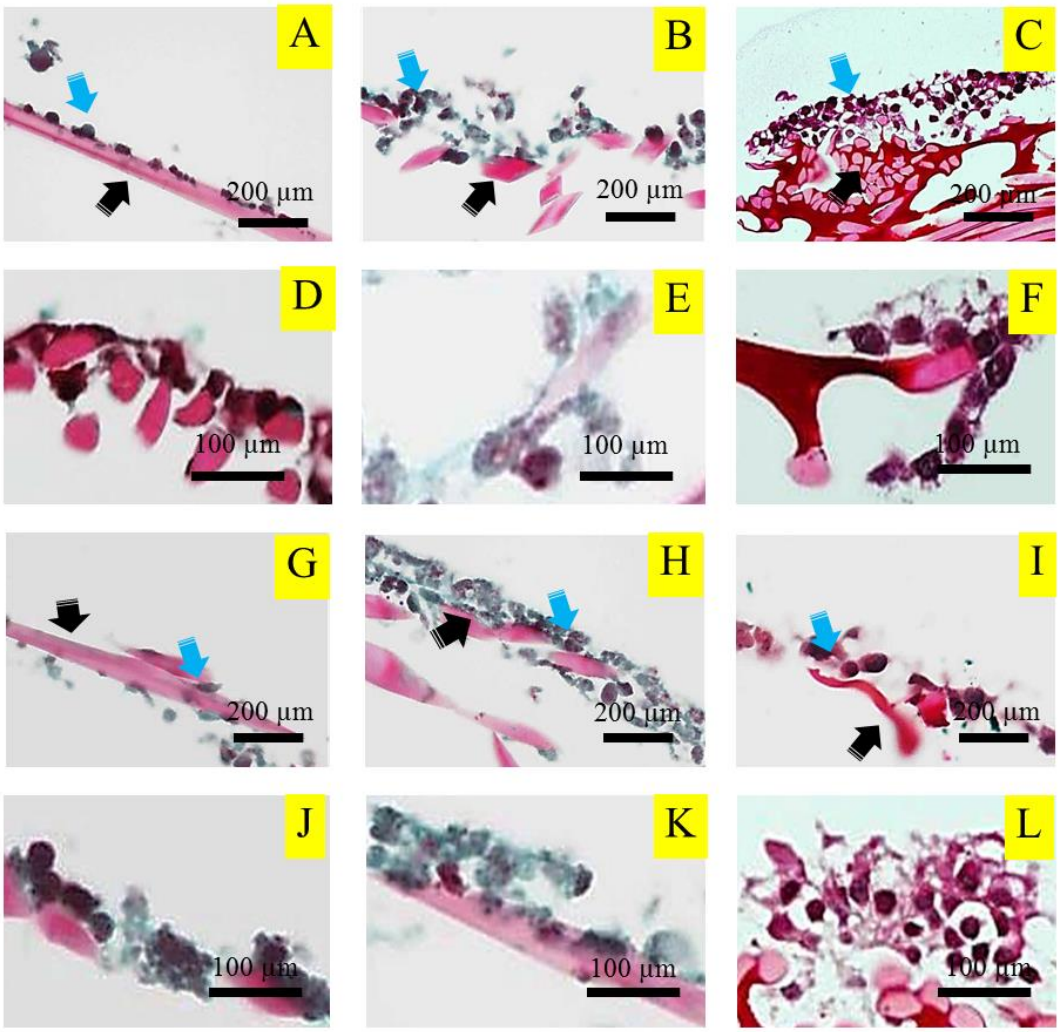

Figure 21. Masson trichrome staining on day 14 and 28 for collagen deposited detecting. The silk fibroin fabric on day 14 (A-B), silk fibroin fabric on day 28 (C-D), silk coated gelatin fabric on day 14 (E-F), silk coated gelatin fabric on day 28 (G-H), silk coated chitosan fabric on day 14 (I-J), silk coated chitosan fabric on day 28 (K-L). The black arrow indicated the silk fibroin fiber, red arrow indicated the L929, the yellow star indicated the collagen matrix.

Biological performance of the coating layer

To observe the cell proliferation of keratinocyte on coating layer was evaluated on day 1, 3, 5 and 7. On day 1, the SF-GT showed more cell proliferation than other groups. On the other hand, SF-CS showed least cell proliferation. The

highest cell proliferation was clearly found on day 5. Especially, SF-GT had higher cell proliferation than others. The report demonstrated that RGD sequences signal in gelatin promoted cell proliferation and attachment of keratinocyte [28]. The results indicated that the gelatin coating layer had the suitable biological performance for mucosa tissue regeneration particularly in keratinocyte layer.

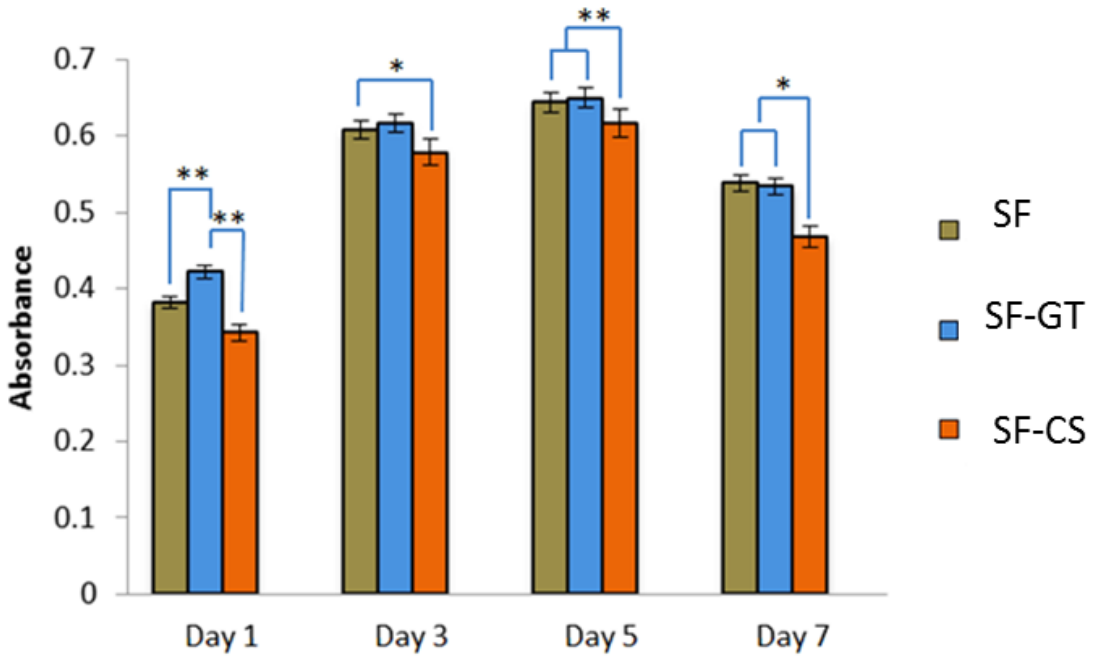

Figure 22. Showed keratinocyte cell proliferation in the silk fibroin fabric on day 1, 3, 5 and 7.

To observe the cell morphology on the silk fabric in all groups, the FDA staining was used on day 1, 3 and 5. The SF and SF-GT clearly showed more cell attachment on the surface than SF-CS for all time points. SF and SF-GT showed the cell migration which covered the whole surface on day 3 and 5. This indicated that the non-coating and gelatin coating showed functionality to induce cell adhesion. This come from RGD sequences which cell could recognize [29]. On the other hand, SF-CS had the cell migration which covered some area on surface for all time points. This might come from the poor cell adhesion on chitosan coating layer that lead to spherical formation of cell organization [30].

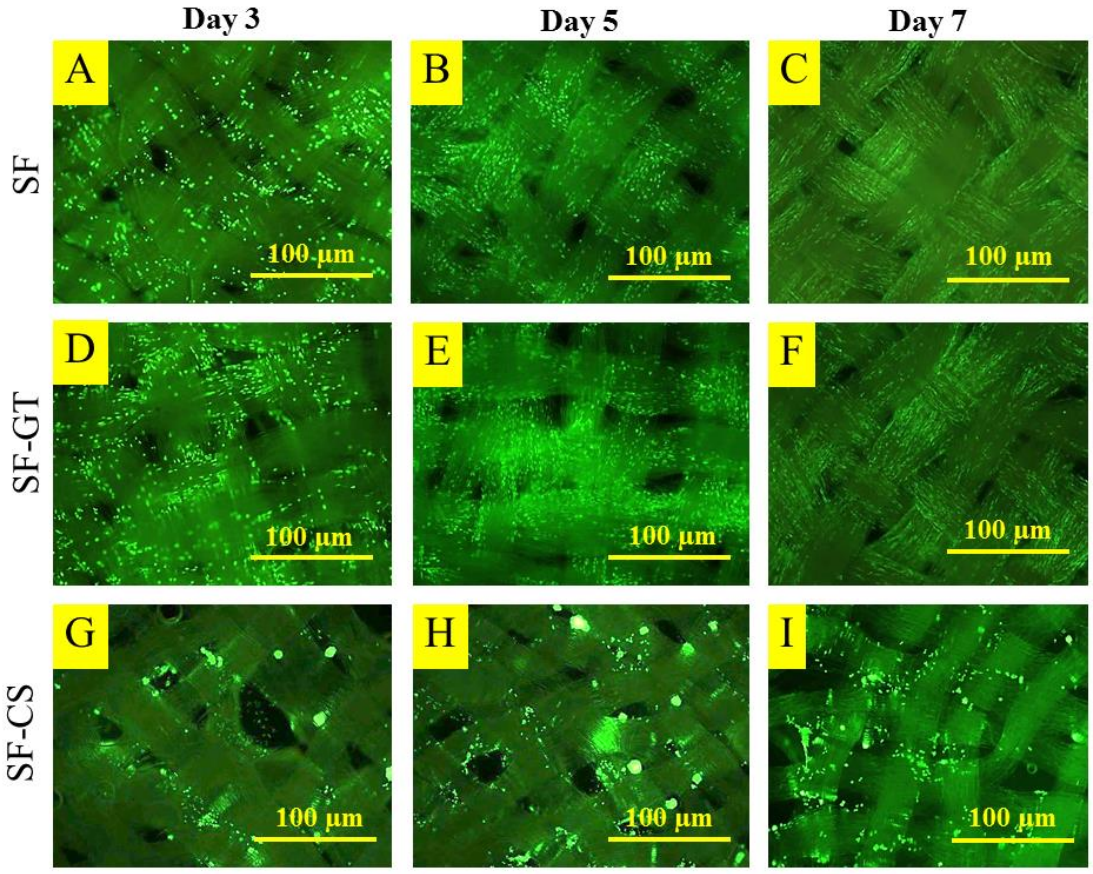

Figure 23. Keratinocyte cell viability staining with FDA on the silk fibroin fabric (A); Coated silk fibroin fabric with gelatin (B); silk fibroin coated chitosan fabric (C); at day 3, 5 and 7.

The morphology of keratinocyte on coating layer was observed at day 3 and 7. The result showed that the SF, SF-GT, and SF-CS supported the cell adhesion and migration. On day 7, SF-GT had more cell attachment than SF and SF-CS. The cell morphology of the keratinocyte showed the spherical pattern when compared with fibroblast cell. Especially, SF-GT showed more cell aggregation than the others. The results indicated that SF-GT showed suitable performance to enhance mucosa tissue regeneration particularly in keratinocyte layer.

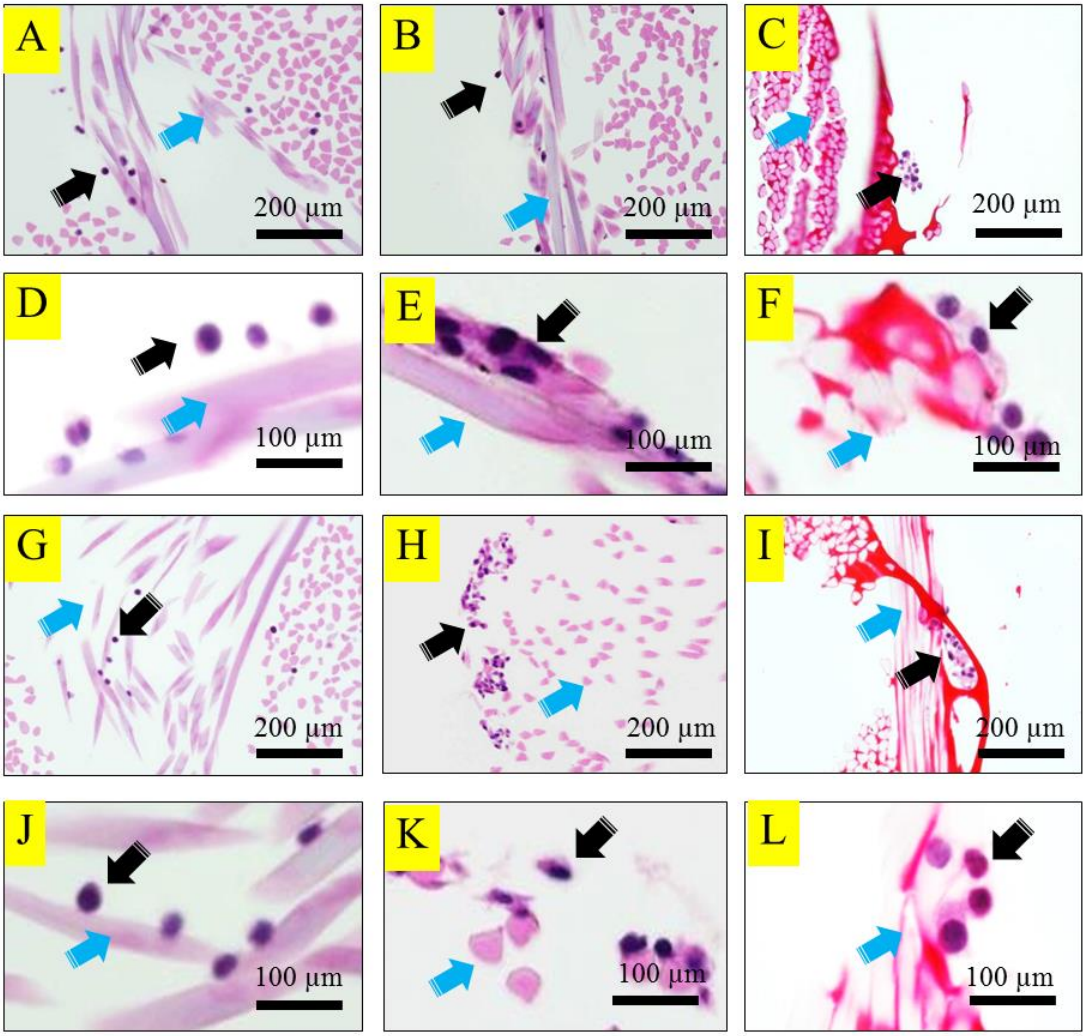

Figure 24. Cell morphology on the silk fabric scaffold on day 3 and 7 by H&E staining. Non coated silk fibroin fabric (Row A) ; silk fibroin coated gelatin fabric (Row B) ; silk fibroin coated chitosan fabric (Row C). The black arrow indicated the L929 fibroblast cell, red arrow indicated the silk fibroin fiber and green arrow indicated the chitosan.

Conclusion

In this research, mimicked anatomical biphasic scaffolds were fabricated with coated silk woven fabric with gelatin and chitosan. The morphology of those scaffolds was devided into two phases; silk woven fabric and coating layer. The silk woven fabric layer showed the covered fiber bundle with gelatin and chitosan. The coating layer which covered the whole surface of fabric had the cue pattern of fiber

bundles. The coated silk fabrics had crystal structure from silk fibroin and amorphous structure from gelatin and chitosan. The coating layer of gelatin showed high stable water structure. The physical performance demonstrated that coated silk woven fabric with gelatin showed suitable swelling behavior and biodegradtion for using as scaffold for construct mucosa tissue. The biological performance of coated silk woven scaffold showed the cell proliferation, viability, morphology which is suitable to construct mucosa tissue. Finally, this research demonstrated that mimicked anatomical biphasic scaffolds based on silk woven fabric/gelatin was promising for construction of mucosa tissue in maxillofacial surgery.

Reference

[1] Florence C, Christine J. Chitosan-based biomaterials for tissue engineering, European Polymer Journal 2013;49:780–792.

[2] Jayakumar R, Prabaharan M, Sudheesh K, Nair SV, Tamura H. Biomaterials based on chitin and chitosan in wound dressing applications, Biotechnology Advances 2011;29:322-327.

[3] Ricardo MP. da Silva PM. Lopez-Perez, Carlos E, Joao FM, Julio SR, Rui LR, Poly(N-Isopropylacrylamide) Surface-Grafted Chitosan Membranes as a New Substrate for Cell Sheet Engineering and Manipulation, Biotechnol. Bioeng 2008;101:1321–1331.

[4] Rana I, Mohammad R, Shahriar HM, Maryam K, Mohsen R. Synthesis and Characterization of Biodegradable Hemostat Gelatin Sponge for Surgery Application, Iranian Journal of Pharmaceutical Sciences. 2008;4:193-200.

[5] Chu HH, Szu KC, Wei YC, Min LT, Rong HC. Effect of the Characters of Chitosans Used and Regeneration Conditions on the Yield and Physicochemical Characteristics of Regenerated Products, International Journal of Molecular Sciences 2015;16:8621-8634.

[6] Nicholas G, Annie B, Bernardo PR, David LK, Lyophilized silk fibroin hydrogels for the sustained local delivery of therapeutic monoclonal antibodies, Biomaterials 2011;32: 2642-2650.

[7] Susan M, Manitha BN, Nisha S, Sreenivasan K, Mariamma J, Annie J. Adult Stem Cells on Methacrylic Acid Grafted Cocoon Silky Fibrous Scaffolds, Trends Biomater. Artif. Organs, 2010;23:137-144.

[8] Parada U, Supatcharin P, Rawee T, Prevalence and Adhesion Properties of Oral Bifidobacterium species in Caries-active and Caries-free Thai Children, Walailak J Sci & 2017;14:645-653.

[9] John AM, Diane GK, Thomas JB. Role of Fibronectin in Collagen Deposition : Fab' to the Gelatin-binding Domain of Fibronectin Inhibits Both Fibronectin and Collagen Organization in Fibroblast Extracellular Matrix, Cell Biology 1982;92:485-492.

[10] Kasoju N, Kubies D, Kumorek MM, Krız J, Fabryova E, Machova L, Kovarova J, Rypacek F. Dip TIPS as a facile and versatile method for fabrication of polymer

foams with controlled shape size and pore architecture for bioengineering applications, PLoS ONE. 2014;9:1–16.

[11] Farokhi M, Mottaghitalab M, Hadjati J, Omidvar R, Majidi M. Amanzadeh A, Azami, S.M. Tavangar, M.A. Shokrgozar, J. Ai, Structural and functional changes of silk fibroin scaffold due to hydrolytic degradation, J. APPL. POLYM. SCI. 2013;131:1–8.

[12] Tao J, Zhen Z, Yi Z, Yi L, Zhejun W, Hua T, Xinyu S, Yining W. Surface Functionalization of Titanium with Chitosan/Gelatin via Electrophoretic Deposition: Characterization and Cell Behavior. Biomacromolecules 2010;11:1254–1260.

[13] Fang W, Nathan W, Eva-Marie R, Trinh V, Xiao H. Comparative studies of regenerated water-based Mori, Thai, Eri, Muga and Tussah silk fibroin films, J Therm Anal Calorim 2015;122:1069–1076.

[14] Antonella M, Luca F, Claudio M. Regenerated Silk Fibroin Films: Thermal and DynamicMechanical Analysis, Macromol. Chem. Phys 2002;203:1658–1665.

[15] Aparna S, Sundararajan VM. Characterization of chitosan–polycaprolactone blends for tissue engineering applications, Biomaterials 2005;26:5500–5508.

[16] Sajjad H, Soo-YP, Shin HL. Preparation, swelling and electro-mechano-chemical behaviors of a gelatin–chitosan blend membrane. Soft Matter 2008;4:485-492.

[17] Swati G, Pratibha PK, Richa G. Mucosal Substitutes for Periodontal Soft Tissue Regeneration. Dentistr 2015;5:1-6.

[18] Jiarong L, Jeremy JM, Lili C. Epithelial–Mesenchymal Interactions as a Working Concept for Oral Mucosa Regeneration. Tissue Engineering: Part B 2011;17:25-31.

[19] Fergal JO, Biomaterials & scaffolds for tissue engineering, Materialstoday 2011;14:88-95.

[20] Steven Bo, Abby C, Kirk J. Hippensteel, Alysha Kishan ,Christopher Gilchrist, N. William Garrigues, David S. Ruch, Farshid Guilak, Dianne Little. Aligned multilayered electrospun scaffolds for rotator cuff tendon tissue engineering. Acta Biomaterialia 2015;24:117–126.

[21] Chiara M, Lorenza D, MariaCristina T, Silvia F. Electrospun silk fibroin–gelatin composite tubular matrices as scaffolds for small diameter blood vessel

regeneration, Journal of Materials Science 2017:28:doi:10.1007/s10856-017-5884-9.

[22] Jingjing L, Ling C, Yabin Z, Lei H, Yuxin L. Promoting Epithelium Regeneration for Esophageal Tissue Engineering through Basement Membrane Reconstitution, ACS Applied Materials & Interfaces 2014;6:4954-4964.

[23] Juthamas R, Siriporn D, Neeracha S, Tanom B, Sorada K. Comparison of Gelatin and Collagen Scaffolds for Fibroblast Cell Culture, Journal of Metals, Materials and Minerals 2006;16:31-36.

[24] Hiromi Y, Yumiko I, Yoko T, Hitoshi S, Kozo T. Identification of fibroin-derived peptides enhancing the proliferation of cultured human skin fibroblasts, Biomaterials 2004;25:467–472.

[25] Alessandro EC, Maurizio S, Andrea C, Domenico D, Francesca S, Serenella A, Massimo M, Saverio B. Cell detachment and apoptosis induction of immortalized human prostate epithelial cells are associated with early accumulation of a 45 kDa nuclear isoform of clusterin, Biochem. J. 2004;28:157–168.

[26] SHI J, DONG N, SUN Z. Immobilization of RGD Peptides onto Decellularized Valve Scaffolds to Promote Cell Adhesion, Journal of Wuhan University of Technology-Mater. Sci. Ed, 2007;22:686-690.

[27] Yu Q, Hui W, Kai W, Ya Y, Ru-YZ, Ick SK, Ke-Qin Z. A Review of Structure Construction of Silk Fibroin Biomaterials from Single Structures to Multi-Level Structures, Int. J. Mol. Sci 2017;18; doi:10.3390/ijms18030237.

[28] Tian Z, Nanping W, Yang X, Tingting D, Xin L, Xiumei M, Jiao S. Electrospun tilapia collagen nanofibers accelerating wound healing via inducing keratinocytes proliferation and differentiation, Colloids and Surfaces B: Biointerfaces. 2016;143:415–422.

[29] Amit KJ, Rohit VD, Sandipto G, Pradip C, Harishankar N, Vivek PS, Geeta RV, Jayesh RB. Bone Healing Evaluation of Nanofibrous Composite Scaffolds in Rat Calvarial Defects: A Comparative Study, J Biomed Nanotechnol 2013;9:2073-2085.

[30] Nitar N, Tetsuya F, Hiroshi T. The Mechanical and Biological Properties of Chitosan Scaffolds for Tissue Regeneration Templates Are Significantly Enhanced by Chitosan from Gongronella butleri. Materials, 2009;2:374-398.

CHAPTER 4

Mimicked pathogenic porous scaffolds based on silk fibroin/gelatin to design ex vivo biomaterials for biomineralization in osteoporosis; morphological formation, physical and biological performance

Abstract

Osteoporosis is a degenerative, tissue disease, which is risky for severely broken bones, leading to the suffering of many patients. In this research, mimicked pathgenic porous scaffolds based on; silk fibroin/gelatin, were designed to evaluate biomineralization in osteoporosis. Silk fibroin (SF) /gelatin (GT) was mixed into solution with different ratios; SF(100:0), (70:30), (50:50), (30:70), and GT(0:100), before being fabricated into porous scaffolds. Then, these scaffolds were observed for morphology, before being analyzed as too pore size and distribution. The physical performance of these scaffolds was tested against biodegradation, and for swelling behavior. The scaffolds were cultured with MG-63 osteoblast cell. Biological performance was tested with cell proliferation, alkaline phosphatase (ALP) activity, calcium contents, calcium deposition and histology. The results demonstrated that; silk fibroin/gelatin of SF/GT(50:50) showed heterogeneous morphology of main porous, incorporated with its network structure. SF/GT (50:50) had suitable physical and biological performance, which could be related to irregular bone remodeling. Finally, the results indicated that SF/GT(50:50) is promising as ex-vivo biomaterials for evaluation of pathogenic structure in osteoporosis.

Materials and methods

Silk fibroin preparation

The silk cocoons were cut into small pieces, and the 0.02 M Na2CO3 was used for sericin removal by boiling at 70 °C, 2 times. After which , the silk fibroin was rinsed with dH2O, until the siricin glue unbound from the silk fibroin fiber. The silk fibroin was kept in a hot air oven for water evaporation. The 9.3 M LiBr was then used in the dissolving process under 70 °C for 4hrs. The LiBr was discharged by this dialysis method, and the silk fibroin solution was prepared at a yield of 3% [1]. To remove the precipitate in the silk fibroin solution, the silk fibroin solution was centrifuged for 20mins at 9000RPM, and the silk fibroin was kept at 4 °C until ready for use. [2]

Gelatin preparation

The gelatin powder was dissolved with dH2O at 50 °C for 30mins, with continues stirring. Then, the gelatin solution was placed at room temperature before being used [3]

Silk fibroin/gelatin scaffold fabrication

Both the silk fibroin and gelatin solution were prepared at 3%, and the ratio of gelatin was designed in; 100, 70, 50, 30 and 0% in silk solution. The mixture of silk fibroin and gelatin was combined by continuous stirring for 5mins. After this, the mixture was poured into 48 well plates. A freeze drying machine was used for 3D, porous scaffold fabrication.

Groups	Details
SF	Silk fibroin porous scaffold
SF/GT (70:30)	Silk fibroin/gelatin porous with ratio of 70:30
SF/GT (50:50)	Silk fibroin/gelatin porous with ratio of 50:50
SF/GT (30:70)	Silk fibroin/gelatin porous with ratio of 30:70
GT	Gelatin porous scaffold

Table 3 The experimental group of silk fibroin/gelatin scaffold

Scanning Electron Microscopy (SEM) Observation

Morphology of the scaffold was observed by Scanning Electron Microscopy (Quanta400, FEI, Czech Republic). A gold, sputter coating machine (SPI Supplies, Division of STRUCTURE PROBE Inc., Westchester, PA, USA) was used for scaffold coating, before investigation by SEM.

Pore size diameter and distribution of scaffold

The SEM image was selected for pore size analysis. ImageJ was used for pore size measurement with randomly area selection (n=25) [4]. The obtained data was calculated and plotted by Qtiplot program.

Swelling testing

The scaffold in all groups was soaked in the PBS at 37 ° C at 30, 60 and 90mins for swelling evaluation. The weight of the scaffolds, before and after,

soaking were used for the swelling calculation following this equation: (Ws –Wd)/Wd ×100, whereas Ws and Wd are the weights of the swollen scaffolds as well as the dry scaffolds, respectively [5].

Degradation

Enzyme was used for the degradation properties of the scaffolds. In that 4mg of Lysozyme powder was dissolved in a ratio of 1ml of PBS (pH=7.4). This, 1ml of lysozyme, was added into each scaffold and incubated at 37 ° C for days 7, 14 and 21, with the lysozyme solution being changed every 3 days of the experiment [6]. The original weight along with the weight remaining on the scaffolds, after degradation, was used for calculation as the percentage of degradation.

Cell culture

MG-63 osteoblast cell was used for biocompatibility of the scaffolds. The passage 4 to 8 of MG-63 osteoblast cells was seeded on the scaffold at a density of around 1×106. The complete alpha-MEM medium (α-MEM, GibcoTM, Invitrogen, Carlsbad, CA) medium included 10% fetal bovine serum, 1% penicillin/streptomycin and 0.1% fungizone. The MG-63 osteoblast cell was maintained in a 5% CO2, 95% air-humidified at 37°C incubation [7]. During, differentiation staging, the MG-63 osteoblast cells were cultured in an osteogenic supplements (OS) medium (OS; 20mM b-glycerophosphate, 50μM ascorbic acid, and 100nM dexamethasone; Sigma-Aldrich) [8].

Cell proliferation

After, osteoblast cell seeding, at days 1, 3, 5 and 7, the cell proliferation rate was evaluated by WST-1 (Roche Diagnostics, Germany). The media were removed and rinses with PBS 2 times following the addition of 10% WST-1 reagent in complete media. Then the scaffolds were incubated for 1hr, and the 200μl of the solution was drained for measurement at 450nm, with the media used as blank.

Alkaline phosphatase activity

The osteoblast cells in the scaffolds were cultured in the OS media condition on days 7, 14 and 21, following the cell lysis method for ALP detection. The 800µl of lysis solution, including 1% TritonX in PBS, was added into the scaffold. The scaffold was then kept at -70 ° C for 1hr, and left at room temperature for 1hr for 3 cycles. The scaffold was crushed and removed to an Eppendorf tube. 12000RPM has used for supernatant, separation from the pellet. The supernatant was used for ALP detection, following the manufacture's instruction (Abcam®, Cambridge, UK) [9].

Calcium contents

The lysis solution of cells, in the scaffolds, at days 7,14 and 21 was used for calcium calcification value by; calcium colorimetric assay (Calcium Colorimetric Assay Kit, BioVision Inc., Milpitas, CA). 30µl of supernatant was added into 96 well plates, and adjusted to a volume of 50µl with dH2O. Upon which, 60µl of the Calcium Assay Buffer and 90µl of a chromogenic reagent were mixed in each well. These were then incubated for 10mins for reaction and measured at a wavelength of 575nm.

Alizarin red staining

The calcium nodule from the osteoblast synthesis activity was examed with alizarin red staining. The MG-63 osteoblast cell was cultured in the osteogenic supplements (OS) medium at days 7 and 14, for calcium detection. The scaffold was rinsed with PBS, then the 2% alizarin red (SigmaAldrich, USA) solution was dropped on the scaffold for 10mins, and washed with tap water. The calcium deposition was observed under a microscope [10].

Histological observing

After, cell culture at days 3 and 7, the scaffolds in all groups were stained with hematoxylin and eosin for detection of both cell attachment and migration.

The scaffold was fixed by 4% formaldehyde at 4 ° C for 24hrs and followed by immersion in paraffin. The paraffin sample was cut into 5μm and placed on a glass slide. Next, the slide was deparaffin in dH2O after which it was continually stained with hematoxylin and eosin.

Results

The morphological structure of scaffolds

After fabrication, the scaffolds showed a white color, which contained a non-difference for their appearance (Figure. 22). Such an appearance showed the sponge, having a rough surface for all samples. The morphology structure of the scaffold was observed by SEM (Figure.23), and the silk fibroin scaffold revealed the connective porous as well as a smooth surface. SF/GT(70:30) and (50:50) showed hierarchical porous structure, which contained the network structure in its main pores (Figure. 23E, F, K, and I). SF/GT (30:70) and GT showed a smaller, more regular shape than the others. Especially, gelatin, which had the smallest pores.

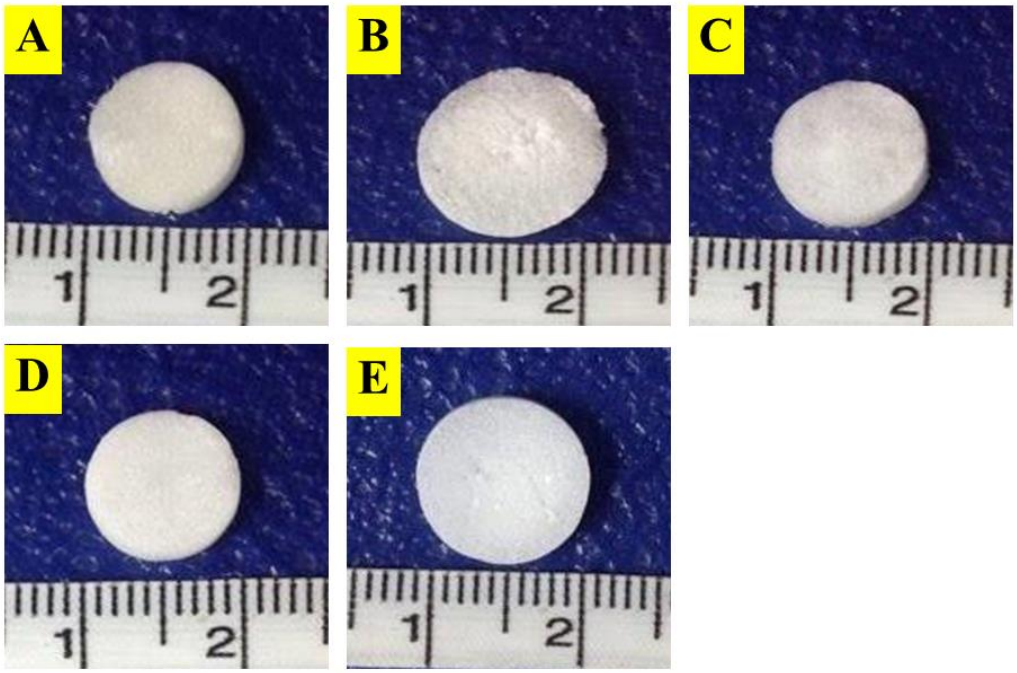

Figure 25. Silk fibroin and gelatin scaffold: (A) SF, (B) SF/GT(70:30), (C) SF/GT(50:50), (D) SF/GT(30:70) , and (E) GT.

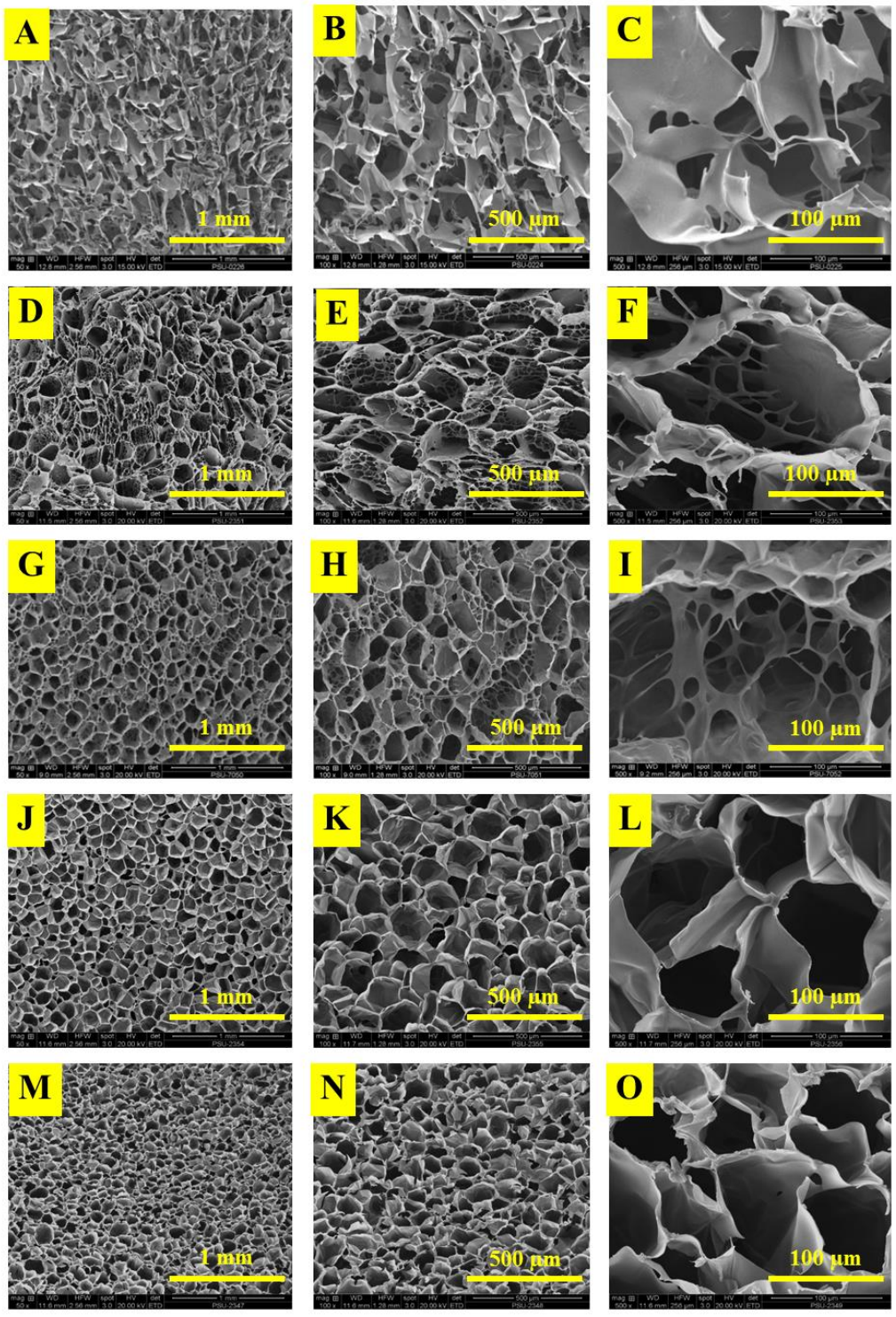

Figure 26. Morphology of SF (A,B,C), SF/GT(70:30), (D,E,F), SF/GT(50:50) (G,H,I), SF/GT(30:70)(K,K,L), and GT (M,N,O).

Pore size diameter and distribution of scaffold

In this research, the mean pore size coupled with pore size distribution was measured and analyzed (Figure. 24). The results showed the mean pore size of silk fibroin/gelatin; SF, SF-GT (70:30), SF-GT(50:50), SF-GT(30:70), and GT is 85.57±10.34, 107.35±27.56, 86.05±15.00, 99.38±15.00 and 80.74±12.35 μm, respectively. For the distribution range of pore sizes, SF, SF-GT(70:30), SF-GT(50:50), SF-GT(30:70), and GT showed 50-120, 30-180, 30-140, 30-170 and 30-130 μm, respectively. The results demonstrated that SF-GT(70:30) showed the largest, mean pore size. Furthermore, the pore size distribution of silk fibroin/gelatin (70:30) is around 30 to 180μm. This is broader than the others. GT had the smallest mean pore size, with the narrowest distribution of pore size being SF, which showed around 50 to 120μm.

Notably, the network structure in the main pore of SF-GT (70:30) and (50:50) had a mean pore size of 44.18±5.67 and 61.20±10.11 μm, respectively (Figure.25). For pore size distribution of network structures, SF-GT (70:30) and (50:50) showed 20-64 and 28-88μm, respectively. SF-GT (70:30) had a larger, mean pore size of network structure than (50:50). Furthermore, pore size distribution of SF-GT (70:30) was broader than (50:50).

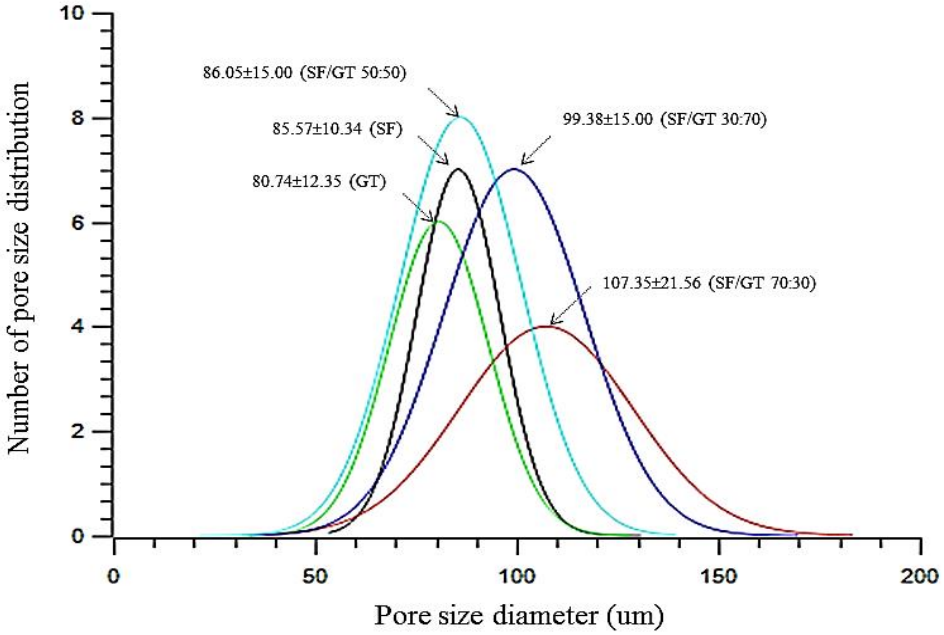

Figure 27. The pore size diameter along with distribution percentage of scaffold in all groups. (A); SF, (B); (70:30), (C); (50:50), (D); (30:70) and GT. The results are displayed as means ± standard deviation (n=50)

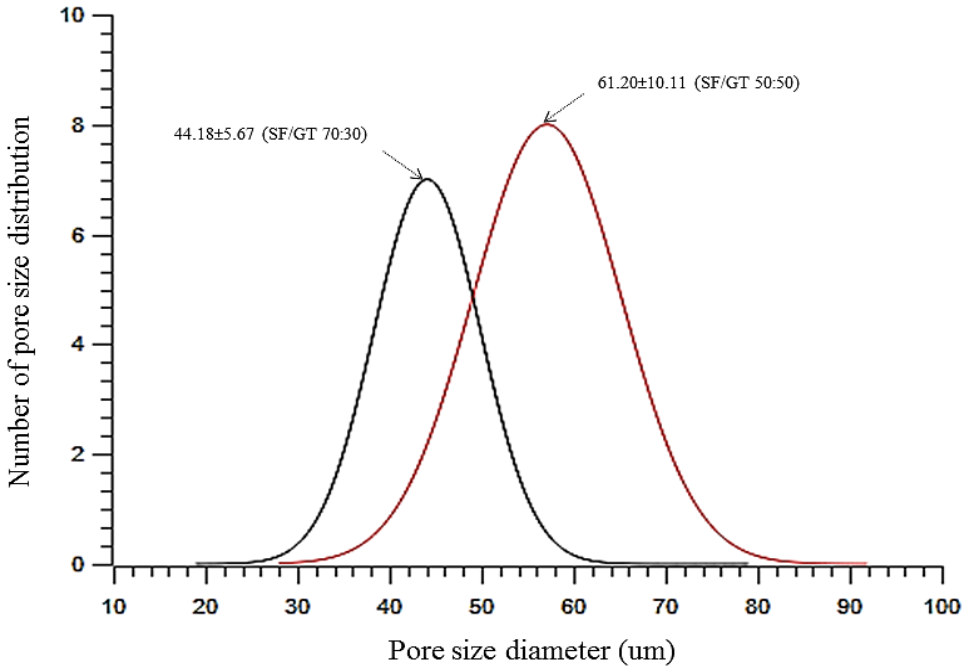

Figure 28. The interconnect pore size as well as distribution of scaffold in SF/GT (70:30) and SF/GT (50:50). The results are displayed as means ± standard deviation (n=50)

Swelling behavior

To determine the gelatin behavior on the swelling property in the scaffold, the scaffold was soaked in PBS at different time points, and the weight of the scaffold, before and after, was calculated (Figure. 26). When the ratio of gelatin increased it effected as to a higher swelling degree. At 30 and 90 mins, SF/GT (30:70) showed a higher swelling percentage than SF/GT (50:50), silk fibroin/gelatin scaffold (70:30) and silk fibroin scaffold, respectively. Except at 60mins, when the silk fibroin/gelatin scaffold (70:30) was higher than the silk fibroin/gelatin scaffold (50:50) at 60mins.

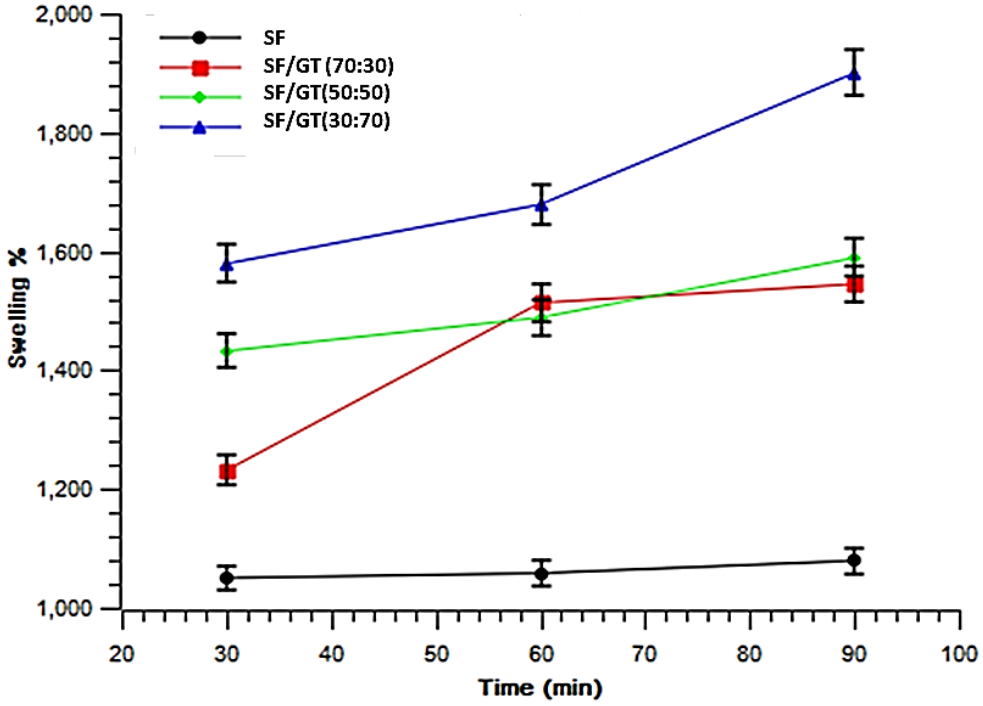

Figure 29. Swelling behavior of scaffolds SF, SF/GT(70:30), SF/GT(50:50), SF/GT(30:70), GT. The results are displayed as means ± standard deviation (n=5)

Degradation of scaffold

The degradation of the scaffold was evaluated by use of Lysozyme enzyme at days 7, 14 and 21(Figure. 27). The increase of the degradation rate was

found at all time points, for all groups. The highest degradation was shown in the group of SF/GT (30:70). Otherwise, the silk fibroin scaffold reviewed a low percentage of degradation, when compared with other groups. When the ratio of gelatin increased it effected the degradation ability of the scaffold. In the group of SF/GT (50:50) there was less degradation than SF/GT (30:70), because of the low ratio of the gelatin. The gelatin rapidly dissolved at temperatures higher than 37 ° C. The morphology and shape of the scaffold was clearly changed in the groups of SF/GT (30:70). The SF/GT (30:70) was digested mostly by the Lysozyme. On day 7, all groups of scaffold had stability in shape, with the exception of the group SF/GT (30:70). The SF/GT (30:70), became lose in shape and holes were found on the surface. This slight degrade was found in the SF/GT (50:50), in the central of the scaffold, which indicated the degradation lesion on day 14. On day 21, good stability was found in both the groups of SF and SF/GT (70:30).

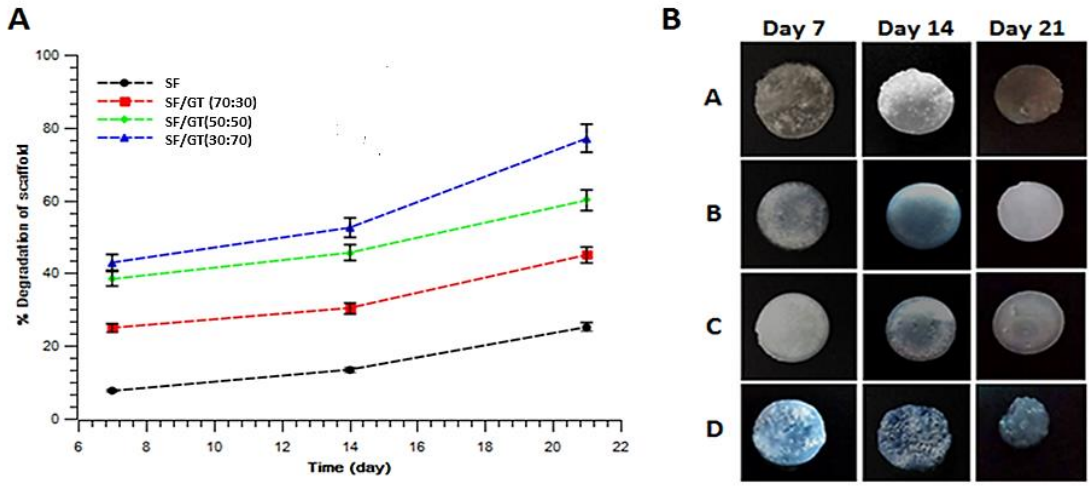

Figure 30. The degradation of scaffolds with lysozyme at days 7, 14 and 21. (A) The degradation of scaffolds in all groups, (B) The morphology of scaffold, after degradation (A) SF, (B) SF/GT (70:30), (C) SF/GT (50:50), (D) SF/GT (30:70). The results are displayed as means ± standard deviation (n=5).

Cell proliferation in scaffolds

The MG-63 osteoblast cell was used to evaluate the biofunctional of scaffolds, in all groups, and the cell proliferation was performed with WST-1 assay on days 1, 3, 5 and 7 (Figure. 28). The trend of the cell proliferation graph expressed the increasing of cell numbers from; day 1 to day 7. On day 1, SF-GT (70:30), (50:50) and (30:70) revealed a significantly higher performance than that of SF and GT. SF revealed higher cell proliferation than GT. On day 3, GT was crumbled in the culture media, because of the temperature being 37 $^{\circ}$C, and the data is therefore not shown on days 3, 5 and 7. The silk fibroin scaffold, that was modified with gelatin, revealed excellent properties in the part of promoting cell proliferation in all ratios. On day 5, SF revealed similar results, with the SF-GT (50:50) and (70:30). SF-GT (30:70) showing higher cell proliferation than other groups, and was significantly different with SF and SF-GT (50:50). On day 7, the SF-GT (50:50) was decreased. In the group of silk fibroin, combined with gelatin, all groups improved their cell proliferation when compared with the silk fibroin scaffold alone.

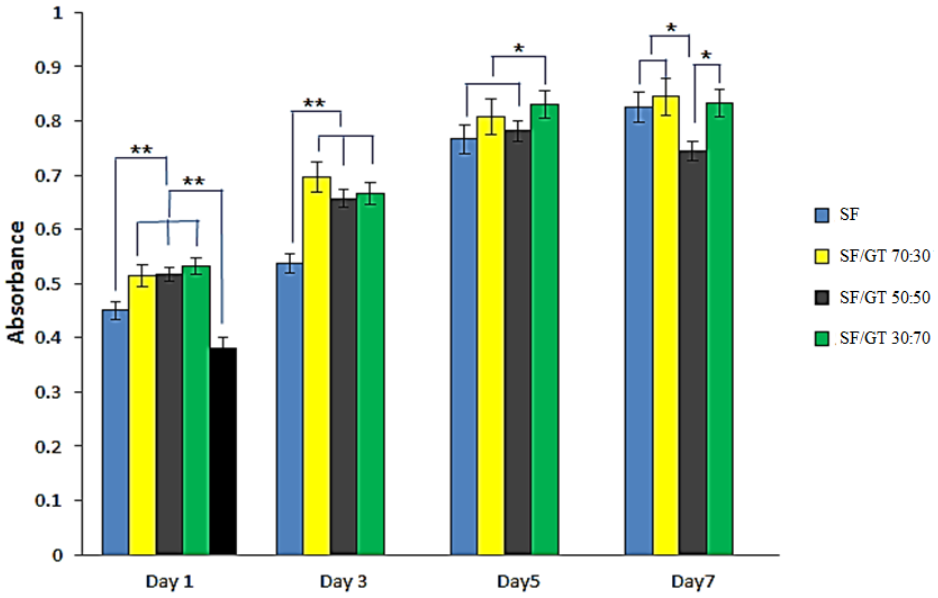

Figure 31. Cell proliferation of osteoblast cell in the scaffold of each group at days 1, 3, 5 and 7. The results are displayed as means ± standard deviation (n=5)

Alkaline Phosphatase (ALP) activity of osteoblasts

The alkaline phosphatase activity was observed at days 7, 14 and 21, during culture in the OS media (Figure. 29). On day 7, the scaffolds in all groups revealed a nonsignificant difference. The SF/GT (50:50) and SF/GT (30:70) were higher in alkaline phosphatase synthesis than SF/GT (70:30) and the SF scaffold and the SF/GT (70:30) was higher than the SF scaffold. Interestingly, both SF and SF/GT increased from day 14, and showed a higher alkaline phosphatase content than that of SF/GT (50:50), (30:70) and (50:50) was also higher than the SF / GT (30:70) on day 21.

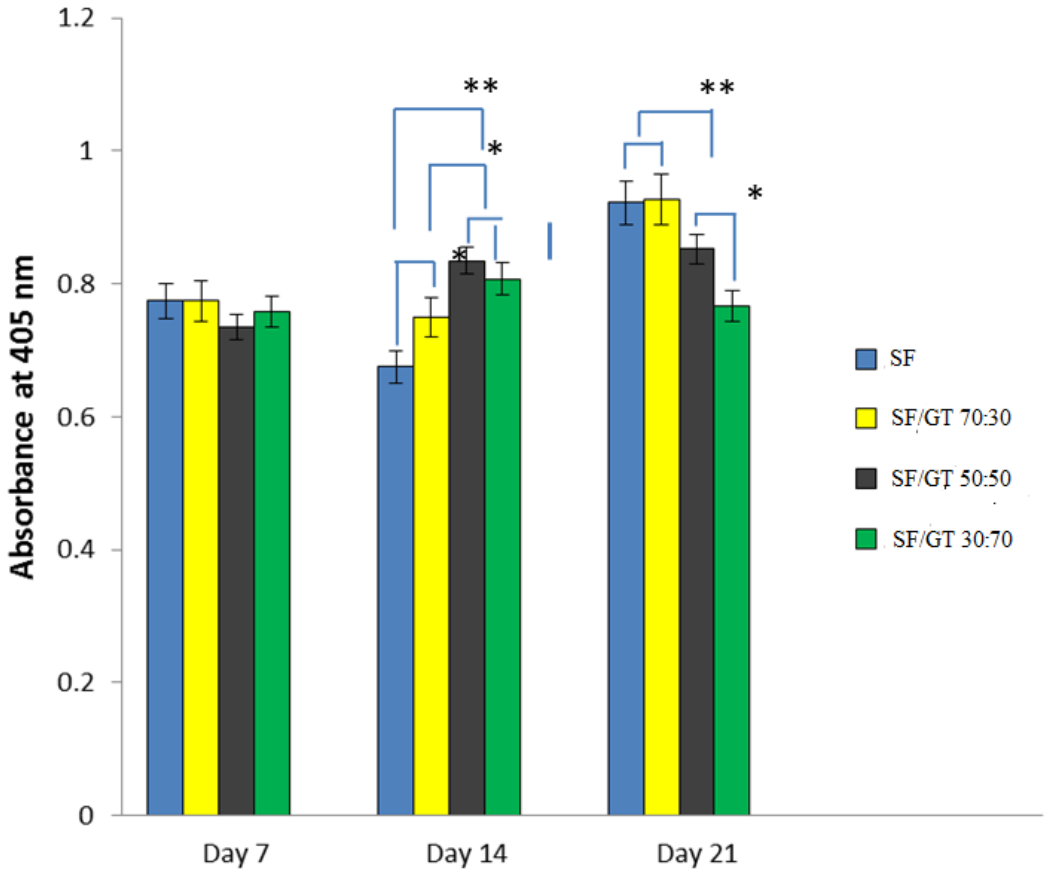

Figure 32. Alkaline phosphatase activity, from osteoblast cell in the scaffold in each group at days 7, 14, and 21. The results are displayed as means ± standard deviation (n=5)

The calcium synthesis from osteoblast was observed a on days 7, 14 and 21, and the calcium content increased when the time increased . (Figure. 30). The SF/GT (70:30) indicated clearly, higher than that of the other groups, especially SF/GT (50:50) and (30:70) on day 7. The SF scaffold rapidly increased from day 7 to day 14, whilst both SF and SF/GT (70:30) were still higher than SF/GT (50:50) and (30:70). The SF/GT (50:50) indicated a higher, calcium synthesis than SF/GT (30:70). On day 21, all groups decreased, with the exception of the group SF/GT (50:50). However, the SF/GT (70:30) remained excellent on calcium synthesis when compared to the other groups.

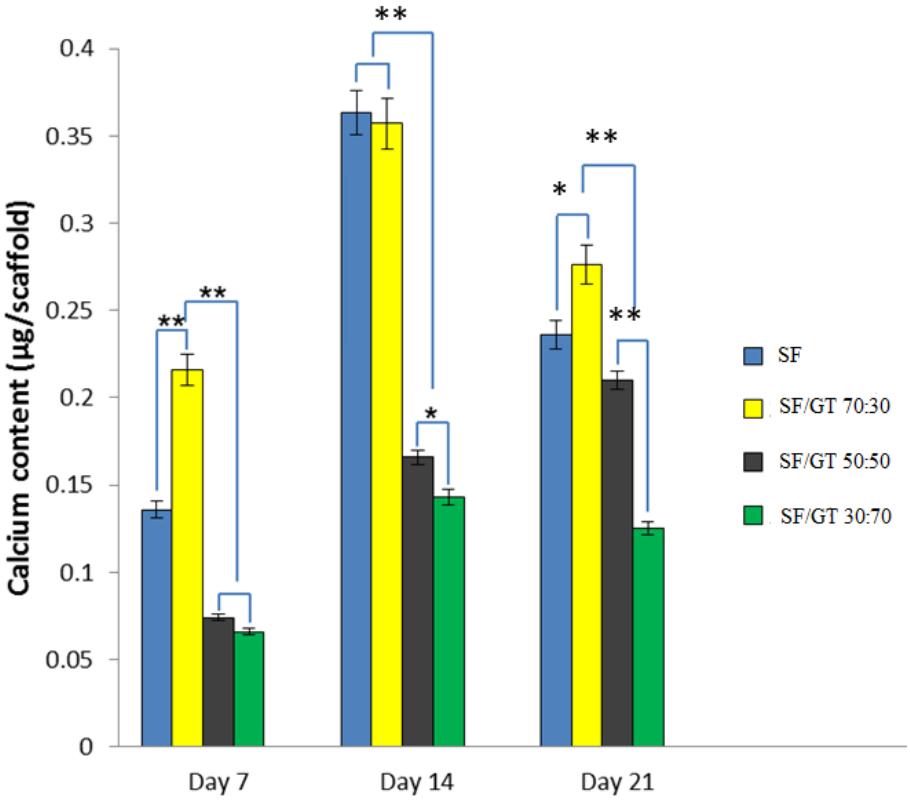

Figure 33. Calcium content, on the scaffolds in each group at days 7, 14, and 21. The results are displayed as means ± standard deviation (n=5).

Calcium deposition on scaffolds

In this research, the morphological structure of calcium nodules, which were deposited on the scaffolds was observed by alizarin red staining at days 7 and 21 (Figure. 31). The results showed all scaffolds had calcium deposition on their porous

structure at; day 7 and 21. The calcium deposition increased by increasing the number of days of testing. For day 7, calcium deposition showed some parts contained a porous structure, and in the case of day 21, calcium deposition demonstrated almost the entire area having a porous structure. Notably, the results showed that the calcium deposition of SF and SF/GT (70:30) had more intensiveness than the others at days 7 and 21. For SF/GT (50:50) and (30:70), there were some non-covered area of porous structure.

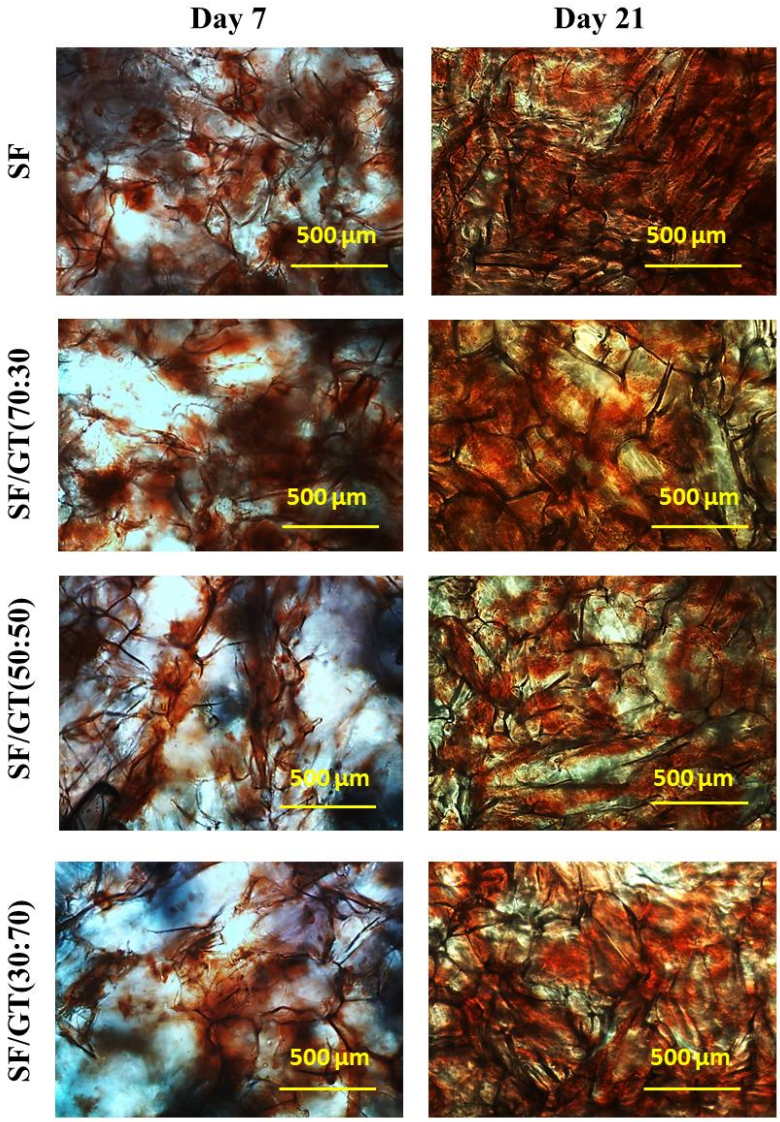

Figure 34. Calcium deposition on scaffolds at days 7, and 21 (n=2)

Histological morphology of scaffolds

The histological morphology was used to present the cell organization on those scaffolds. The results demonstrated that all scaffolds had cell adhesion on the porous structure at days 3 and 7 (Figure. 32). For day 3, silk fibroin with gelatin showed good cell adhesion as well as distribution in the porous structure, and these cell adhesions, self-organized into the large aggregation. On the other hand, silk fibroin, without gelatin, showed only fair cell adhesion coupled with distribution. Such cell adhesion, expressed the small aggregation on its porous structure. For day 7, silk with and without, gelatin at a ratio of; SF/GT (70:30) and (30:70), demonstrated better cell adhesion and distribution than the others. Those cell adhesions expressed formation into extending and spreading on its porous structure. In the case of ratio; SF/GT (50:50) and (30:70), the scaffolds showed a loose and large porous structure. Notably, there were some light cell adhesions on the structures of SF/GT (50:50).

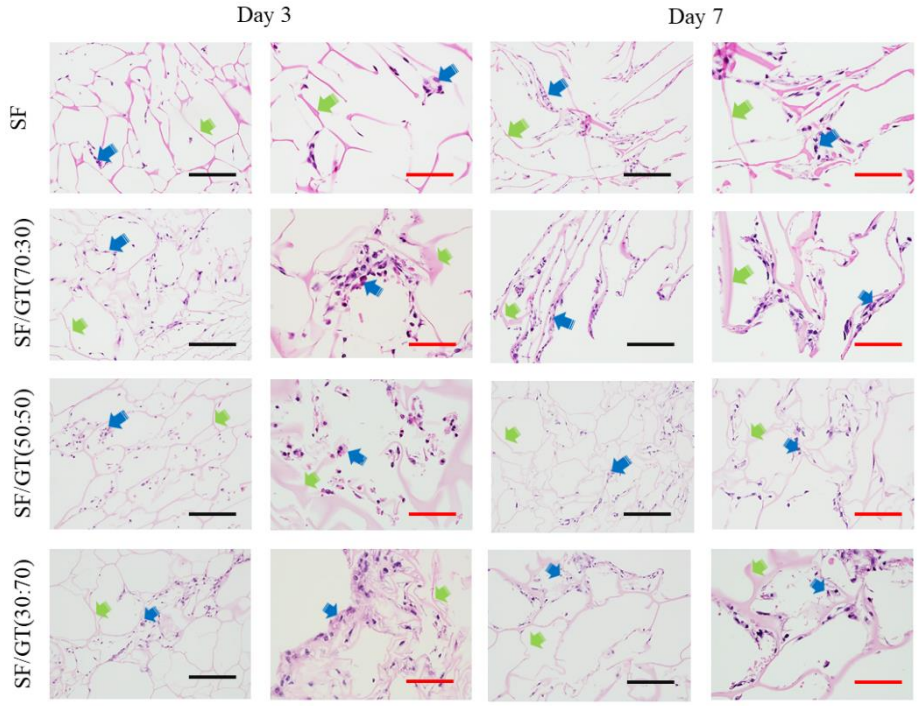

Figure 35. The histology of cell mophology on porous of scaffolds at different time points; days 3 and 7. (n=2) Blue arrow; Cells, Green arrow; Scaffold, Green scale bar; 100 μm, Red scale bar; 50 μm.

Discussion

Morphological formation of mimicked pathogenic porous structure of osteoporosis

In this research, pathogenic, porous structures were mimicked for use as ex vivo biomaterials in the evaluation of biomineralization in osteoporosis. The similar pores of osteoporosis were mimicked into heterogeneous and homogeneous structures, because some reports demonstrated that the different pores have an effect on the pathogenic structure of osteoporosis [11].

The results revealed that silk fibroin, with a gelatin scaffold of SF/GT (70:30) and (50:50) had heterogeneous porous. Such heterogeneous porous demonstrated the main pores, which had a network structure inside. The main pores as well as network structure came from the silk fibroin and gelatin, respectively. This was generated from the mixed bi-component of scaffolds, which has different molecular hydrophillicity of silk fibroin and gelation. The difference has an effect on irregular interfacial tension between that of bi-components and ice, crystals during the process of freeze drying [12, 13]. In those ratios, silk fibroin, which had low hydrophillicity than gelatin, self-organized into the main porous structure. Such main porous structures might come from the high interfacial tension between silk fibroin and ice crystals during freeze drying. For the network porous structure, the hydrophilic gelatin shows lower interfacial tension. This leads to the formation of the small porous network.

On the other hand, silk fibroin, gelatin, and SF/GT (30:70) demonstrated a homogenous, porous structure. For the single component of silk fibroin and gelation, the results demonstrated a homogeneous, porous structure, because there were no second components to interfere with them,during freeze drying. For the ratio of; 30:70, the result indicated that the gelatin was the main component which dominanted the minor silk fibroin component. Additionally, this also had an effect on the homogeneous, structural occurrence of that ratio. According to the morphological formation, the results can relate to irregular bone remodeling, which is the pathogenic porous structure of osteoporosis. There are some reports on irregular expression of heterogeneous

morphology during bone remodeling [14]. Nevertheless, the other physical performance which is related to the pathogenic porous structure of osteoporosis was undertaken to clarify performance of those scaffolds as ex-vivo biomaterials.

Physical performance of mimicked pathogenic porous structure of osteoporosis

In this research, biodegradability as well as swelling behavior was presented as physical performance of pathogenic porous formation, which relates to the extracellular matrix (ECM) organization during osteoporosis.

First, the results demonstrated that the mimicked scaffolds, with different contents of gelatin, showed different degradability. The scaffolds with gelatin showed more degradation than those without gelatin. This is because gelatin is the protein, which is easily degraded with lysozyme [15, 16]. Therefore, the scaffolds with a high content of gelatin demonstrated more degradability than those with low content. Notably, the degradability can be represented as stability of the scaffolds. The result indicated that scaffolds with gelatin had lower stability than those without gelatin. This can related to the different degree of osteoporosis, which has different stability of ECM [17]. The Silk fibroin component in mimicked scaffolds refers to the stable performance of ECM, during bone formation [18, 19]. On the other hand, gelatin implies to the non-stable performance of ECM, during bone re-sorption. The results demonstrated that the non-stable scaffolds, with gelatin, can be related to more pathogenic porous structure of osteoporosis.

Second, the results could be related to the dynamic behavior of mimicked scaffolds, which showed in situ physical expression during osteoporosis. The swelling behavior was used to present this dynamic behavior. The results indicated that scaffolds of silk fibroin, with non-stable gelatin, had more swelling behavior than those without gelatin. This is because, gelatin shows the hydrophilicity, which can enhance the swelling behavior. Interestingly, some research related the swelling behavior to the dynamic behavior of ECMs [20]. That research showed that the dynamic behavior was

dependant on the non-stable components as well as hydrophilicity in ECMs. ECMs, which have main non-stable components and hydrophilicity, oftenshows unique dynamic behavior [21]. Therefore, mimicked scaffolds with gelatin are possibly to imply the unique, dynamic behavior of ECM, which is the in situ physical expression of pathogenic porous formation during osteoporosis. Nevertheless, biological performance was undertaken to evaluate the feasibility of these scaffolds, as ex vivo biomaterials of biomineralization on pathogenic porous structure, in osteoporosis.

Biological performance of mimicked pathogenic porous scaffolds

In this research, the biological performance of cell proliferation, calcium synthesis and deposition, and hisological organization on mimicked scaffolds is important for the evaluation of biomineralization on pathogenic porous structure in osteoporosis. Osteoblast cell proliferation and viability was, therefore, selected to evaluate said erformance. For cell proliferation, the results demonstrated that there were some different cell proliferations, at different time periods. For the early stage, around days 1 and 3, the scaffolds with gelatin showed higher cell proliferation than those without gelatin. This is because; the gelatin has a unique functional expression of RGDs in their molecules [22]. These RGDs, act as the domain that cells can recognize to adhere to [23]. This leads to the enhancement of cell proliferation [24]. For the middle stage, approximately at day 5, the scaffold with high contents of gelatin (30:70) had more cell proliferation than those with a low content. This result, possibly comes from the homogenous porous, which had no network, showing sufficient, free spaces for cell proliferation. For the later stage, around day 7, the scaffolds with a low content of gelatin (70:30) increased, slightly to the same level of cell proliferation as scaffolds with a high content (30:70). This might be that the network of gelatin in the main silk pores of (70:30) was degraded. This leaded to the emergange of free spaces for cell proliferation. Furthermore, the main silk pores might have suitable stability of structure and function to enhance cell proliferation. Notably, the fair gelatin content in a ratio of;

50:50, showed unique, decreasing lower levels of cell proliferation than the others. This possibly comes from more degradability of those gelatin networks in the porous structure. This increased degradability might be the cause of non-stability, which in turn leads to a decrease of cell proliferation [25]. Moreover, main silk pores are possibly shown to be a non-suitable structure and functionality for the promotion of cell proliferation.

According to the biological performance of cell proliferation, the results indicated that the stability as well as morphological structure of pores had an effect on cell proliferation. The heterogeneous structure of stable main pores, incorporated with non-stable networks, showed unique performance in the enhancement of cell proliferation. Especially SF/GT (70:30), which showed unique cell proliferation. On the other hand, the non-stable main pore incorporated, with a non-stable network showed low cell proliferation. This can related to the pathogenic porous structure of osteoporosis. Some research demonstrated that the low cell proliferation has an effect on osteoporosis [26]. Our results showed that the non-stable structure along with heterogeneous of main pores, incorporated with network structure, had performance similar to pathogenic porous formation of irregular bone remodeling during osteoporosis [14]. This represented the pathogenic structure of osteoporosis. However, to clarify the performance, bone formation on the scaffolds was undertaken.

In this research, ALP activity, calcium content and morphology of calcium organization were presented as markers for biological performance of calcium synthesis and deposition on scaffolds. First, ALP activity is generally used to analyze calcium synthesis from osteoblast at the early stage of bone formation. In this research, there were no differences of calcium synthesis in all scaffolds at day 7. This indicated that a suitable structure and function of all scaffolds had the role to activate calcium synthesis for all samples. Then, the calcium synthesis of silk fibroin, with gelatin was lower than without gelatin at day 14. The results demonstrated that gelatin is the component which had the role to promote calcium synthesis. This comes from the

RGDs and suitable dynamic behavior in gelatin, which plays the role to enhance calcium synthesis [27]. For day 21, the silk fibroin with low amounts of gelatin had lower calcium synthesis than the others. This possibly comes from the non-stable gelatin, which had a high dynamic behavior. This leads to slight functions to promote calcium synthesis at this time period.

Second, calcium content is the marker, which can relate to the biological performance of the scaffolds. The results demonstrated that the calcium content of silk fibroin, with and without low gelatin, (70:30) was higher than the others at day 7. This may have arisin from their stability, thus enabling them to capture calcium from osteoblast [28]. Silk fibroin with low gelatin (70:30) was higher in calcium content than that of silk fibroin without gelatin. Notably, silk fibroin with low gelatin showed the highest calcium content. The results possibly came from its stability and having a suitable amount of gelatin. This leads to high capability for calcium capturing from osteoblast. For day 14, silk fibroin, with and without low gelatin had non-significant differences of calcium content. They were, however, higher than the others. The results indicated that the maintained, stable structure and function of those scaffolds showed suitable performance to capture calcium from osteoblast in high amounts [29]. In contrast to this, silk fibroin, with high gelatin and a non-stable structure, had a unique, dynamic behavior causing it to only slightly capture calcium slightly . For day 21, silk fibroin, with and without, high gelatin demonstrated higher calcium content than the others. This was especially true for silk fibroin with a low gelatin content of; 70:30, which revealed to have the highest calcium content. This indicated that its maintained, stable structure and suitable expressed function of scaffolds has the role to promote calcium capturing. Controversy, silk fibroin with high gelatin had a low calcium content. This possibly came from the non-stable structure, which was dominant over its expressed biological function, leading to slight calcium capturing.

Third, the morphology of calcium deposition on scaffolds was observed by alizarin red staining. For the early stage, at day 7, silk fibroin, with and without, low

gelatin showed more, dense calcium deposition than the others. This comes from the stable structure and expressed function that showed performance to capture calcium [30]. Once again, controversy, the silk fibroin with high gelatin demonstrated a non-stability and dynamic behavior. This lead to loose calcium deposition on the scaffolds. At the later stage, day 21, silk fibroin, with and without low gelatin, showed complete, fused calcium deposition covering the whole structure of the scaffolds. This is because the maintained, stable structure and function can support calcium deposition. For the silk fibroin with high gelatin, the non-stable structure and function is the cause of incomplete calcium deposition covering only some parts of the scaffolds.

According to biological performance of scaffolds, the results can be related to the pathogenic porous structure of osteoporosis. The mimicked scaffolds, which showed structural stability and dynamic functional behavior, were the main effects on promotion of biomineralization. Especially, scaffolds which had major, stable structural component and minor components of dynamic functional behavior, this being having the most effectiveness for biomineralization. This possibly demonstrated the normal biomineralization with this condition.

On the other hand, the scaffolds which had major components of dynamic, functional behavior and minor stable, structural components showed only slight biomineralization. The degree of the bone formation depended on the ratio of these structures and behaviors. This might be similar to the irregular biomineralization during osteoporosis. This demonstrated that those scaffolds were suitable as ex-vivo biomaterials to represent the pathogenic porous structure for biomineralization in osteoporosis. Nevertheless, to clarify mimicked pathogenic porous structure for biomineralization of osteoporosis, further histological observing was undertaken.

The histological organization was observed to evaluate the performance of the mimicked scaffolds as ex vivo biomaterials. The results demonstrated that silk fibroin, with gelatin, showed more cell aggregation in the pores than those without gelatin at day 3. This might come from RGDs in gelatin, that can enhance cell adhesion.

Furthermore, the non-stability and dynamic behavior of gelatin is possibly the cause of cell aggregation [31]. Whereas , silk fibroin without gelatin demonstrated cell extension which adhered in the pores. This indicated that silk fibroin. without gelatin, had the stability to promote cell adhesion, which in turn leads to cell extension . At day 7, the loose structural organization of scaffolds of 50:50 and 30:70 is possibly the cause of gelatin degradation. The light cell adhesion of 50:50 might came from the non-stability and dynamic behavior in their structure. Notably, the results showed dense cell aggregation on the loose structural scaffold at day 7. This is probably the cause from the plentiful debris of degraded gelatin, which can encourage the RGDs to enhance cell aggregation [32].

According to the biological performance of histological organization, the results indicated that the stability and dynamic behavior of those scaffolds was the main causes having an effect on cell organization on porous structures. The stability and non-dynamic behavior could promote dense cell adhesion on said porous structure. In contrast, non-stability and dynamic behavior lead to light cell adhesion on the porous structure. As a result, the stability and dynamic behavior could be related to the pathogenic porous structure of osteoporosis. This can be related to bone remodeling, as the stable structure acts as the substrate for strong cell adhesion, which leads to extending and spreading [33]. This shows performance similar to the bone formation [34]. The dynamic, behavior expressed performance as bone resorption [35]. For the pathogenic structure of osteoporosis, those bone formations and resorptions showed irregular demonstration [36]. The dynamic behavior of bone resorption expresses hyper-function that lead to the osteoporosis [37]. This related to the mimicked scaffolds of silk fibroin with high dynamic behaviors of gelatin. Those scaffolds demonstrated performance similar to the pathogenic structure of osteoporosis. Especially, 50:50, which showed distinguish expression of histological organization, again this is similar to poor bone remodeling during osteoporosis formation.

Conclusion

In this research, the mimicked pathophysiologic scaffolds, based on silk fibroin/gelatin, was presented for the use as ex-vivo biomaterials for the evaluation of osteoporosis. The results indicated that the stability of structure, morphology and dynamic behaviors are the triggers to evaluate these scaffolds. The non-stable porous structure, heterogeneous morphology and dynamic behavior of scaffolds showed suitable performance, which is similar to the pathogenic structure of osteoporosis. Especially, the SF/GT 50:50, which showed heterogeneous morphology, which has a main pore incorporated with network structures, while also demonstrating dynamic behavior. The SF/GT 50:50 has the biological performance, similar to poor bone remodeling in the pathogenic structure of osteoporosis. These performances of SF/GT 50:50 indicated that it is promising as a ex-vivo biomaterial to evaluate the pathogenic structural formation of osteoporosis.

Reference

[1] Chang G, Kim HJ, Kaplan DL, Vunjak-Novakovic G, Kandel RA. Porous silk scaffolds can be used for tissue engineering annulus fibrosus. Eur Spine J 2007;16:1848–1857.

[2] Yan LP, Silva-Correia J, Correia C, Caridade SG, Fernandes EM, Sousa RA, Mano JF, Oliveira JM, Oliveira AL, Reis RL. Bioactive macro/micro porous silk fibroin/nano-sized calcium phosphate scaffolds with potential for bone-tissueengineering. Nanomedicine 2013;8:359–378.

[3] Imani R, Rafienia M, Emamia SH, Kabiria M, Rabban M. Synthesis and Characterization of Biodegradable Hemostat Gelatin Sponge for Surgery Application. Iranian Journal of Pharmaceutical Sciences 2008;4:193-200.

[4] Kasoju N, Kubies D, Kumorek MM, Krız J, Fabryova E, Machova L, Kovarova J, Rypaek F. Dip TIPS as a facile and versatile method for fabrication of polymer foams with controlled shape size and pore architecture for bioengineering applications. PLoS ONE 2014;9:1–16.

[5] Guziewicz N, Best A, Perez-Ramirez B, Kaplan DL. Lyophilized silk fibroin hydrogels for the sustained local delivery of therapeutic monoclonal antibodies. Biomaterials 32;2011:2642–2650.

[6] Chang G, Kim HJ, Kaplan DL, Vunjak-Novakovic G, Kandel RA. Porous silk scaffolds can be used for tissue engineering annulus fibrosus. European Spine Journal 16;2007:1848–1857.

[7] Liu X, Zhao M, Lu J, Ma J, Wei J, Wei S. Cell responses to two kinds of nanohydroxyapatite with different sizes and crystallinities. International Journal of Nanomedicine 7;2012:1239–1250.

[8] Kim BS, Kang HJ, Lee J. Improvement of the compressive strength of a cuttlefish bone-derived porous hydroxyapatite scaffold via polycaprolactone coating, Journal of Biomedical Materials Research Part B: Applied Biomaterials 101;2013:1302–1309.

[9] Ji H. Lysis of cultured cells for immunoprecipitation. Cold Spring Harb Lab Protoc 2010;2010:1–5.

[10] Wang YH, Liu Y, Maye P, Rowe DW. Examination of mineralized nodule formation in living osteoblastic cultures using fluorescent dyes. Biotechnology 22;2006:1697–1701.

[11] Bono CM, Einhorn TA. Overview of osteoporosis:pathophysiology and determinants of bone strength. Eur Spine J 12;2003:90-96.

[12] Matsumoto A, Chen J, Collette AL, Kim UJ, Altman GH, Cebe P, Kaplan DL. Mechanisms of Silk Fibroin Sol-Gel Transitions. J. Phys. Chem. B 110;2006:21630-21638.

[13] Baldino L, Cardea S, Reverchon E. Loaded Silk Fibroin Aerogel Production by Supercritical Gel Drying Process for Nanomedicine Applications. Chemical Engineering Transactions 49;2016:343-348.

[14] Lloyd AA, Wang ZX, Donnelly E. Multiscale Contribution of Bone Tissue Material Property Heterogeneity to Trabecular Bone Mechanical Behavior. J Biomech Eng. 137;2015:0108011–0108018.

[15] Yang Z, Xu LS, Yin F, Shi YQ, Han Y, Zhang L, Jin HF, Nie YZ, Wang JB, Hao X, Fan DM, Zhou X. In vitro and in vivo characterization of silk fibroin/gelatin composite scaffolds for liver tissue engineering. Journal of Digestive Diseases 13;2012:13:168–178.

[16] Ratanavaraporn J, Damrongsakkul S, Sanchavanakit N, Banaprasert T, Kanokpanont S. Comparison of Gelatin and Collagen Scaffolds for Fibroblast Cell Culture. Journal of Metals, Materials and Minerals 6(2006)31-36.

[17] B. Clarke, Normal Bone Anatomy and Physiology. Clin J Am Soc Nephrol 3;2008:131-139.

[18] Yao D, Liu H, Fan Y. Silk scaffolds for musculoskeletal tissue engineering. Experimental Biology and Medicine 241;2016: 238–245.

[19] Polo-Corrales L, Latorre-Esteves M, Ramirez-Vick JE. Scaffold Design for Bone Regeneration. J Nanosci Nanotechnol 14;2014:15-56.

[20] Gao Y, Liu S, Huang J, Guo W, Chen J, Zhang L, Zhao B, Peng J, Wang A, Wang Y, Xu W, Lu S, Yuan M, Guo Q. The ECM-Cell Interaction of Cartilage Extracellular Matrix on Chondrocytes. BioMed Research International 2014;2014:1-8.

[21] Muiznieks DL, Keeley FW. Molecular assembly and mechanical properties of the extracellular matrix: A fibrous protein perspective. Biochimica et Biophysica Acta 1832;2013:866-875.

[22] Davidenko N, Schuster CF, Bax DV, Farndale RW, Hamaia S, Best SM, Cameron RE. Evaluation of cell binding to collagen and gelatin: a study of the effect of 2D and 3D architecture and surface chemistry. J Mater Sci: Mater Med 27;2016:1-14.

[23] Bellis SL. Advantages of RGD peptides for directing cell association with biomaterials. Biomaterial 32;2011:4205-4210.

[24] Rivera-Chacon DM, Alvarado-Velez M, Acevedo-Morantes CY, Singh SP, Gultepe E, Nagesha D, Sridhar S, Ramirez-Vick JE. Fibronectin and vitronectin promote human fetal osteoblast cell attachment and proliferation on nanoporous titanium surfaces. J Biomed Nanotechnol 9;2013:1092-1097.

[25] Sung HJ, Meredith C, Johnson C, Galis ZS. The effect of scaffold degradation rate on three-dimensional cell growth and angiogenesis. Biomaterials 25;2004:5735–5742.

[26] Li C, Wei G, Gu Q, Wang Q, Tao S, Xu L. Proliferation and Differentiation of Rat Osteoporosis Mesenchymal Stem Cells (MSCs) after Telomerase Reverse Transcriptase (TERT) Transfection. Med Sci Monit. 21;2015:845–854.

[27] Han WT, Liu J, Tang M, Chen W, Cheng L, H. Xu HHK. Induced Pluripotent Stem Cell-derived Mesenchymal Stem Cell Seeding on Biofunctionalized Calcium Phosphate Cements. Bone Research 4;2013:371-384.

[28] Polo-Corrales L, Latorre-Esteves M, Ramirez-Vick JE. Scaffold Design for Bone Regeneration. J Nanosci Nanotechnol 14;2014:15-56.

[29] Takagishi Y, Kawakami T, Hara Y, Shinkai M, Takezawa M, Nagamune T. Bone-Like Tissue Formation by Three-Dimensional Culture of MG63 Osteosarcoma Cells in Gelatin Hydrogels Using Calcium-Enriched Medium. Tissue Engineering 12;2006:927-937.

[30] Yaghoobi M, Hashemi-Najafabadi S, Soleimani M, Vasheghani-Farahani E, Mohammad Mousavi S. Osteogenic Differentiation and Mineralization on Compact Multilayer nHA-PCL Electrospun Scaffolds in a Perfusion Bioreactor. Iran J Biotechnol 14;2016:41-49.

[31] Georges PC, Janmey PA. Cell type-specific response to growth on soft materials. J Appl Physiol 98;2005:1547–1553.

[32] Jenna L. Wilson, Todd C. McDevitt. Stem Cell Microencapsulation for Phenotypic Control,Bioprocessing, and Transplantation. Biotechnol Bioeng 10;2013:667-682.

[33] Vernerey FJ, Farsad M. A mathematical model of the coupled mechanisms of cell adhesion, contraction and spreading. J Math Biol 68;2014:989-1022.

[34] Joy A, Cohen DM, Luk A, Anim-Danso E, Chen C, J. Kohn, Control of Surface Chemistry, Substrate Stiffness, and Cell Function in a Novel Terpolymer Methacrylate Library. Langmuir 27;2011:1891-1899.

[35] Komarova SV, Smith RJ, Dixon SJ, Sims SM, Wahl LM, Mathematical model predicts a critical role for osteoclast autocrine regulation in the control of bone remodeling. Bone 33;2003:206-215.

[36] Feng X, McDonald JM. Disorders of Bone Remodeling. Annu Rev Pathol 6;2011:121-145.

[37] Melo NDO, Serakides R. Effect of the physical activity on normal bone and on the osteoporosis prevention and treatment. Rev Bras Med Esporte 12;2006:149-152.

CHAPTER 5

Biomineralized scaffolds of chitosan with bicomponent calcium phosphate based on bioispiration of bone remodeling for maxillofacial tissue engineering; Morphology and performances

Abstract

Biomineralzed scaffold is an attractive materials for maxillofacial tissue engineering. In this research, bioinspiration of bone remodeling was used to design and fabricate those scaffolds. Chitosan was mixed with 2, 4, 6, and 8% of bicomponent calcium phosphate (BiCP) into acidic solution before neutralized with basic solution. Then, the neutralized solution was fabricated into scaffolds by freeze drying. Mophology of scaffolds was observed with Scanning Electro Microscopy (SEM). Physical performance of scaffolds was evaluated with swelling property and degradation. Afterward, those scaffolds were cultured by osteoblasts. Biological performance of scaffolds was evaluated with total protein synthesis, cell vibility and proliferation, Alkaline Phosphatase (ALP) activity, calcium contents, and histology. The results showd scaffolds of chitosan with BiCP which had morphology of calcium deposition on chitosan fibers. The physical performance of those scaffolds demonstrated low swelling property and high degradation with increasing of BiCP concentration. Biological performance showed that scaffold with BiCP could induce total protein synthesis, cell viability and proliferation, ALP activity, and calcium content. The histology of cultured scaffolds with BiCP showed cell adhesion, elongation which was similar to osteoblast organization of bone formation. Finally, the results indicated that a scaffold with BiCP is promising for maxillofacial tissue engineering particularly in 2 and 4% of bicomponent calcium phosphate.

Materials and methods

Chitosan preparation

The shrimp chitosan powder (Marine Bio Resources Co.,Ltd) was dissolved in 0.1 M acetic acid with ratio 2% chitosan. After dissolving the chitosan solution was stirred for 24 hrs, the bubble was removed in this step. The chitosan solution was filtered through cheesecloth.

Construction of BiCP with chitosan

The BiCP (Bicomponent calciumphospate) powder which had the ratio of hydroxyapatite:tricalcium phosphate (1:1) was added into the chitosan solution with difference concentration including 2%, 4%, 6% and 8% (W/V). After combination process, the chitosan/BiCP solution was stirred for 15 min for homogeneous mixture. After that, the chitosan /BiCP solution was injected into the 1 M NaOH via the syringe. When the solution form into fibril that has the BiCP infiltrated in the fibril, the fibril was rinsed with dH2O for 3 times to remove the alkaline solution and adjusted pH in neutral phase. The cheesecloth has been used for filtering the micro fibril from solution. Next, the micro fibril was contained in the 15 ml tube continue to weighted for equal condition and centrifuge at 1500 rpm for 10 min. Then, the micro fibril scaffold was cut into 2 mm thickness and diameter about 10 mm. The freeze drying machine was used for water evaporation. The experiment was divided in 5 groups;

Groups	Detail
Chitosan	Chitosan without bicomponent calciumphosphate
Chitosan/2% BiCP	Chitosan with 2% of bicomponent calciumphosphate (W/V)
Chitosan/4%BiCP	Chitosan with 4% of bicomponent calciumphosphate (W/V)
Chitosan/6% BiCP	Chitosan with 6% of bicomponent calciumphosphate (W/V)
Chitosan/8% BiCP	Chitosan with 8% of bicomponent calciumphosphate (W/V)

Table 4. The experimental groups

Morphology analysis

The scaffold in all groups was observed the surface structure and the thickness by Scanning Electron Microscopy (SEM), (Quanta400, FEI, Czech Republic). The samples were pre-coated with gold using a gold sputter coater machine (SPI supplies, Division of STRUCTURE PROBE Inc., Westchester, PA USA).

Swelling properties

The scaffold in all groups was soaked in PBS in different time point 15, 30 and 60 min to check swelling properties. Weighing of the scaffold was collected before and after soaking with PBS to calculate the weigh increasing follow this equation (Ws –Wd)/Wd ×100, where Ws and Wd are the weights of the swollen scaffold and the dry scaffold, respectively [1].

Degradation analysis

To observe the degradation rate of scaffold in each group was incubated with lysozyme (4 mg/ml of PBS) enzyme with deference time, including 0, 5, 10, 15 and 20 days. The scaffold in all groups was weighed before and after soaking for collect weighs loosing, degradation rate [2].

Cell proliferation, WST-1

Cell proliferation was assessed using a WST-1 (Roche Diagnostics GmbH, Mannheim, Germany). The measurement of cell proliferation was performed on days 1, 3, 5 and 7, following the manufacture’s protocol. The scaffold was washed with PBS and added 850 µl fresh media containing 10% of WST-1 reagent. Next, incubated for 50 min and continue to measure at absorbance 450 nm using a microplate reader (Biotrak II, UK).

Cell viability

The cell viability in scaffold was evaluated by FDA staining after day 3 and 5. The scaffold was removed the media and rinsed with PBS for 2 times. The fresh media was added into the scaffold and combined with 5 µl of 5 mg/ml in acetone, incubated at 37 °C for 5 mins. Next, the scaffold was rinsed with PBS and continues observing the live cell under the confocal microscope [3].

Alkaline phosphatase activity

The ALP activity was performed by Alkaline Phosphatase liquicolor (Human, Germany) on day 7, 14 and 21. The cell in scaffold was lysis with 1% TritonX in PBS and freeze thaw 3 cycle in -80 $^{\circ}$C for 1 h and room temperature. After that, the scaffold in the lysis was centrifuged for precipitate separation. The lysis solution was used for ALP activity analysis following the ALP kit following the manufacturing [4].

Total protein synthesis

The cell lysis solution on day 7,14 and 21 was used for protein analysis following the manufacturer's instructions (Pierce BCA Protein Assay kit, Thermo Scientific, USA). The standard curve was plotted by bovine serum albumin.

Calcium content

The calcium content was evaluated with the calcium colorimetric assay kit (Biovision). The cell lysis solution was used for calcium detection following the manufacturer's instructions.

Histology analysis

The scaffold in all groups was stained with hematoxylin and erosin at day 3 and 5 for observing the cell migration and morphology of scaffold. The cell in scaffold was fixed with 4% formaldehyde at 4 $^{\circ}$C for 24 h. Next, move the scaffold into

paraffin and cut at 5 μm. The sample was placed on the glass slide and stained with H&E and observed the cell under microscopy.

Statistical analysis

All data were shown as mean ± standard deviation. The samples were measured and statistically compared by one-way ANOVA and Tukey's HSD test (SPSS 16.0 software package). A $P < 0.05$ was accepted as statistically significant.

Results

Morphology of scaffolds

After preparation, mixed solution of chitsan with BiCP which was adjusted with NaOH showed the distribution of fibril bundles in aqueus media (Figure. 33A). The dense bundles of fibers demonstrated after rinse with dH_2O (Figure. 33B).

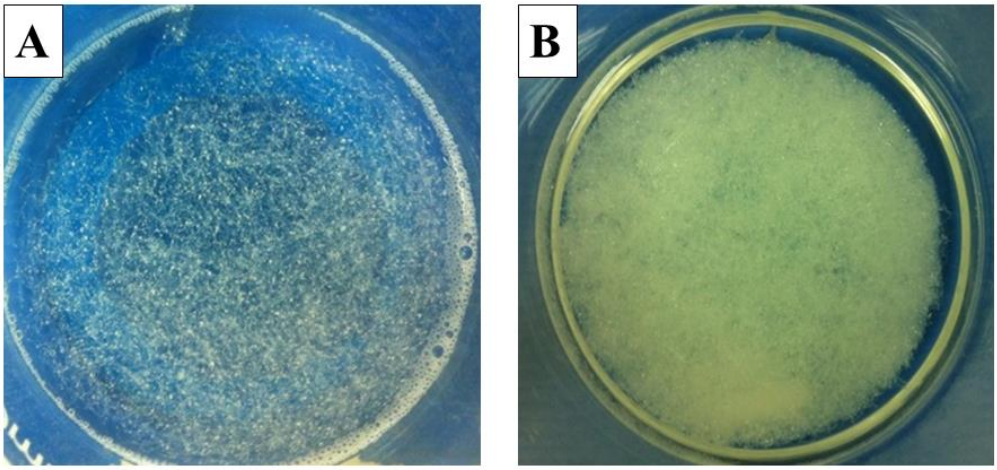

Figure 36. The chitosan/BiCP solution adjused with NaOH (A) and Chitosan/BiCP after rinsing with dH2O (B).

After rinsing with dH2O, all samples were fabricated into 3D scaffolds by freeze drying (Figure 34). The results showed that the chitosan and 2% BiCP/chitosan group were revealed the loose structure when compared to other groups. The compact

structure was found in groups that adding 4%, 6% and 8% of BiCP in chitosan scaffold. The adding BiCP was availed in dense structure.

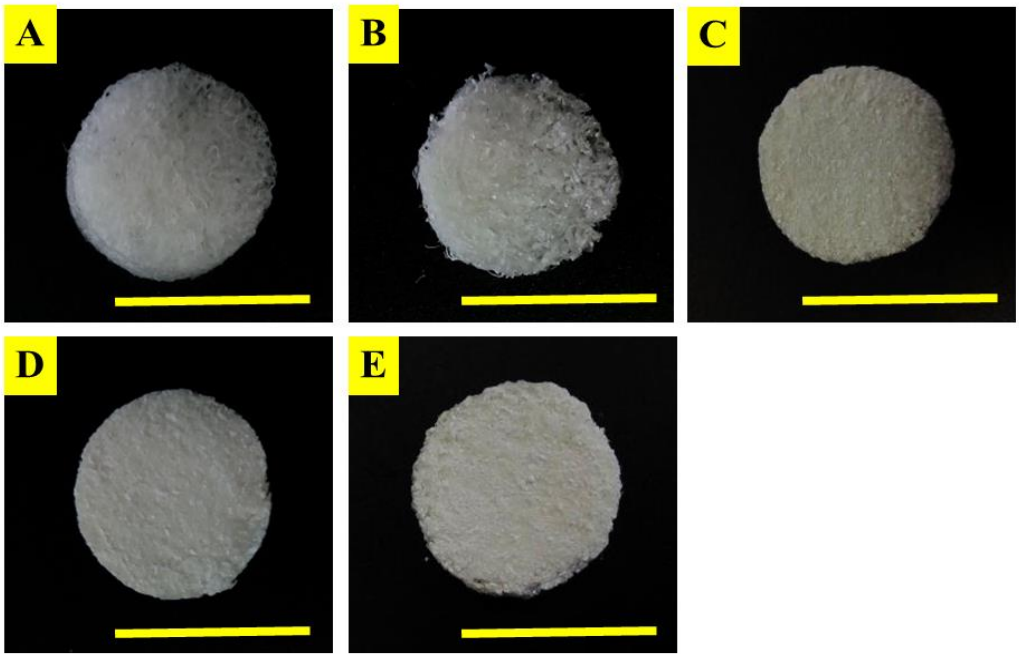

Figure 37. The morphological structure of the scaffold in all groups; A) Chitosan, B) Chitosan/2% BiCP, C) Chitosan/4% BiCP, D) Chitosan/6% BiCP, and E) Chitosan/8% BiCP. Scale bar; 10 mm

The morphology and structure of the scaffold were observed by SEM (Figure 35), the scaffold had porous structure in all groups particularly in chitosan. The chitosan showed the regular porous structure and distribution. Furthermore, that structure found the slightly roughness on the surface. On the other hand, the irregular porous structure was found in chitosan with BiCP. Chitosan with BiCP had clusters of particle which distributed and infiltrated in the porous structure. BiCP was adhered on porous surface of scaffold. Notably, there are some parts of scaffolds demonstrated self-organization of dense particular clusters which deposited on the fibril structure of chitosan particularly in high content of BiCP (Figure 35H, K, and N). Especially, the

high content of 8% BiCP showed more dense formation of particular cluster than the others.

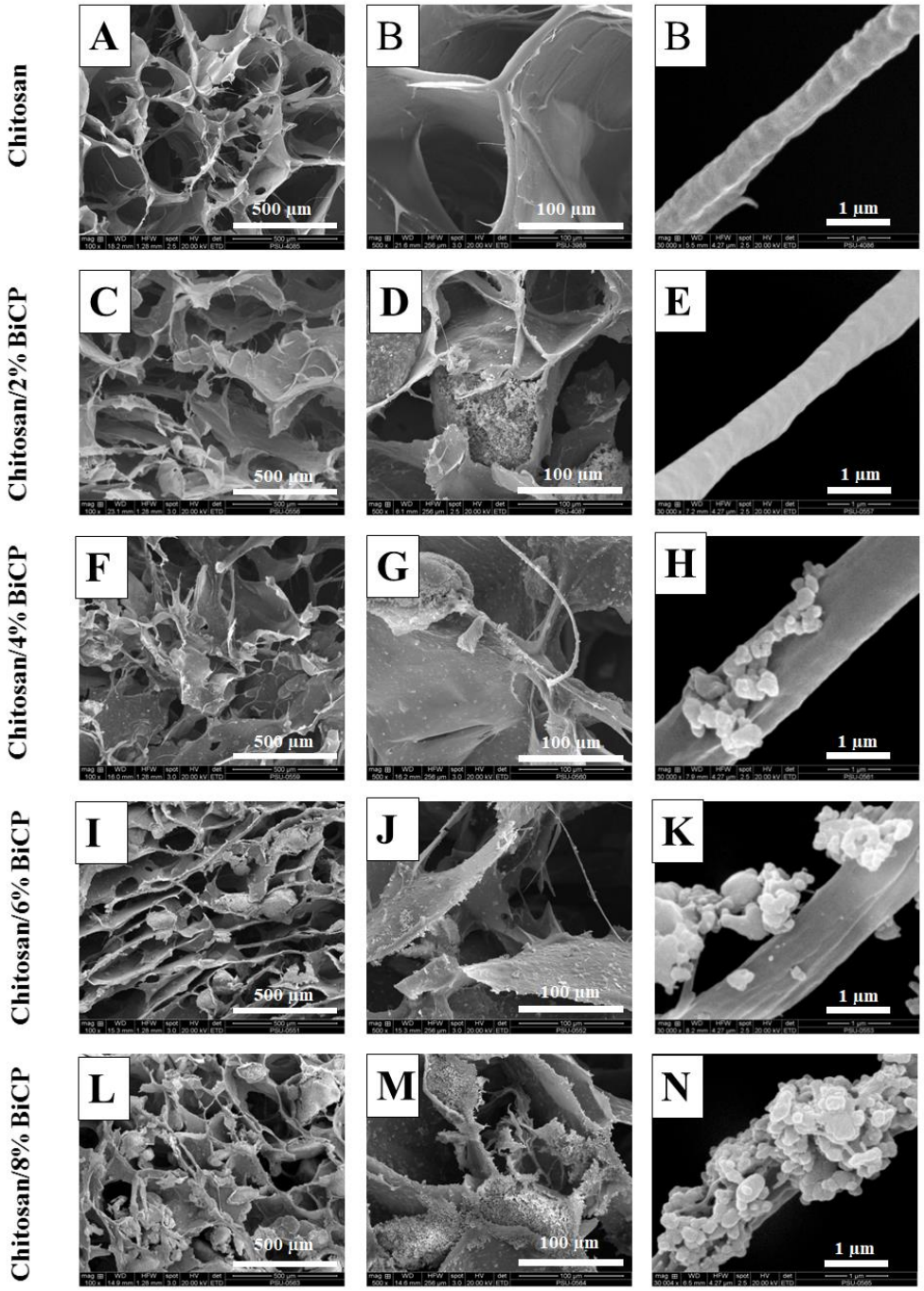

Figure 38. Morphology from SEM image of scaffolds

Swelling property

The swelling properties of the scaffolds were evaluated at 37 °C in the PBS, the swelling properties at 15, 30 and 60 min (Figure 36). The result showed three groups of swelling properties; high, fair, and poor swelling. Chitosan showed performance of the high swelling property. Chitosan/2% BiCP was the fair swelling property. Chitosan/4%, 6%, and 8% BiCP demonstrated poor swelling property. Notably, the swelling property decreased with increasing of BiCP.

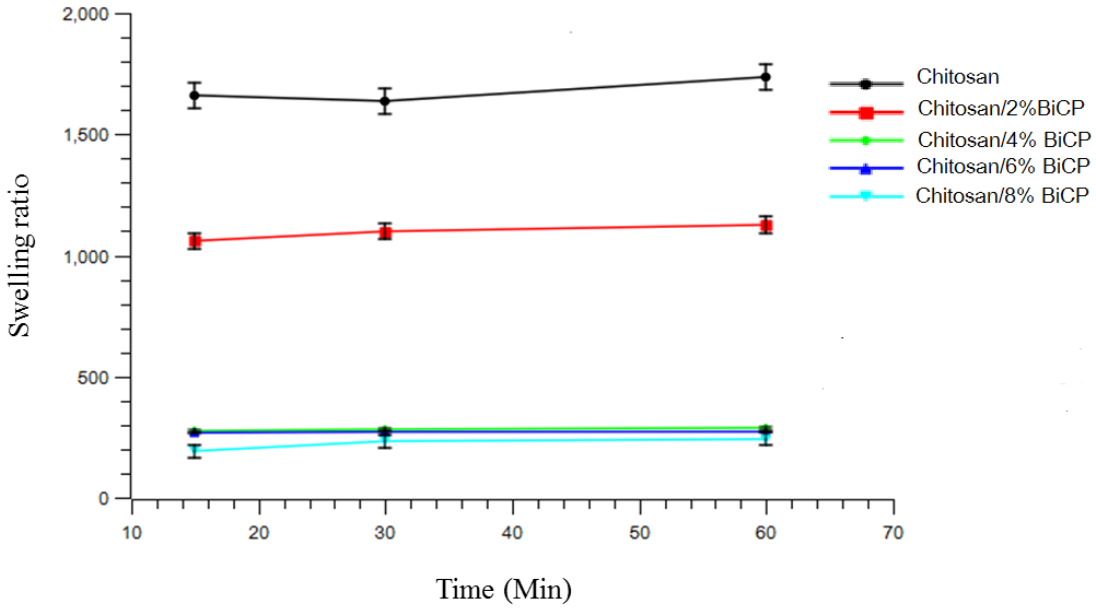

Figure 39. The swelling properties of the scaffolds in the PBS solution at 37 °C.

Degradation

To evaluate physical functionality, scaffolds were tested by degradation with lysozyme (Figure 37). This function was related to the application for tissue regeneration. The results showed that the degradation of all samples increased by increasing of time point. For day 7, chitosan/6% BiCP had the highest degradation. That chitosan/6% BiCP was still the highest degradation at day 14. For day 21, chitosan/4% and 6% showed the highest degradation. Chitosan with BiCP demonstrated

higher degradation than chitosan without BiCP. Notably, chitosan with low concentration of 2% and high content of 8% BiCP had non-different with chitosan at day 7.

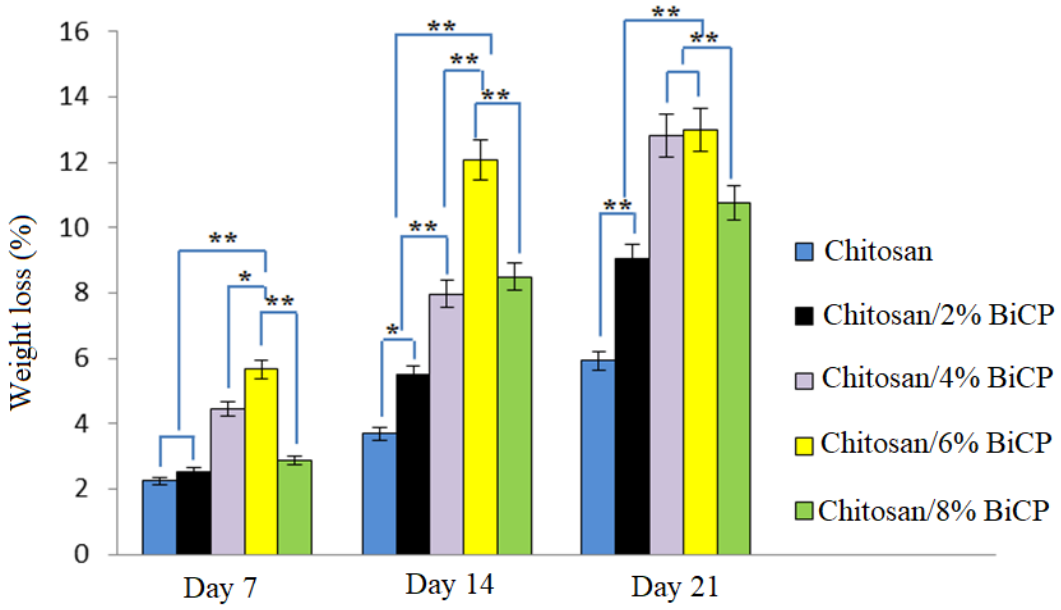

Figure 40. The degradation of scaffold in all groups after incubating with lysozyme at 37 °C.

Total protein synthesis

The protein synthesis from the osteoblast in the scaffold was evaluated (Figure 38). On day 7, the chitsan with BiCP can improve the protein synthesis of the osteoblast cell when compare to chitosan without BiCP . The chitosan/6% BiCP revealed the highest protein synthesis, but non significant difference with the chitosan/8% BiCP. However, chitosan/ 6 and 8% BiCP was higher than chitosan without BiCP, chitosan/2 and 4%BiCP. The chitosan/8% BiCP indicated that the highest value of protein synthesis on day14 and significant difference from all groups. The chitosan /2% BiCP to 6% BiCP showed non significant between group, but significantly higher than chitosan without BiCP. On day 14, all groups revealed the lower trend and chitosan/8% BiCP still higher than other groups.

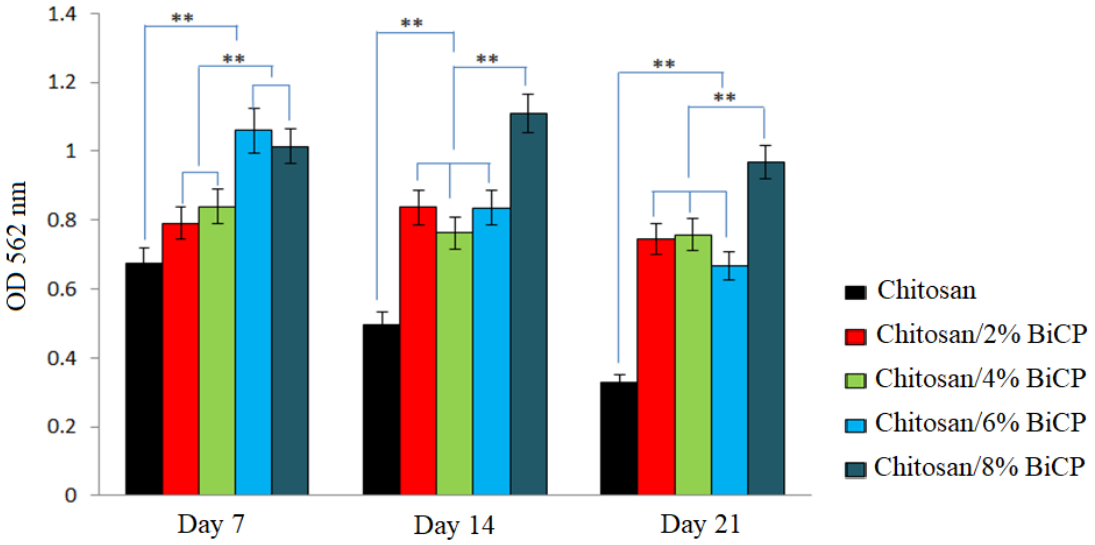

Figure 41. The protein synthesis of osteoblasts after culture in the scaffold in all groups at day 7, 14 and 21

Cell viability

The cell viability in the scaffold was detected by FDA staining under the confocal microscopy day 3 and 5, the cell was indicated in the green luminance (Figure 39). On day 3, the slightly cell viability was found in the chitosan and chitosan/4%BiCP scaffold. The chitosan/2% BiCP reviewed the cluster of cell viability, the abound of cell was found in the chitosan/6% and 8% of BiCP. The cell viability was clearly increased from day 3 to day 5, all groups of scaffold showed the good cell adhesion.

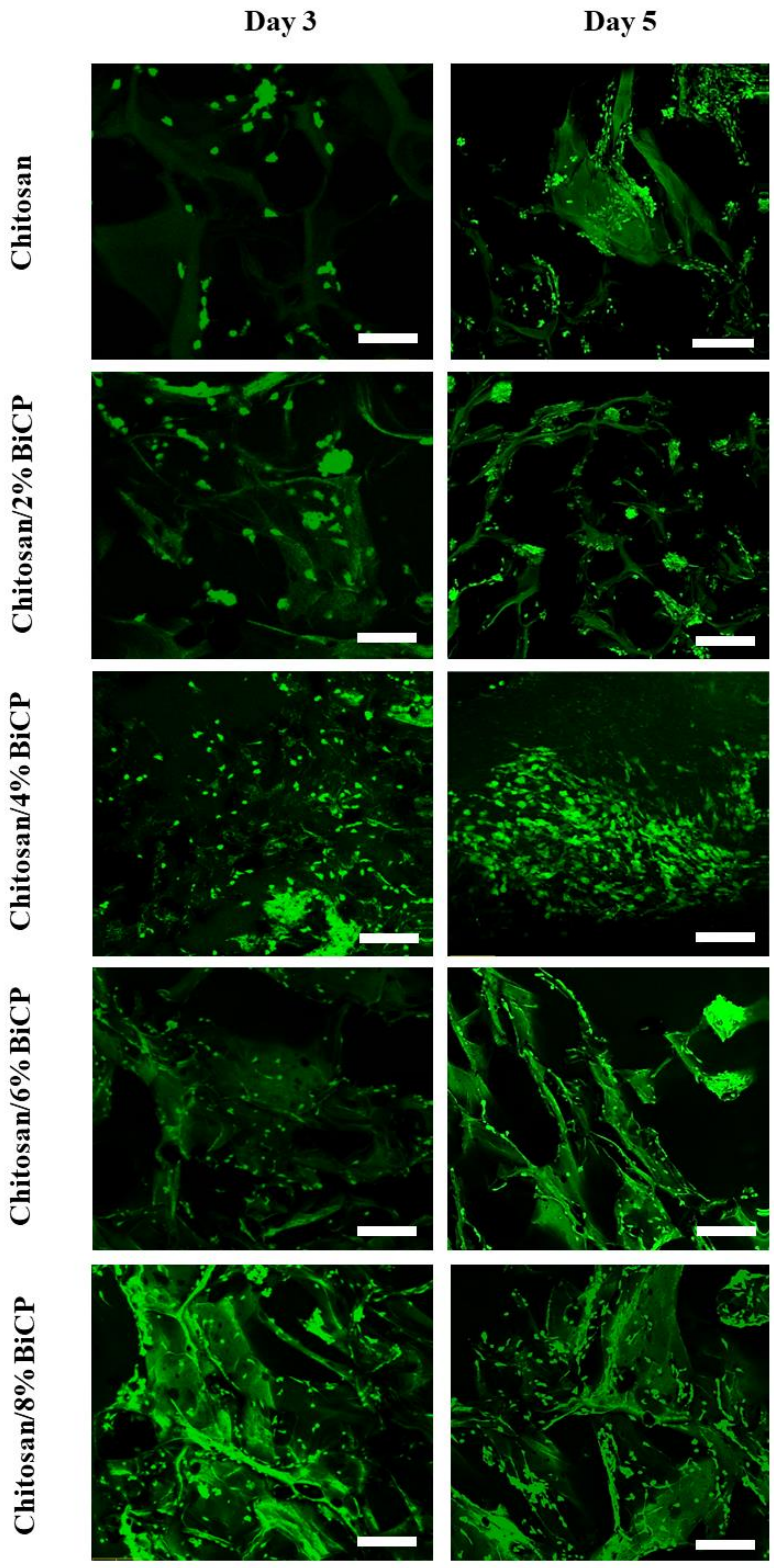

Figure 42. The cell viability of osteoblast in the scaffolds after staining with FDA at day 3 and 5. Scale bar; 200 μm

Cell proliferation

The cell proliferation was used to present biological performance. The result showed that cell proliferation continuously increased from day 1 to day 5, except day 7 that became lower (Figure 40). On day 1, the chitosan/2% BiCP in scaffold showed the highest cell proliferation when compared to other groups. The chitosan/2% BiCP scaffold was significantly higher than chitosan/6% BiCP and chitosan. On day 3, the chitosan/8% BiCP revealed a higher value than other groups and significantly different than chitosan. Moreover, after mixing chitosan with BiCP in all concentration was improved the osteoblast cell proliferation than chitosan without BiCP. On day 5, the chitosan/%8 BiCP still revealed a higher value than other groups. On the other hand, the chitosan/2% BiCP showed the significant difference value than all groups in day 7.

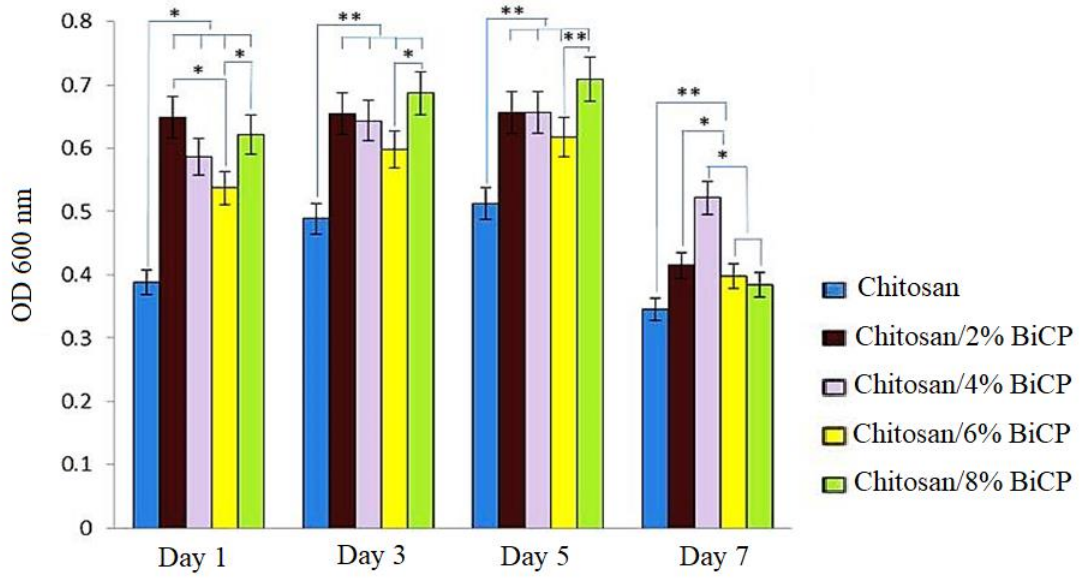

Figure 43. Cell proliferation of osteoblast cell on the scaffold in all groups on day 1, 3, 5 and 7.

Alkaline phosphatase (ALP) activity

After the cell culture in the OS media at 7, 14 and 21, the ALP activity was evaluated for the performance of osteoblast cell in the scaffold (Figure 41). On day

7, the chitosan scaffold with BiCP revealed the higher ALP activity than the chitosan group. The chitosan/2%, 4%, 6% and 8% BiCP were showed the similarly on the ALP activity and continue as same as on day 14. The chitosan/2% BiCP on day 21 revealed the higher ALP value than other groups but not significantly different. The chitosan scaffold showed the lower ALP activity when compared to the other groups.

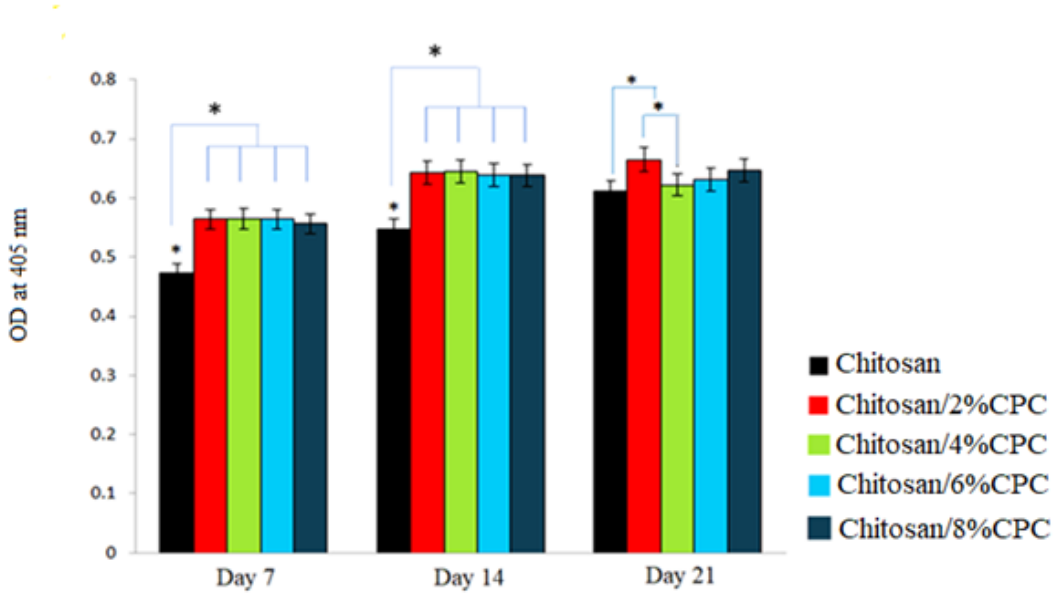

Figure 44. The ALP activity of osteoblasts in scaffolds after culture in OS media at day 7, 14 and 21.

Calcium content

The calcium analysis was used for evaluating the osteoblast performance on the differentiation stage in the scaffold (Figure 42). On day 7, the chitosan/8% BiCP reviewed lower in calcium synthesis than other groups and significantly different with chitosan/2% and /6% BiCP. The chitosan/2% BiCP was showed the significantly different on the calcium synthesis when compared to other groups on day 14. Moreover, the chitosan/6% BiCP was significantly higher than chitosan/8% BiCP. The calcium synthesis became lower on day 21, the chitosan/2% BiCP was good performance when compared with other concentrations of BiCP.

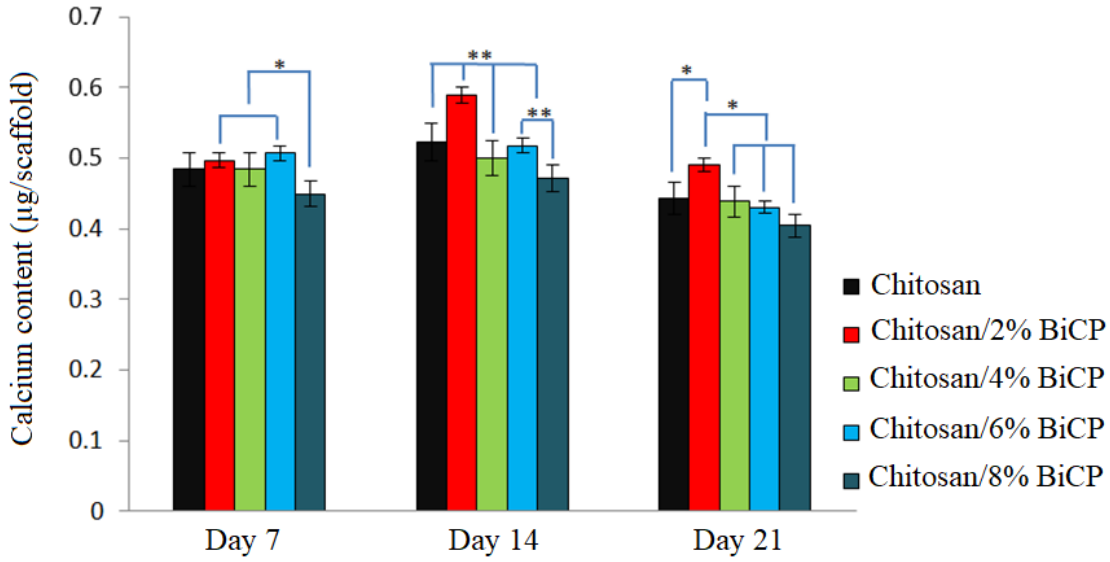

Figure 45. The calcium analysis of osteoblasts in scaffolds at difference time point at 7, 14 and 21

Histology

The morphology of the cell attachment and the arrangement in inside the scaffold was observed by H&E staining (Figure 43). The H&E staining show the chitosan can be hold the BiCP particle and protect the BiCP particle dispersion. Moreover, all groups clearly indicated that the increasing trend of cell number, except the chitosan group. On day 3, the good cell adhesion, elongation, formation into dense structure was found in the groups of chitosan with 2%, 4%, 6% and 8% BiCP, mostly cell was specific adhere to the BiCP nodule. In the chitosan without BiCP, the cell revealed the globular shape when compare to other groups. On day 5, the scaffold in all groups showed the good cell migration and attachment on the scaffold, except the chitosan group that showed cell less migration and circular structure.

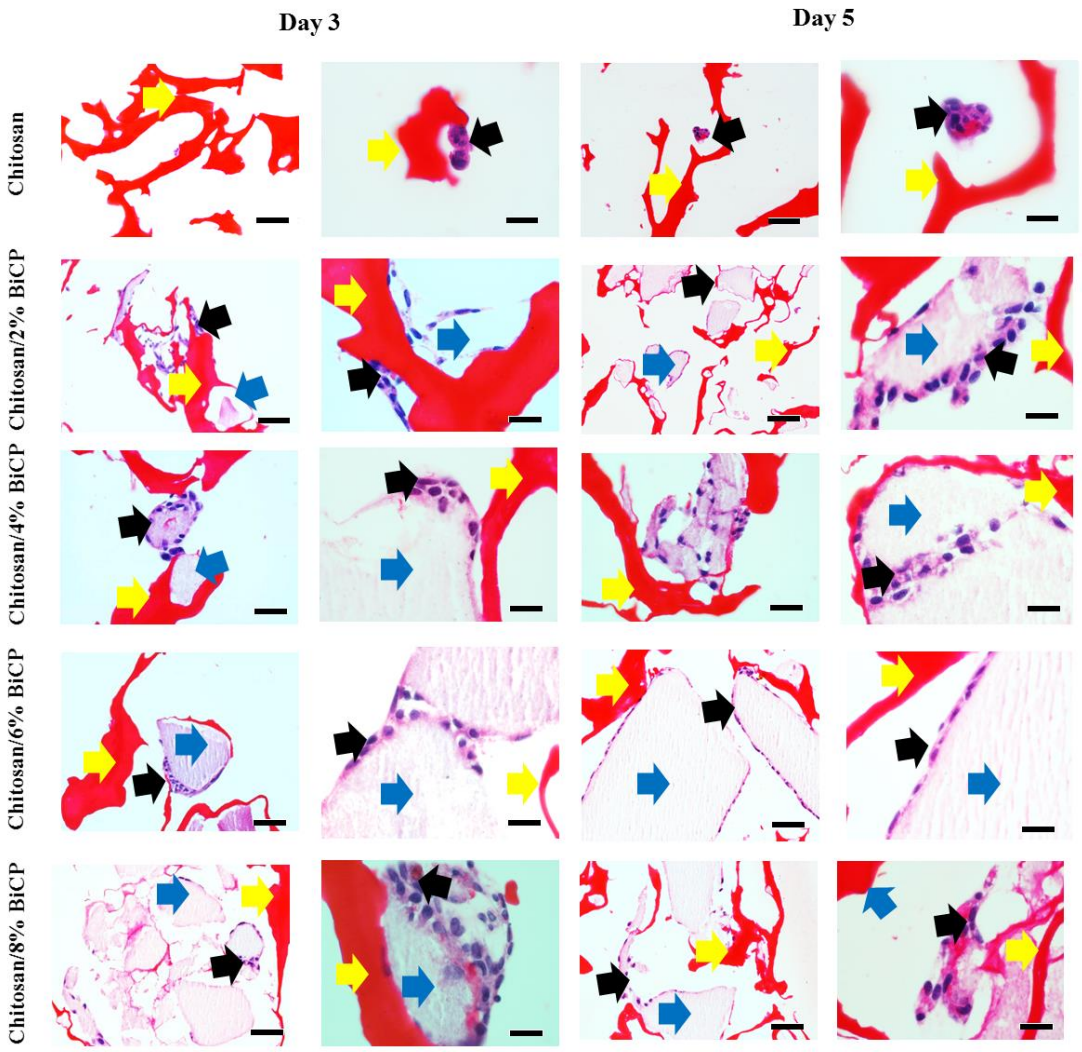

Figure 46. Histology of cultured osteoblast cell in scaffolds at difference time point at 3 and 5. Yellow, Blue, and Black arrows point chitosan, bicomponents calcium phosphate, and osteoblasts. Scale bar : 100 μm

Conclusion

In this research, chitosan with bicomponent calcium phosphate was fabricated into biomineralized scaffolds based on bioinspiration of bone remodeling. The results showed morphological formation of calcium phosphate deposition on chitosan fiber which is similar to biomineralization in bone remodeling. Physical performance of biomineralized scaffolds demonstrated dynamic behavior of swelling property and degradation which related to bone remodeling. Furthermore, biological performance of

biomineralized scaffolds was suitable to enhance bone formation. Finally, the results were deduced that biomineralized scaffolds based on bioinspiration of bone remodeling is promising for maxillofial tissue engineering particularly in chitosan with 2 and 4% of bicomponent calcium phosphate.

References

[1] Guziewicza N, Besta A, Perez-Ramireza B, Kaplan DL. Lyophilized silk fibroin hydrogels for the sustained local delivery of therapeutic monoclonal antibodies. Biomaterials. 32;2011:2642–2650.

[2] Chang G, Kim HJ, Kaplan D, Vunjak-Novakovic G, Kandel R. Porous silk scaffolds can be used for tissue engineering annulus fibrosus. European Spine Journal. 16:2007:1848–1857.

[3] Li TT, Ebert K, Vogel J, Groth T. Comparative studies on osteogenic potential of micro- and nanofibre scaffolds prepared by electrospinning of poly(ε-caprolactone). Progress in Biomaterials. 2;2013:1–13.

[4] Ji H. Lysis of cultured cells for immunoprecipitation. Cold Spring Harb Lab Protoc 2010:1–5.

CHAPTER 6

Bioactive composite hydrogel of agarose/ TiC-coated carbon nanoparticle for bone healing; morphological formation and biological performance

Abstract

Incomplete bone healing is a critical problem for many patients. An alternative choice to solve that problem is to create a bioactive composite hydrogel of agarose/TiC-coated carbon nanoparticles. In this research, agarose was mixed with different amounts of TiC-coated carbon nanoparticles (10, 50, 100, and 200 mg) before forming into hydrogels. Molecular organization and behaviors were characterized by FT-IR, DSC, and DMA. The morphologies of the TiC-coated carbon nanoparticles and hydrogels were observed with TEM, SEM, and LM. Wettability was analyzed by water contact angle measurement. Osteoblast cells were cultured on the hydrogels. Cell viability, adhesion, and proliferation were observed and analyzed. The biological performances for the purpose of bone healing were measured by ALP activity, osteocalcin synthesis, calcium deposition, and protein absorption. The results demonstrated that composite hydrogels showed molecular organization and behaviors via nanoparticle-agarose interaction. The composite hydrogels displayed low softness. They had morphology of networks of fused clusters of TiC-coated carbon nanoparticles in the agarose matrix. Those composite hydrogels showed bioactive functionalities to induce cell viability, adhesion, and proliferation. Furthermore, the composite hydrogels had unique ALP activity, osteocalcin synthesis, calcium deposition, and protein absorption. Finally, the results indicated that composite hydrogels are promising to induce bone healing.

Materials and methods

TiC/agarose hydrogel gel preparation

The TiC nanoparticles were prepared following the procedure in previous research [32]. The nanoparticles were added into 1% agarose solutions at different amounts: 10 mg; 50 mg; 100 mg; and 200 mg. The agarose without TiC was used as the control. The solutions were then poured into 48-well plates followed by drying at room temperature for 24 h. The samples were classified into 5 groups (Table.1)

Groups	Detail
Control	Agarose hydrogel without TiC
10 mg	Agarose hydrogel with 10 mg of TiC (w/v)
50 mg	Agarose hydrogel with 50 mg of TiC (w/v)
100 mg	Agarose hydrogel with 100 mg of TiC (w/v)
200 mg	Agarose hydrogel with 200 mg of TiC (w/v)

Table 5 The sample groups of TiC/agarose hydrogels

Morphological observation

The morphologies and structures were observed by scanning electron microscopy (SEM, JSM-5800LV, JEOL, Japan) and transmission electron microscopy (TEM, JEOL JEM-2010) at 35 kV and 200 kV, respectively.

Wettability of the membranes (water contact angle)

Membrane samples in each group were cut into 2×2 cm and at random in 3 points in different areas for hydrophilic and hydrophobic surface testing using the sessile drop technique (Dataphysics, Model OCA15EC, Filderstadt, Germany).The membrane was fixed with metal plate. Then, water was dropped on surface of membrane. The angle of water drop was measured, the 5 membranes in each group was used for water contact evaluation.

Differential scanning calorimetry (DSC)

After cutting the membrane into small pieces, the membranes were put in an aluminium pan and covered with a lid. Next, the samples in the pan were move into the differential scanning calorimetry (DSC7: Perkin-Elmer, USA). The temperature was set at a range of 25 to 300 °C and analyzed by increments of 5 °C

Dynamic mechanical analysis (DMA)

The membranes were cut into rectangular shapes before insertion in the Dynamic Mechanical Analyzer (DMA 1, Mettler-Toledo, USA). The condition was set for dynamic tension force of 4 Hz for 60 min at 37 °C under nitrogen gas at 20.0 ml/min.

Fourier transform infrared spectroscopy (FT-IR)

The molecular arrangementd of the membranes were observed with FT-IR (EQUINOX55, Bruker, Ettlingen, Germany). The range was set to 400–4000 cm^{-1} using the KBr disc technique.

Cell culturing

The 2×10^4 MG-63 osteoblast cell line was maintained in complete alpha-MEM medium (α-MEM, GibcoTM, Invitrogen, Carlsbad, CA, USA) with 10% fetal bovine serum, 1% penicillin/streptomycin and 0.1% Fungizone®. The cells were cultured in the agarose hydrogels with TiC under 5% CO_2 and 95% humidified air at 37 °C in an incubator. In the differentiation stage, the MG-63 osteoblast cells were cultured in osteogenic supplemented (OS) medium (OS: 20 mM b-glycerophosphate; 50 μM ascorbic acid; and 100 nM dexamethasone [Sigma-Aldrich]) [33].

Cell proliferation (AlamarBlue™)

Cell proliferation was evaluated with alarmarBlue® cell viability reagent (Invitrogen, Germany) after cell seeding in the agarose hydrogels with TiC on days 1,

3, 5, and 7. The media was removed and rinsed with PBS several times. The 10% alamarBlue reagent was added in the complete media and added to each group of the experiment after incubation at 37 °C for 1 h. An amount of 200 µl of solution was used for OD measurements.

Cell viability

The cells in each group were stained with fluorescein diacetate (FDA) on days 1 and 3 to observe cell viability. The media was removed from the TiC construct in agarose and washed with PBS 2 times. Fresh media was added in the agarose gel and 5 µg/ml of acetone was added in the fresh media and kept at room temperature for 5 min. The agarose gel was rinsed with PBS and observed under fluorescence microscopy [34].

Alizarin red staining

After culturing on days 7, 14, and 21, the agarose gel was removed, rinsed with PBS, and fixed with 4% formaldehyde for 15 min. The 2% alizarin red (Sigma-Aldrich, USA) solution was used to stain each group for 10 min, rinsed with dH_2O, and observed for calcium nodules under a microscope [35].

Protein synthesis

The cells were cultured in OS media on days 7, 14, and 21 to measure the protein. The TiC constructed in agarose was rinsed with PBS after removing the media. Then 800 µl of 1% Triton X was added in each group and frozen at –80 °C for 1 h and at room temperature for 1 h for 3 cycles. The agarose was crushed and removed to Eppendorf tubes. A centrifuge machine was used to separate the supernatant from the pellet. A cell lysis solution was used for the protein measurement following the manufacturer's instructions (Pierce BCA Protein Assay kit, Thermo Scientific, USA).

Alkaline phosphatase activity

A lysis solution was used for ALP activity using the Alkaline Phosphatase LiquiColor® Test (Human, Germany) on days 7, 14, and 21 following the manufacturer's instructions [36].

Osteocalcin assay

The lysis solution on day 7, 14 and 21 was used for the osteocalcin assay (Mouse Osteocalcin Enzyme Immunoassay kit, BT-470; Alfa Aesar Co, Inc., USA) following the manufacturer's instructions.

Statistical analysis

The data are represented as mean ± standard deviation, one-way ANOVA and Tukey's HDS test (SPSS 16.0 software package) was used for statistical measurements and comparisons. A $p < 0.05$ was accepted as statistically significant.

Results

Morphology of TiC-coated carbon nanparticles

The morphologies of the TiC-coated carbon nanoparticles are shown as SEM and TEM images (Fig. 1). The results based on the SEM image showed that the particles were approximately 40 nm in size and agglomerated. The TEM image revealed clearly a core-shell structure of the particles. An ultra-thin layer of TiC (shell) was formed on a carbon particle (core) due to the template growth mechanism of the reaction. The formation mechanism was already discussed in our previous work [37].

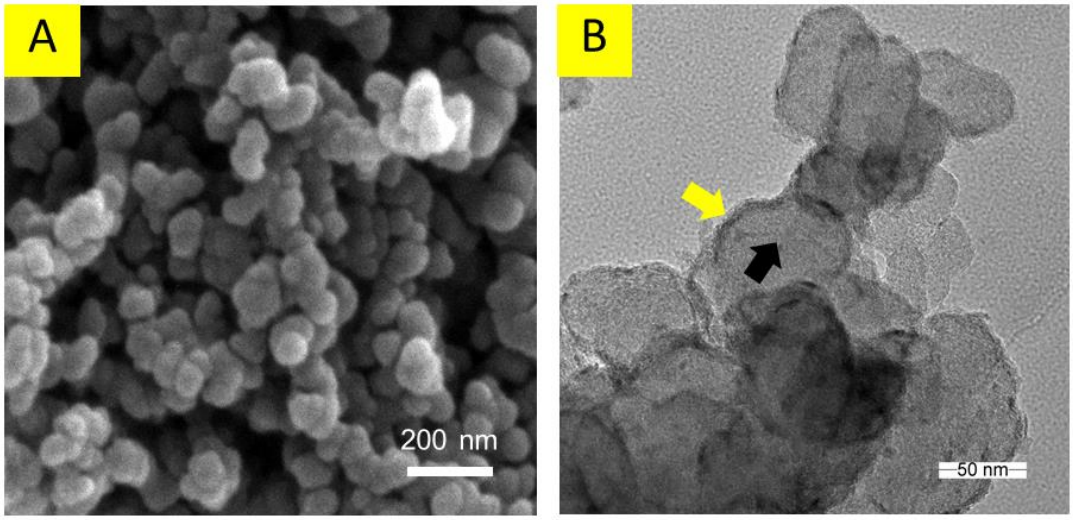

Figure 47. SEM image (A) and TEM image (B) of TiC-coated carbon nanoparticles. The yellow arrow indicates TiC coating layer and the black arrow designates the carbon core.

Morphologies of the hydrogels

TiC-coated carbon nanoparticles in agarose solutions were prepared before the hydrogels were formed. There were differences between the solutions. The results demonstrated that the transparency of the solutions decreased as the amount of nanoparticles increased (Fig. 2). The solution without nanoparticles was bright and colorless. The brightness of the solutions decreased as the amount of nanoparticles increased. The colors transformed from light gray to dark black from 10 to 500 mg of nanoparticles. Furthermore, the solutions had a homogenous texture.

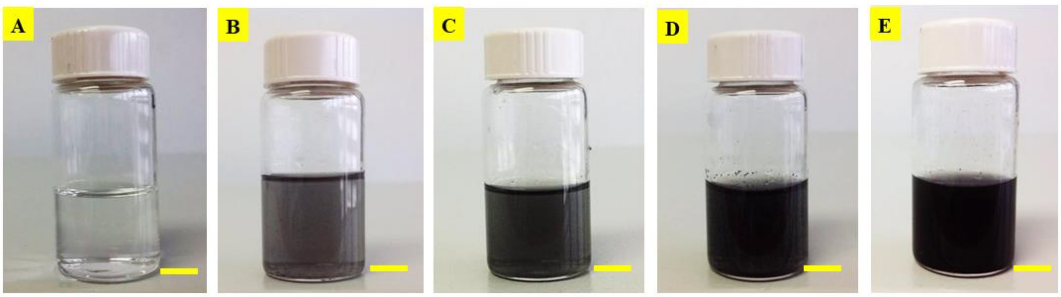

Figure 48. Agarose solutions at different concentrations of TiC-coated nanoparticles: agarose hydrogel without TiC-coated carbon nanoparticles (A); agarose hydrogels with 10 mg (B); 50 mg (C); 100 mg (D); and 200 mg (E) of TiC-coated carbon nanoparticles. The scale bar represents 1 cm.

After hydrogel formation, the appearances of the specimens were different (Fig. 3). The hydrogels displayed more turbidity than the solutions. The hydrogel without nanoparticles were white. On the other hand, the hydrogels with nanoparticles changed from light gray to dark black.

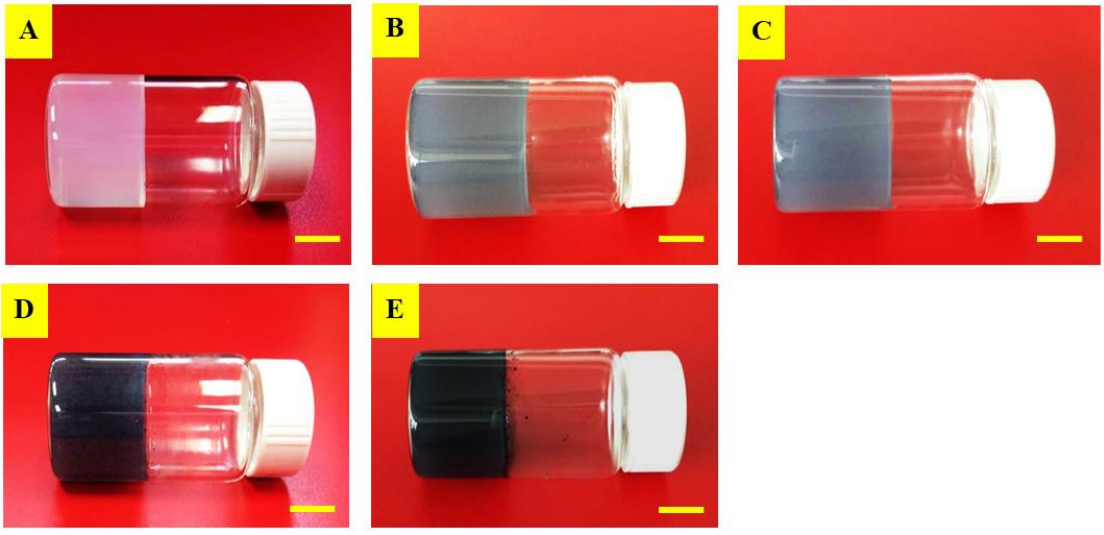

Figure 49. Hydrogel stages in agarose at different amounts of TiC-coated nanoparticles: agarose hydrogel without TiC-coated carbon nanoparticles (A); agarose hydrogels with 10 mg (B); 50 mg (C); 100 mg (D); and 200 mg (E) of TiC-coated carbon nanoparticles. The scale bar represents 1 cm.

Hydrogels were prepared into membranes for cell culturing. Fig. 4 shows the membranes after removal from the molds. The results demonstrated that the transparencies of the hydrogels decreased as the amount of nanoparticles increased and the hydrogels became darker.

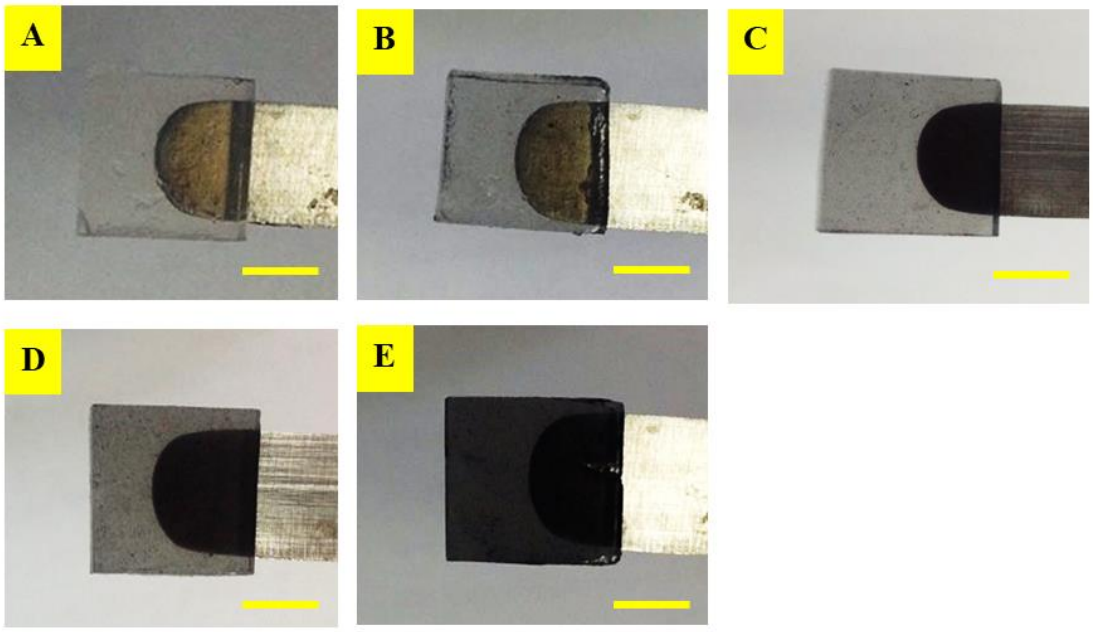

Figure 50. Agarose hydrogel membranes at different amounts of TiC-coated nanoparticles: agarose hydrogel without TiC-coated carbon nanoparticles (A); agarose hydrogels with 10 mg (B); 50 mg (C); 100 mg (D); and 200 mg (E) of TiC-coated carbon nanoparticles. The scale bar represents 5 mm.

The morphologies of the membrane hydrogels were observed by light microscopy (LM) (Fig. 5) and SEM (Figs. 6 and 7). The morphological structure, surface, and cross-sectional views of the hydrogels were observed. The images from LM demonstrated that the agarose hydrogel without the TiC-coated carbon nanoparticles had a clear continuous phase. The agarose hydrogel with TiC-coated carbon nanoparticles showed a discontinuous phase. The continuous phase was distributed in a continuous texture. The discontinuous phases indicated that the clusters became fused together as the amount of particles increased.

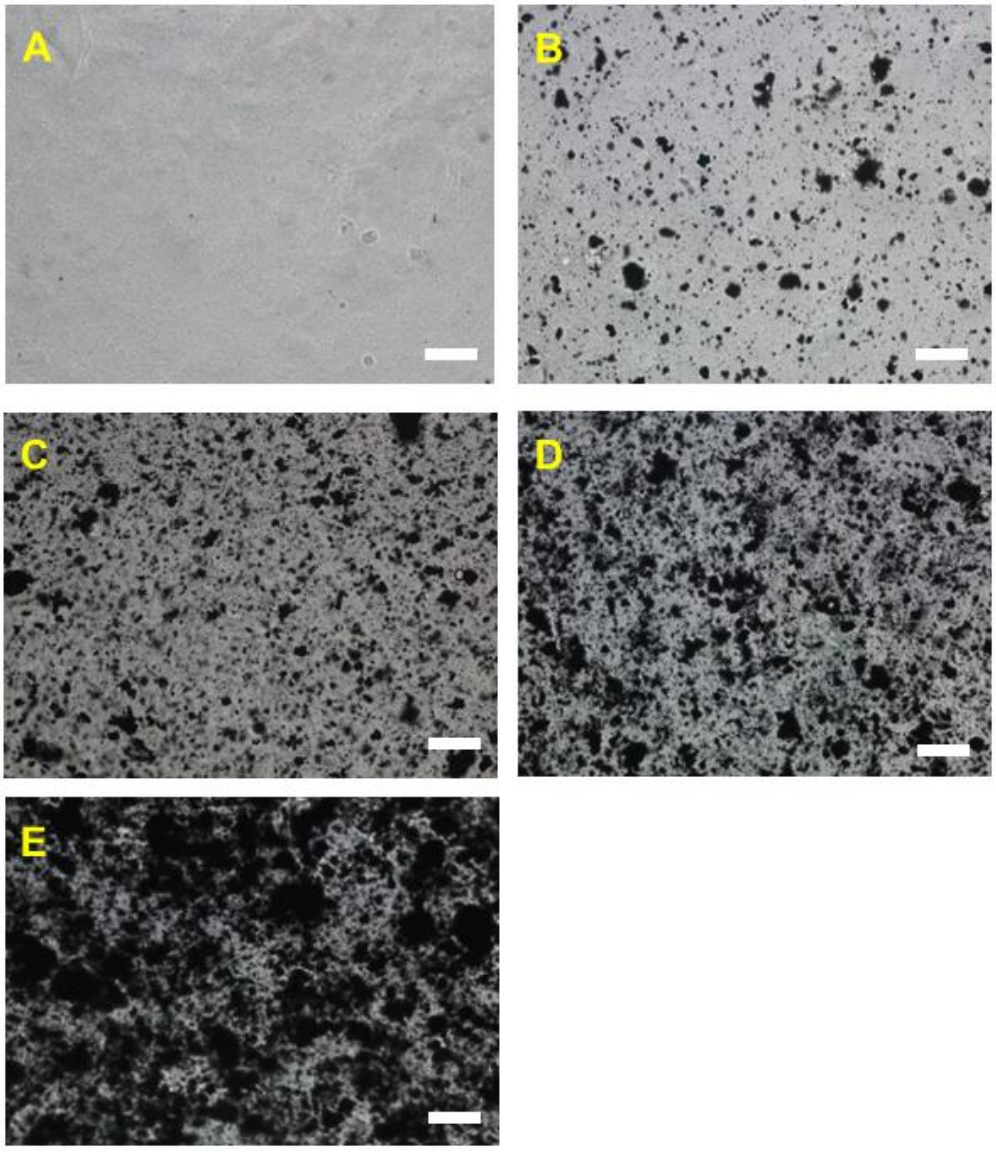

Figure 51. LM images of agarose hydrogel: without TiC-coated carbon nanoparticles (A); agarose hydrogels with 10 mg (B); 50 mg (C); 100 mg (D); and 200 mg (E) of TiC-coated carbon nanoparticles. Scale bar represents 200 μm.

SEM was used to better view the morphology of the hydrogel samples. The surface morphology showed some clusters of particles attached to the surface of the hydrogels with TiC-coated carbon nanoparticles (Fig. 6). The clusters were bigger as the amount of particles increased. The 200 mg nanoparticle samples displayed the biggest clusters of nanoparticles (Fig. 6E).

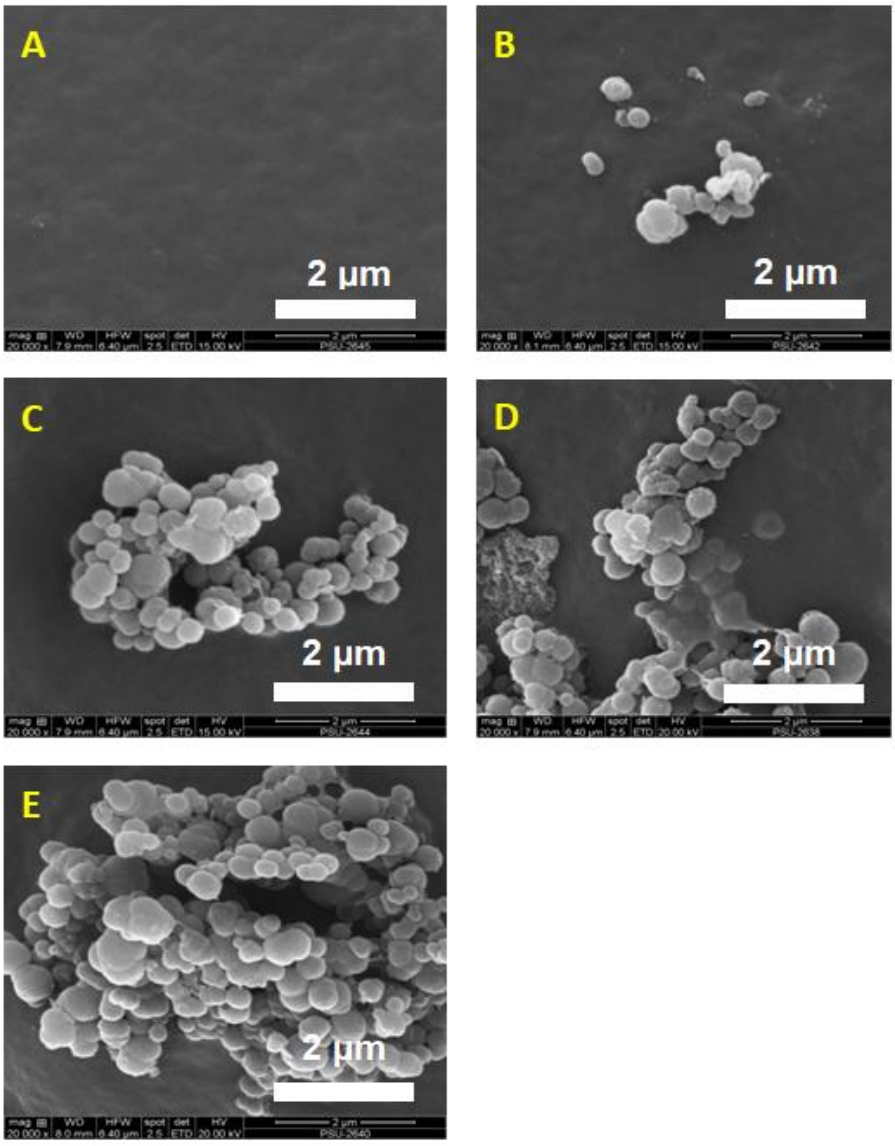

Figure 52. SEM surface images of agarose hydrogels: without TiC-coated carbon nanoparticles (A); agarose hydrogels with 10 mg (B); 50 mg (C); 100 mg (D); and 200 mg (E) of TiC-coated carbon nanoparticles.

The cross-sectional morphologies of the hydrogels with TiC-coated carbon nanoparticles showed multiple layers of fused clusters which aligned in the horizontal direction (Fig. 7). The multiple layers became denser as the amount of particles increased, particularly in the hydrogels with 100 and 200 mg of nanoparticles (Figs. 7D and E). In the case of

hydrogels without and with 20 mg of nanoparticles, the morphology showed a non-prominent formation of multiple layers (Figs. 7A and B).

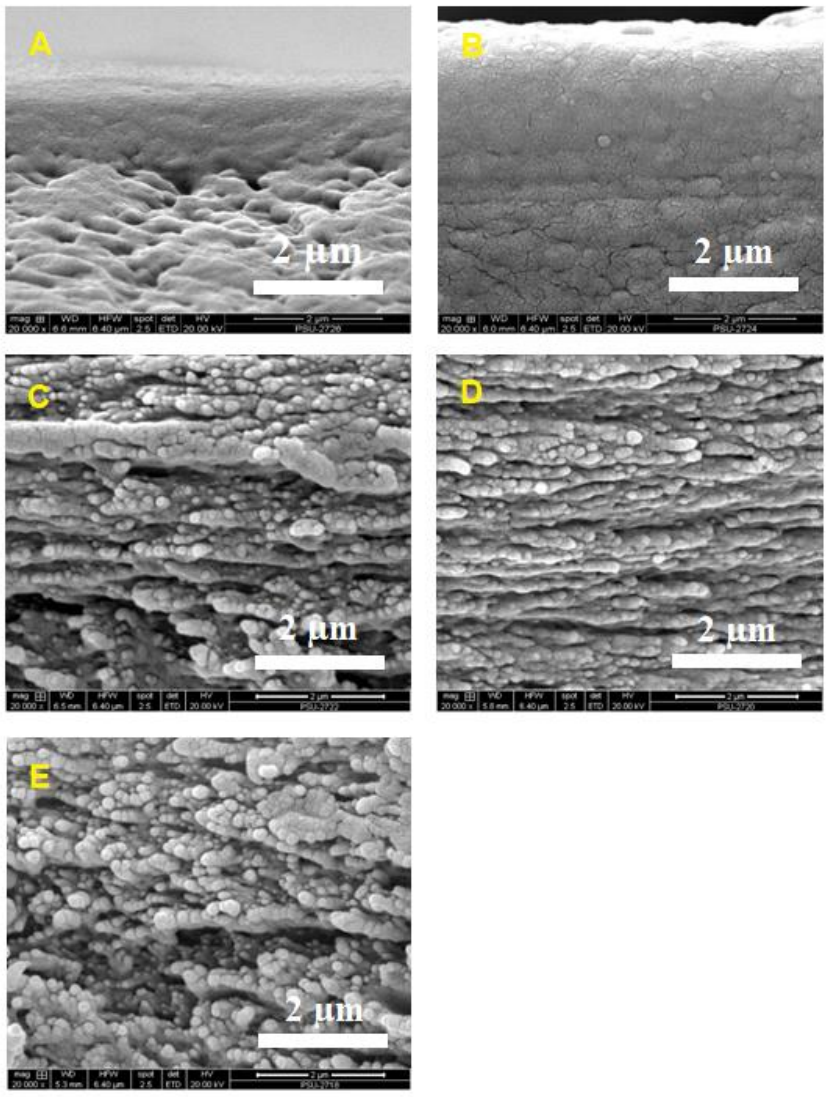

Figure 53. SEM cross-sectional images of agarose hydrogels: without TiC-coated carbon nanoparticles (A); agarose hydrogels with 10 mg (B); 50 mg (C); 100 mg (D); and 200 mg (E) of TiC-coated carbon nanoparticles.

FT-IR Spectroscopy

FT-IR spectroscopy was used to characterize the molecular organization of the hydrogels (Fig. 8). The results showed seven peaks at around 3360 (O-H bond

stretching) [38], 2920 (C-H bond stretching) [39], 1640 (water bending) [40], 1370 (C-H bond bending) [41], 1150 (C-O-C stretching) [42], and 1040 (glycosidic bonding) cm^{-1} [43]. The O-H of the control, 10, 50, 100, and 200 mg appeared around 3365, 3365, 3362, 3366, and 3359 cm^{-1}, respectively. The C-H of the control, 10, 50, 100, and 200 appeared around 2925, 2901, 2900, 2899, and 2898 cm^{-1}, respectively. Water bending of the control, 10, 50, 100, and 200 mg showed wavenumbers at around 1640, 1640, 1641, 1639, and 1640 cm^{-1}, respectively. The C-O-C stretching of the control, 10, 50, 100, and 200 demonstrated the same wavenumber at around 1151 cm^{-1}. Glycosidic bonding of the control, 10, 50, 100, and 200 mg appeared around 1040, 1040, 1040, and 1039 cm^{-1}, respectively.

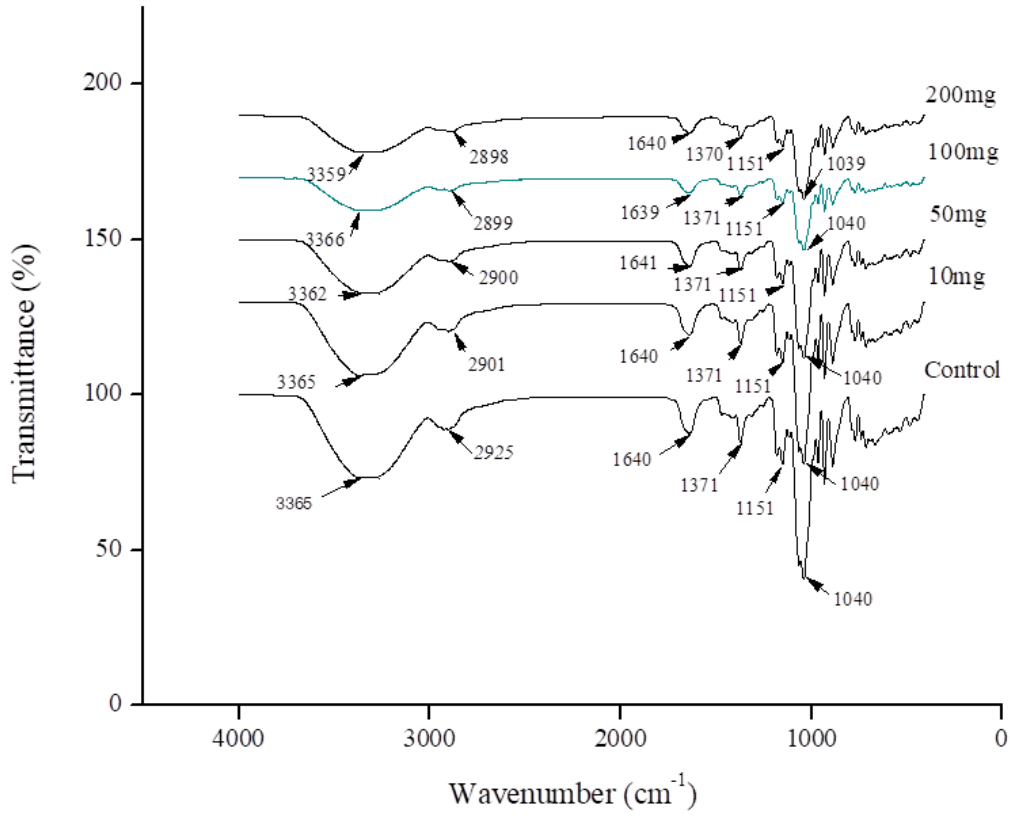

Figure 54. FT-IR spectroscopy analysis of the hydrogels in all groups.

DSC characterization

DSC was selected to characterize structural organization of the hydrogels in this research (Fig.9 and 10). The results showed two regions in the DSC spectrum which refer to the structural organization of the hydrogels (Figure 8). The first region is the peak at around 60 to 70 °C. This is the dehydration peak of the hydrogels [44]. The second region is the peak at around 250 to 350 °C. This is the melting temperature of the hydrogels. The dehydration peaks of the control, 10, 50, 100, and 200 mg hydrogels appeared around 60.6, 68.5, 68.4, 69.8, and 66.2 °C, respectively. The peak area of dehydration of the control, 10, 50, 100, and 200 mg hydrogels were 124.1, 332.7, 229.3, 289.7, and 209.5 J/g, respectively.

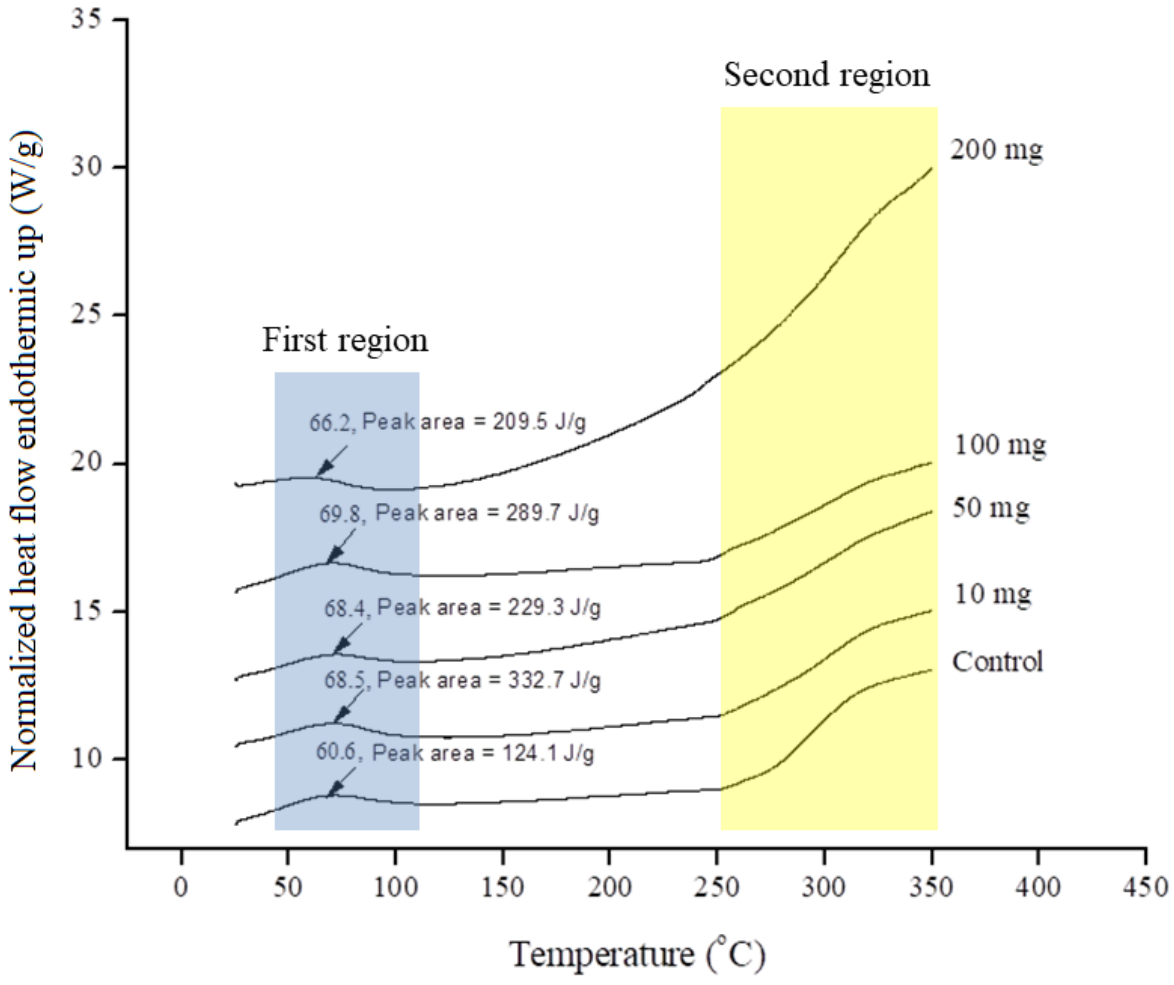

Figure 55. The DSC thermogram of the hydrogels in all groups.

The melting temperatures of the hydrogels are shown in Figure 10. The melting temperature of the control, 10, 50, 100, 200 mg hydrogels appeared around 313.7, 318.2, 316.6, 318.7, and 321.3 ^{o}C, respectively. The peak areas of the 10, 50, 100, 200 mg hydrogels appeared at around 291.4, 133.6, 62.8, 62.0, and 119.8 J/g, respectively.

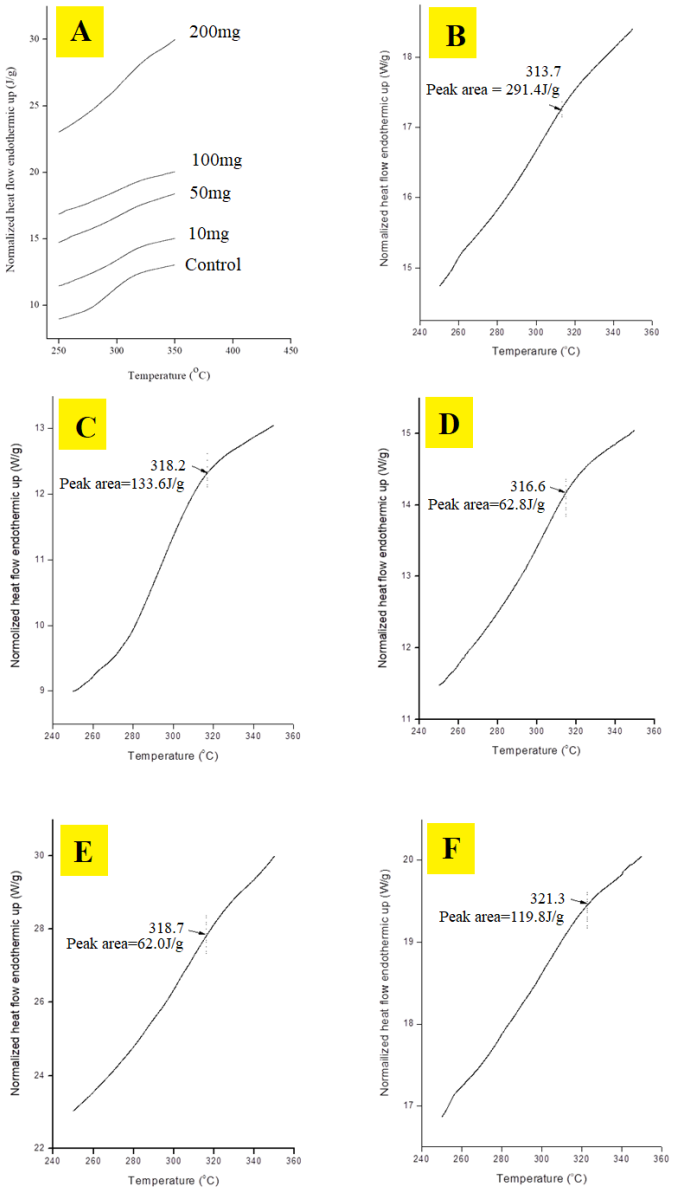

Figure 56. DSC thermograms: each hydrogel of all groups at the second region (A); control (B); 10 mg (C); 50 mg (D); 100 mg (E); 200 mg (F)

Dynamic mechanical analysis (DMA)

DMA was selected to characterize molecular behavior of hydrogels in this research (Fig.11). The tanδ was used to analyze energy dissipation which refers to the softness and hardness of the materials. Soft materials showed large energy dissipation. On the other hand, hard materials demonstrated small amounts of energy dissipation [45]. Principally, the existence of broad and large peaks in the DMA spectrum demonstrated large energy dissipation [46].

The results showed three groups in the DMA spectrum: 1) agarose without nanoparticles; 2) agarose with 10, 50, and 100 mg of nanoparticles; and 3) agarose with 200 mg of nanoparticles. The agarose without nanoparticles showed the existence of tanδ peaks. The second group had a decrease in the tanδ value from 0 to 10 min. The agarose with 200 mg of nanoparticles had no peaks of tanδ and showed a steady curve from 0 to 10 min.

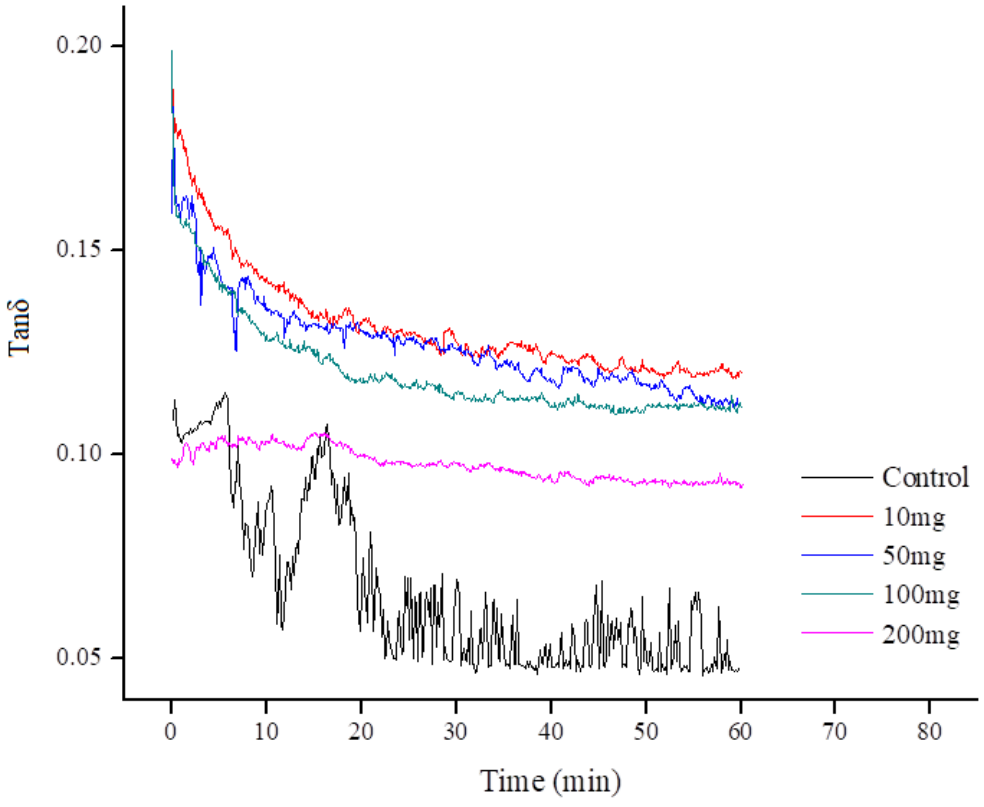

Figure 57. DMA spectrum of hydrogels of all groups

Water contact angle

The hydrophobicities of the membranes were evaluated by water contact measurements (Fig.12). The control and 200 mg had higher contact angles of about 52.42° and 53.84° respectively. The 10 mg, 50 mg, and 100 mg hyrogels showed a similar trend; however, the 100 mg hydrogel had a lower contact angle at around 24.08°. This result indicated that the modified agarose with TiC nanoparticles had increased hydrophilicity properties of the membranes, except the 200 mg hydrogel. Although all groups showed contact angles less than 90°, a water contact angle less than 90° indicates hydrophilicity.

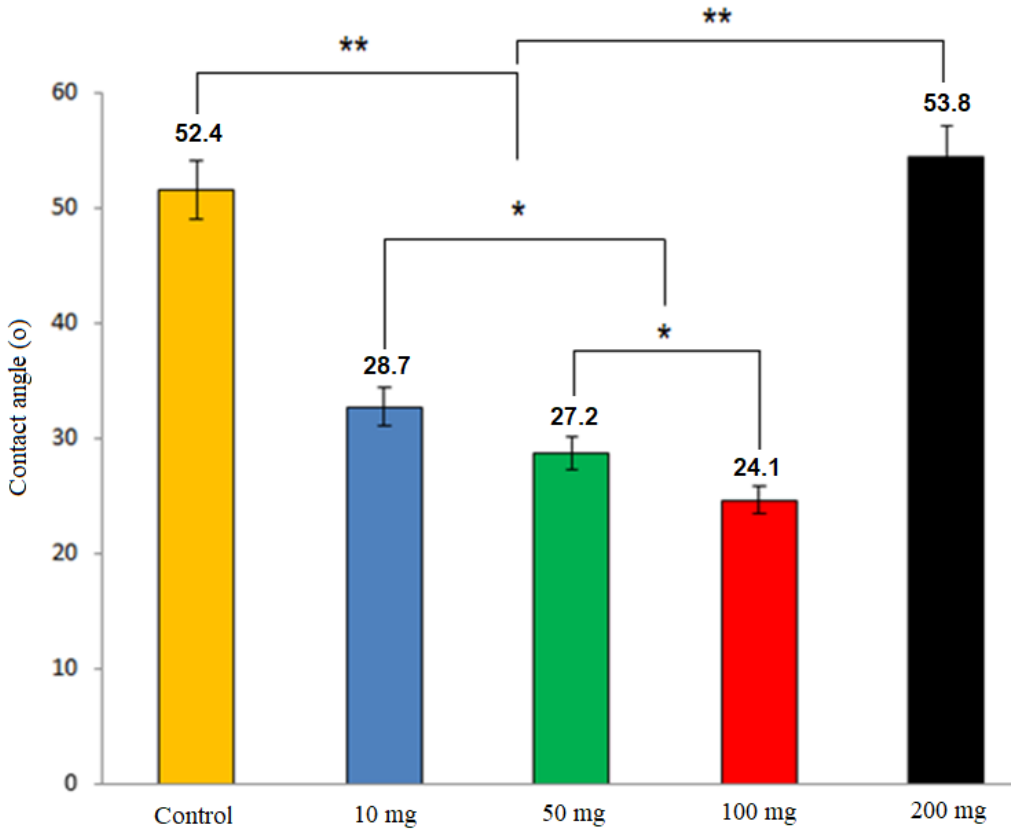

Figure 58. Water contact angles of the hydrogels in all groups.

Cell viability on the hydrogels

The cultured hydrogels were observed by a fluorescence microscope for cell viability (Fig. 13). Cell viability was observed with FDA staining after days 3 and 5. On day 3 the control and 10 mg showed less cell viability than the other groups. The 50 mg, 100 mg, and 200 mg hyrogels had higher cell viability. Cell viability increased as time elapsed. Cell viability clearly increased from day 3 to day 5, especially in the 50 mg, 100 mg, and 200 mg hydrogels.

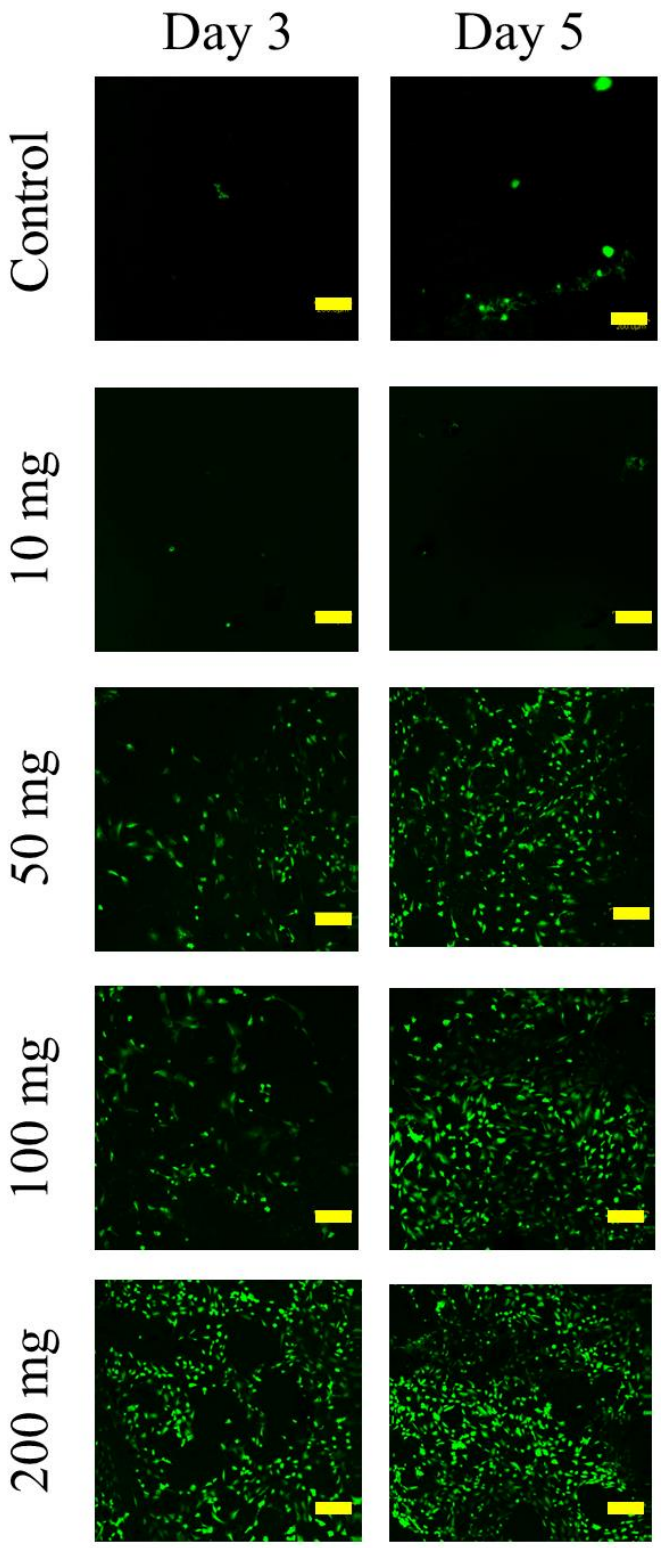

Figure 59. Fluorescence microscopy images of the cells in cultured agarose hydrogels: without TiC-coated carbon nanoparticles (A) and the agarose hydrogels with TiC-coated carbon nanoparticles at days 3 and 5. Scale bar 200 μm

Cell adhesion on the hydrogels

Cell adhesion on the hydrogels appeared as circular structures on the surface of the hydrogel with the TiC-coated carbon nanoparticles (Fig. 14). The hydrogels with TiC-coated carbon nanoparticles showed an elongated morphology of the cells. The hydrogel with the greatest amount of TiC-coated carbon nanoparticles (200 mg) distinctly showed cell adhesion and spreading on the clusters of the nanoparticles.

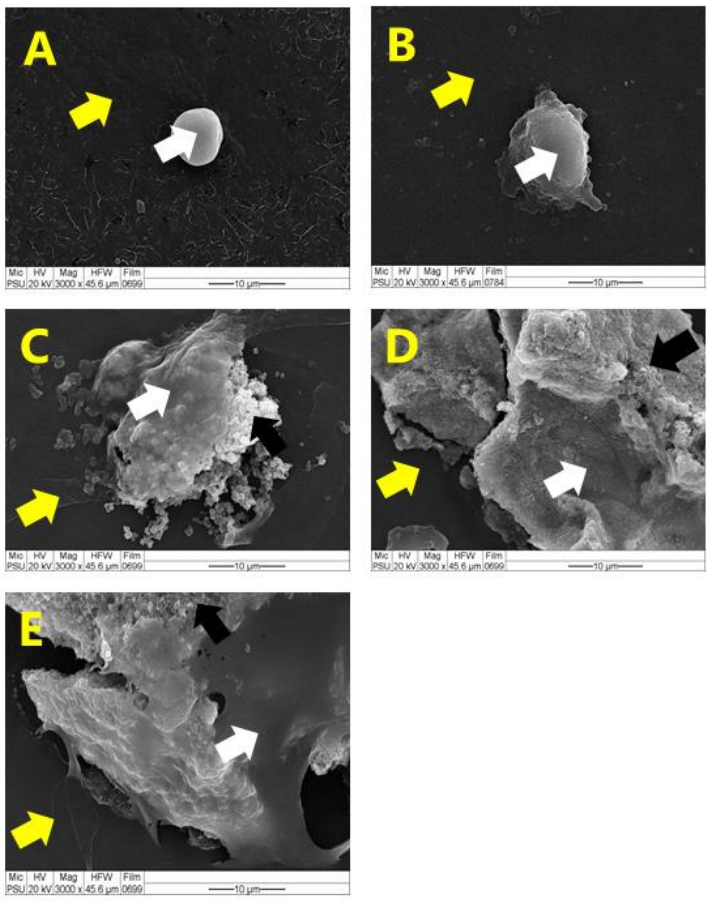

Figure 60. SEM images of cell adhesion on agarose hydrogel: without TiC-coated carbon nanoparticles (A); agarose hydrogels with 10 mg (B); 50 mg (C); 100 mg (D); and 200 mg (E) of TiC-coated carbon nanoparticles at day 3. Yellow arrows indicate the agarose texture, white arrows indicate cell adhesion, and black arrows indicate clusters of TiC-coated carbon nanoparticles.

Cell proliferation on the hydrogels

Cell proliferation was evaluated with AlarmarBlue on days 1, 3, 5, and 7. The trend indicated increased proliferation as time increased (Fig. 15). The 10 mg, 50 mg, and 100 mg hydrogels showed better cell proliferation than the control and 200 mg hydrogel on day 1. On day 3, the 10 mg, 50 mg, and 100 mg hydrogels still had significantly higher cell proliferation than the control and the 200 mg hydrogels and the 200 mg hydrogel showed higher cell proliferation than the control but the difference was not significant. Cell proliferation clearly increased from day 3 to day 5. Cell proliferation on the 200 mg hydrogel increased nearly to the levels of the 10 mg, 50 mg, and 100 mg hydrogels but the result was not significant. However, the hydrogels with TiC revealed significantly higher cell proliferation than the control. Cell proliferation was not significantly different between the 10 mg, 50 mg, and 100 mg hydrogels. However, with the exception of the 10 mg hydrogel, cell proliferations of the 50 mg and 100 mg hydrogels were higher than the control and 200 mg groups.

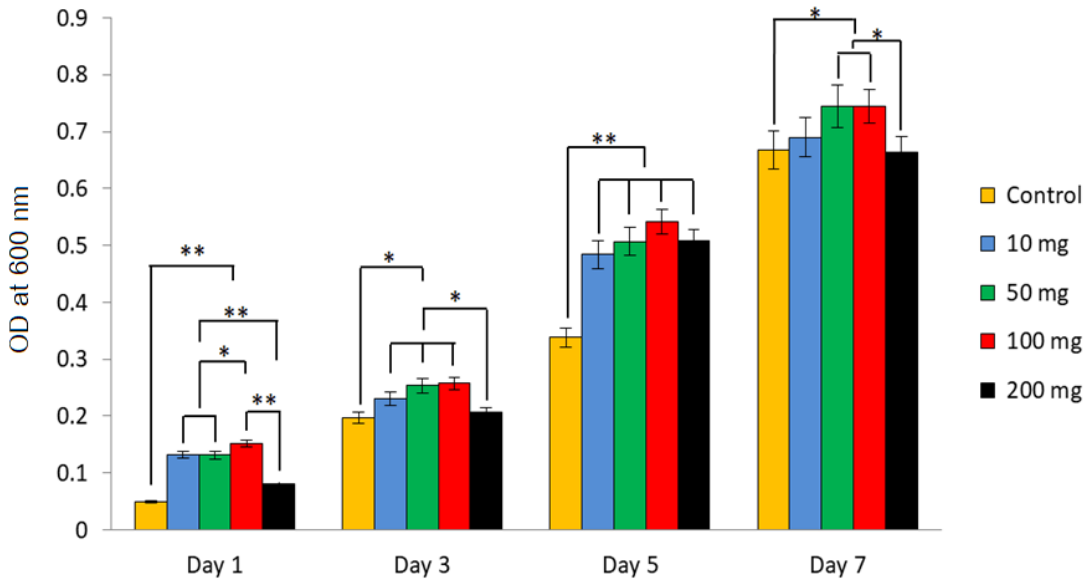

Figure 61. Cell proliferation of the agarose hydrogels with and without TiC-coated carbon nanoparticles at days 1, 3, 5, and 7.

ALP activity on the hydrogels

ALP activity was chosen as the biomarker to evaluate the biological performance in the early state of bone formation. At day 7, the results demonstrated that composite hydrogels of agarose with 10, 50, and 100 mg of particles had more ALP activity than the agarose without particles and agarose with 200 mg of particles (Fig. 16). Agarose with 100 mg of particles showed the most ALP activity. At day 14, the composite hydrogels of agarose with 50, 100, and 200 mg of particles had higher ALP activity than the agarose without particles and agarose with 10 mg of particles. Notably, the agarose hydrogel with 10 mg of particles had higher ALP activity than the agarose without particles. At day 21, the results showed no differences of ALP activity between any of the samples.

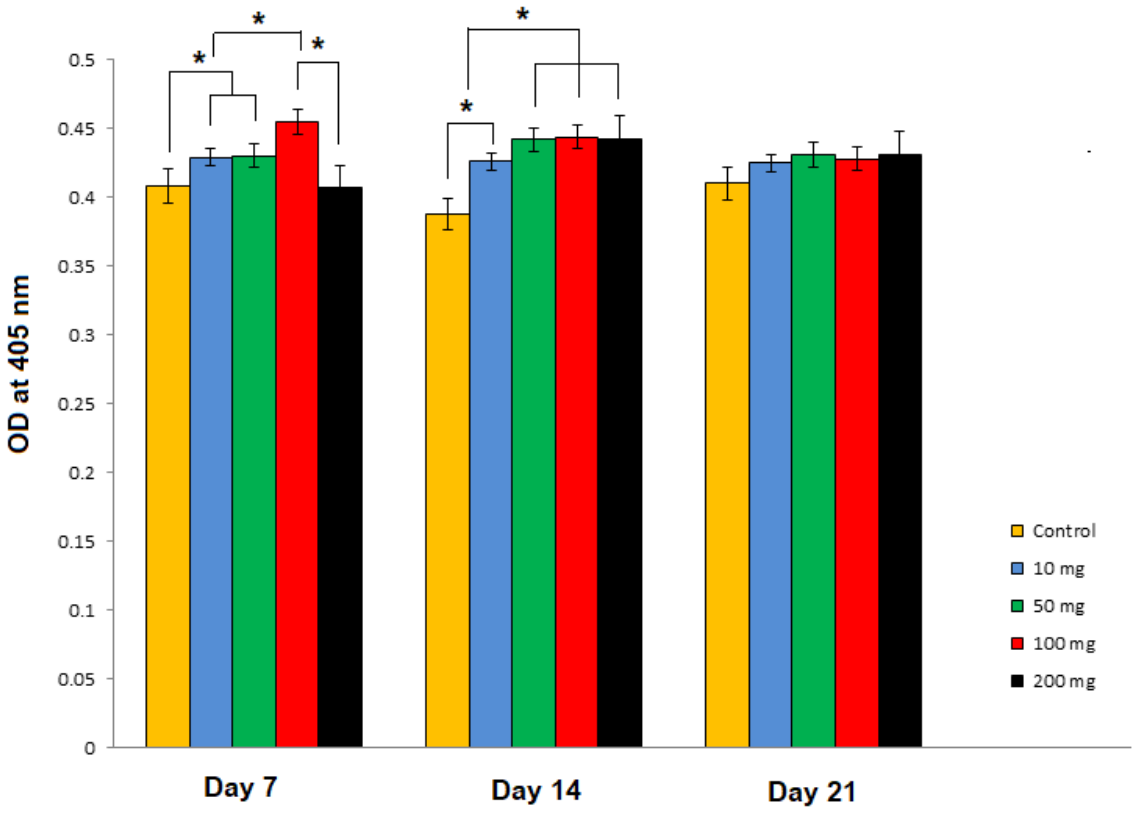

Figure 62. ALP activity of agarose hydrogels with and without TiC-coated carbon nanoparticles at days 1, 3, 5, and 7.

Calcium deposition on the hydrogels

Calcium deposition was also selected as a biomarker to evaluate biological performance. Calcium deposition is an indicator of the later state of new bone formation. The results demonstrated calcium deposition on all samples (Fig. 17). The red nodules identified the calcium clusters stained with Alizarin red. The agarose hydrogel showed some calcium deposition on the surface. However, the composite agarose hydrogels demonstrated high amounts of calcium deposition. Calcium deposition increased as the amounts of particles increased. The hydrogel with the highest amount of TiC-coated carbon nanoparticles (200 mg) displayed the most unique calcium deposition.

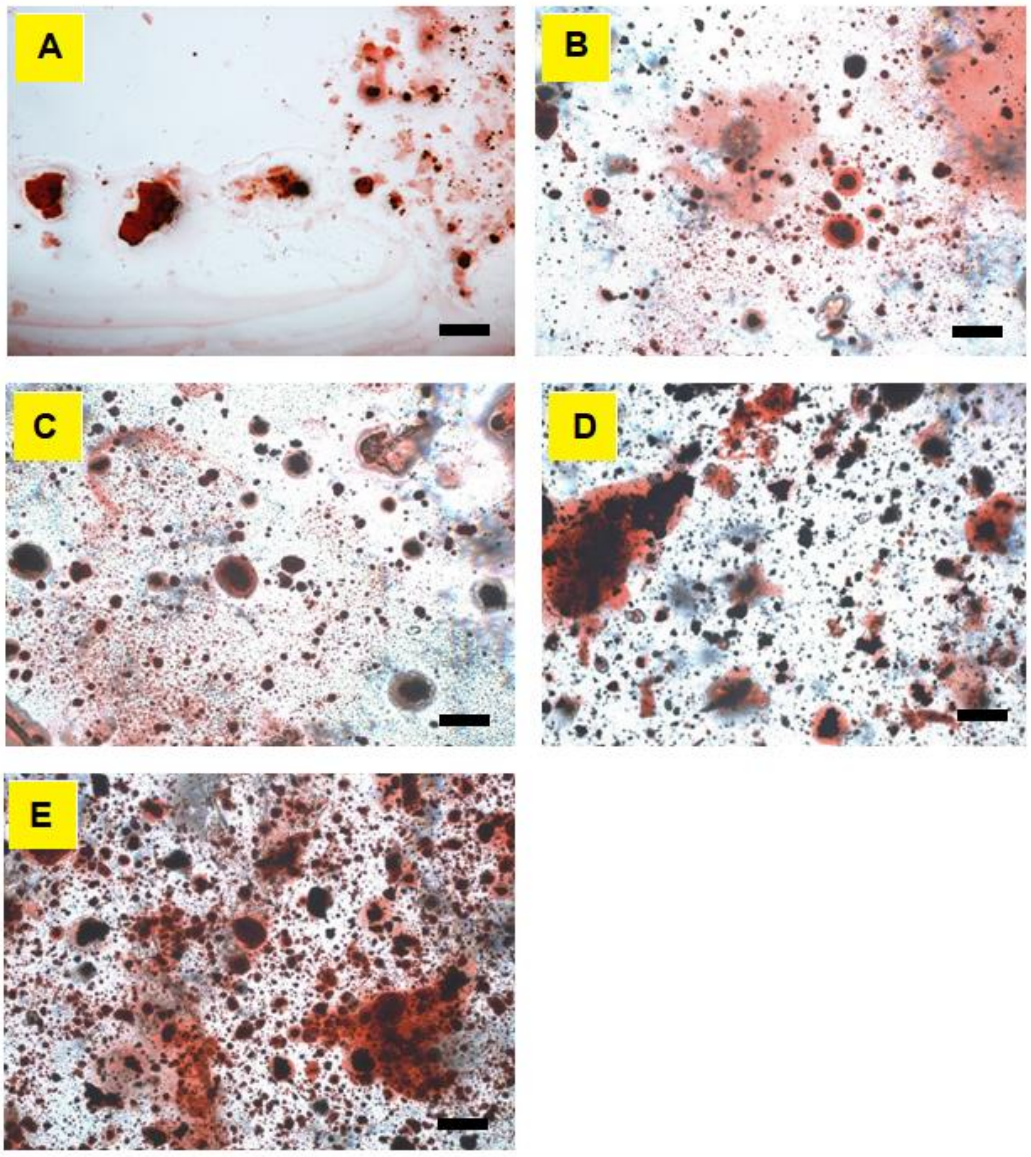

Figure 63. Calcium nodules on agarose hydrogels with and without TiC-coated carbon nanoparticles were detected with alizarin red staining on days 7: control A); 10 mg B); 50 mg C); 100 mg D); and 200 mg E). The red areas indicate calcium nodules. Scale bar 200 μm

Protein synthesis on the hydrogels

Protein synthesis was evaluated by the BCA kit on days 7, 14, and 21. On day 7, the 100 mg hydrogel showed a significantly higher percentage of protein synthesis compared with the other groups. The control, 10 mg, and 50 mg hydrogels

revealed no significant differences between them, but these groups were significantly lower than the 200 mg hydrogel (Fig.18). Protein synthesis became lower on day 14 and especially in the 50 mg hydrogel which showed significantly lower protein synthesis than the others. All groups showed similar protein synthesis except the 50 mg hydrogel. The control clearly showed a decrease in protein synthesis compared to the other hydrogels. All groups of TiC particles revealed rather similar results on day 21.

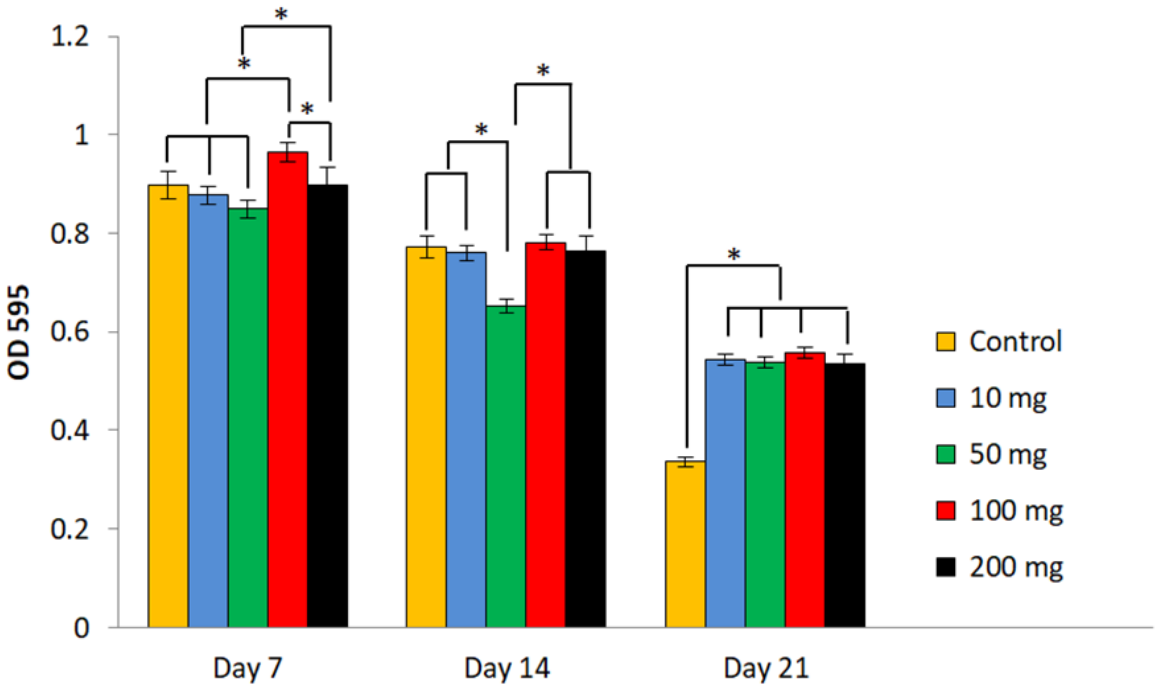

Figure 64. Protein synthesis of cells on agarose hydrogels with and without TiC-coated carbon nanoparticles at days 7, 14, and 21.

Osteocalcin synthesis on the hydrogel

Osteocalcin synthesis was evaluated with the Mouse Osteocalcin Enzyme Immunoassay kit, BT-470 (Alfa Aesar, USA) on days 7, 14, and 21. The results showed that osteocalcin increased as time elapsed (Fig.19). On day 7, the control was lower than the other groups. The modified agarose hydrogels (10 mg, 50 mg, 100 mg, and 200 mg) all showed good performance on osteoclacin synthesis, especially the 200 mg hydrogel. The 50 mg and 100 mg hydrogels clearly had increased osteocalcin

synthesis from day 7 to day 14 and the 200 mg hydrogel showed significantly higher synthesis than other groups. The control hydrogel showed the lowest amount of osteocalcin synthesis. The 100 mg and 200 mg hydrogels did not have significantly different osteocalcin synthesis on day 21. However, the 50 mg hydrogel had higher osteocalcin synthesis than the 10 mg and control hydrogels. The 100 mg and 200 mg hydrogels were also significantly higher than other groups.

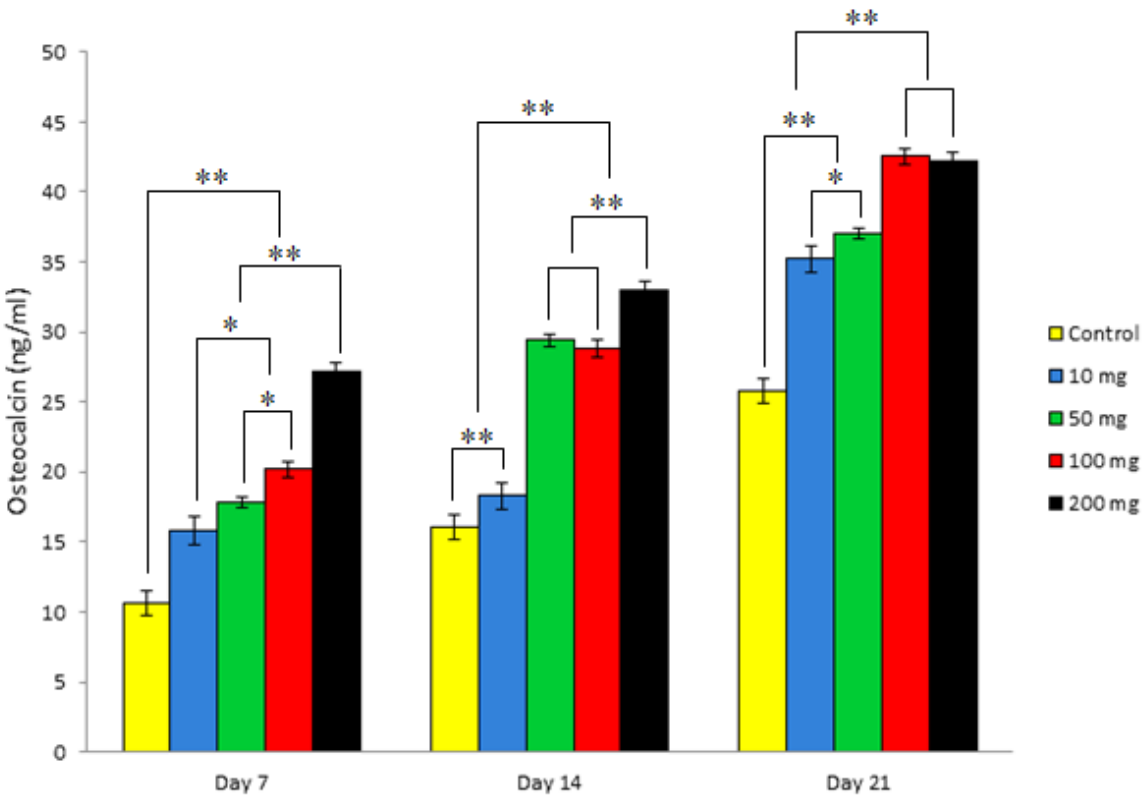

Figure 65. Osteocalcin synthesis on days 7, 14, and 21 after measurements with Mouse Osteocalcin Enzyme Immunoassay kit, BT-470.

Discussion

Physical appearance and performance of hydrogels

After preparation, the bioactive composite hydrogels were observed for physical appearance and performance. The hydrogels with different amounts of TiC coated carbon black nanoparticles had different colors. The hydrogels with high

amounts of nanoparticles were darker than the hydrogels with low amounts. This was due to the higher light absorbance of the high amounts of nanoparticles in the hydrogels [47]. The hydrogels with nanoparticles showed more turbidity than the hydrogel without nanoparticles. This was due to light scattering of the aggregations of nanoparticles [48].

The water contact angle was selected to evaluate the hydrophilicity of the materials. Principally, the materials which have a water contact angle greater than 90^{o} are identified as hydrophilic [49]. The results demonstrated that the hydrogels with nanoparticles showed greater hydrophilicity than the hydrogel without nanoparticles. This was due to the nanoparticles which provided a hydrophilic layer of TiC on their surface [50]. Interestingly, the over loading of nanoparticles in the 200 mg hydrogel had lower hydrophilicity than the other hydrogels. Particle aggregation led to the reduced hydrophilicity of the hydrogel [51]. Importantly, the various hydrophilicities of the hydrogels are critical because hydrophilicity has an effect on the biological performance, particularly in cell behavior [52]. Cell behavior offers important clues on how to evaluate the potential of hydrogels for use in bone healing. Therefore, this hypothesis was undertaken.

Molecular organization and behavior of hydrogels

FT-IR, DSC, and DMA were selected to characterize the hydrogels. The results of FT-IR characterization showed molecular organization of the hydrogels via chemical group interaction and mobility. There were two groups of molecular organization: 1) hydrophilic and 2) hydrophobic chemical groups.

The hydrophilic groups were mainly O-H which showed fluctuation of molecular organization as the amount of nanoparticles increased. The hydrogels with nanoparticles showed lower O-H wavenumbers than without nanoparticles. This indicated molecular organization via interaction of the O-H groups. The hydrophobic groups were mainly C-H which had decreasing wavenumbers as the amount of nanoparticles increased. This showed molecular organization via interaction of the C-H

groups. The result demonstrated that water bending showed the fluctuation of wavenumbers as the amount of nanoparticles increased. This indicated that water showed interaction and mobility in the molecular organization of the hydrogels with nanoparticles. Nevertheless, to comprehend water organization in hydrogels, DSC was used for characterization.

DSC characterization initially showed that the hydrogels with nanoparticles had higher dehydration temperatures than the hydrogel without nanoparticles. This indicated that the water in the hydrogels with nanoparticles self-organized with greater stability than without nanoparticles. Furthermore, the hydrogels with nanoparticles had higher peak areas than without the nanoparticles. Therefore, water organization in the hydrogels with nanoparticles had more regularity than the hydrogel without nanoparticles. The results also demonstrated that the hydrogels with nanoparticles had higher melting temperatures of the agarose than without nanoparticles which indicated that the hydrogels with nanoparticles had higher structural stability of the agarose than without nanoparticles. Interestingly, hydrogels with nanoparticles showed lower peak areas than without nanoparticles. This occurred because hydrogels with nanoparticles had higher irregular structures of agarose than without nanoparticles. This indicated that the hydrogels with nanoparticles showed structural stability which comes mainly from the agarose-nanoparticle interaction [53].

In the case of DMA which was selected to characterize molecular behavior of the hydrogels, the results showed that the hydrogel without nanoparticles had tanδ peaks related to energy dissipation of the material [54]. Principally, energy dissipation was indicated the softness of the material [55]. Therefore, the results demonstrated that the hydrogel without nanoparticles showed more softness than without nanoparticles. This was the result of the molecular mobility of agarose. The hydrogel with 200 mg of nanoparticles had a steady graph of DMA. This indicated that the hydrogel with a high amount of nanoparticles had the lowest softness. This showed the non-molecular mobility of agarose. In the case of hydrogels with 10, 50, and 100

mg, they showed decreasing curves before they reached the steady state. This indicated a fair amount of molecular mobility of agarose.

According to our results of molecular organization and behavior, the hydrogels with nanoparticles had unique molecular organization via the nanoparticle-agarose interaction. This led to low molecular mobility of agarose which reflected the low softness of the hydrogels. Interestingly, some reports demonstrated that the softness of materials acted as clues for cell regulation [56]. Nevertheless, to prove this was related to our results, further testing of the biological functions was undertaken.

Morphological formation of nanoparticles and hydrogels

The observed morphological formations of the nanoparticles and hydrogels were related to the biological performances. The results showed a nano-thin layer of TiC coating on the carbon nanoparticles. The nanoparticles organized themselves into aggregations via the physical forces [57]. The morphological formations of the hydrogels demonstrated that the nanoparticles organized themselves into a network of fused clusters which acted as a discontinuous phase or reinforcement part of composite hydrogels [58]. That discontinuous phase was distributed within the continuous phase or matrix of the composite hydrogels [59,60]. The network of fused clusters was also formed by the physical interaction between the particles. The cross-sectional image of the morphological formation showed multiple layers of nanoparticles that aligned themselves in a horizontal direction. This possibly resulted from the surface tension between air/hydrogel and substrate/hydrogel. Surface tensions can force nanoparticles to align themselves into a horizontal direction [61].

Cell behaviors on the hydrogels

Cell behaviors, cell viability, adhesion, and proliferation on hydrogels were described in this research. The results demonstrated that a high amount of nanoparticles enhanced cell viability. The hydrogel with the highest amount of

nanoparticles showed high bioactive surface area of TiC with more unique cell viability than the hydrogels with lower amounts and without nanoparticles [62]. In the case of cell adhesion, hydrogels with higher amounts of nanoparticles influenced the induction of cell adhesion, elongation, and spreading. TiC layers which have bioactive functionality might be the main effect to enhance cell adhesion [63]. However, the fluctuation of surface nanoparticle clusters can act as nodes for cell creeping which might be the cause of cell elongation and spreading. The higher amounts of nanoparticles had more bioactive functionality to induce cell proliferation than the lower amounts of nanoparticles [64].

Expression of bone healing

ALP activity, osteoclacin, calcium deposition, and protein absorption on hydrogels represent expressions of bone healing in this research. Principally, ALP activity and osteocalcin are the biomarkers related to the early state of bone healing [65]. The results demonstrated that hydrogels with higher amounts of nanoparticles showed more bioactive functionality to induce ALP activity and osteocalcin than lower amounts of nanoparticles. This occurred because greater amounts of TiC nanoparticles have an overall greater surface area than lower amounts of nanoparticles. This demonstrated that TiC showed the unique bioactive function to enhance ALP activity and osteocalcin [66].

The results indicated that the TiC layer of nanoparticles had the important role of promoting calcium deposition. This was due to the TiC layer which had the bioactive performance to act as a suitable substrate for calcium deposition [67]. Furthermore, the greater amount of nanoparticles had more surface area. The greater amount of high surface area contributed to the increased calcium deposition [68].

Finally, protein absorption on the hydrogels was related to the secreted biological signals during osteoblast cell growth. This is the biomarker related to bone healing [69]. Notably, the TiC layer performs as a bioactive substrate to capture

secreted proteins from osteoblast cells [70]. Interestingly, some reports demonstrate that the secreted biological signals of protein act as molecules connected to cells [71]. The connecting has an effect on the expression of cell behavior which leads to the induction of bone healing [72] .

The results of biological performance indicated that hydrogels with nanoparticles showed suitable performance to induce bone healing.

Conclusions

Agarose/TiC-coated carbon nanoparticles were fabricated into composite hydrogels for bone healing. The composite hydrogels showed the molecular organization and behavior via nanoparticle-agarose interaction which led to low softness. They had the morphological formation of a network of fused clusters of nanoparticles in the matrix and showed hydrophilic functionality. The composite hydrogels with the bioactive TiC-coated carbon nanoparticles demonstrated the important role of inducing cell adhesion, elongation, and spreading, and the composite hydrogels were able to enhance cell proliferation. Furthermore, they could promote the expression of the biomarkers including ALP activity, osteocalcin synthesis, calcium deposition, and protein absorption which are related to the biological performance of bone healing. Finally, this research indicated that composite hydrogels of agarose/TiC-coated carbon nanoparticles are a promising approach to bone healing.

References

[1] Henkel J, Woodruff MA, Epar DR, Steck R, Glatt V, Dickinson IC, Choong PE, Schuetz MA, Hutmacher DW. Bone Regeneration Based on Tissue Engineering Conceptions A 21st Century Perspective. Bone Res 2013;1:216–248.

[2] Einhorn TA, Gerstenfeld LC. Fracture healing: mechanisms and interventions, Nat Rev Rheumatol 2015;11:45–54.

[3] Wang W, Yeung KWK. Bone grafts and biomaterials substitutes for bone defect repair: A review. Bioact Mater 2017;2:224–247.

[4] Rau JV, Antoniac I, Cama G, Komlev VS, Ravaglioli A. Bioactive Materials for Bone Tissue Engineering, Biomed Res Int 2016;2016:1-3.

[5] Raucci MG, Guarino V, Ambrosio L. Biomimetic Strategies for Bone Repair and Regeneration, J Funct Biomater 2012;3:688–705.

[6] Short AR, Koralla D, Deshmukh A, Wissel B, Stocker B, Calhoun M. Hydrogels That Allow and Facilitate Bone Repair, Remodeling, and Regeneration, J Mater Chem B Mater Biol Med 2015;3:7818–7830.

[7] Gianluca T, Arianna DM, Antero O, Marta R. Composite Hydrogels for Bone Regeneration, Materials 2016;9:1-24.

[8] Yodmuang S, McNamara SL, Nover AB, Mandal BB, Agarwal M, TAN N, et al., Silk microfiber-reinforced silk hydrogel composites for functional cartilage tissue repair. Acta Biomater 2015;11:27–36.

[9] Zhao F, Yao D, Guo R, Deng L, Dong A, Zhang J. Composites of Polymer Hydrogels and Nanoparticulate Systems for Biomedical and Pharmaceutical Applications, Nanomaterials (Basel) 2015;5:2054–2130.

[10] Qinyuan C, Yang J, Xinjun Y. Hydrogels for Biomedical Applications: Their Characteristics and the Mechanisms behind Them, Gels 2017;3:1-15.

[11] Ahmed EM. Hydrogel: Preparation, characterization, and applications: A review, J Adv Res 2015;6:105–121.

[12] Varoni E, Tschon M, Palazzo B, Nitti P, Martini L, Rimondini L. Agarose Gel as Biomaterial or Scaffold for Implantation Surgery: Characterization, Histological and Histomorphometric Study on Soft Tissue Response, Connect Tissue Res. 2012;53:548-554.

[13] Chao PG, Yodmuang S, Wang X, Sun L, Kaplan D, Vunjak NG. Silk hydrogel for cartilage tissue engineering. J Biomed Mater Res B Appl Biomater 2010;95:84–90.

[14] Tozzi G, Mori DA, Oliveira A, Roldo M. Composite Hydrogels for Bone Regeneration, Materials 2016;9:1-24.

[15] Kondiah PJ, Choonara YE, Kondiah PP, Marimuthu T, Kumar P, du Toit LC, Pillay V. A Review of Injectable Polymeric Hydrogel Systems for Application in Bone Tissue Engineering. Molecules 2016;21:1-31.

[16] Li X, Xu H, Chen ZS, Chen G. Biosynthesis of Nanoparticles by Microorganisms and Their Applications, Journal of Nanomaterials 2011;2011:1-16.

[17] I. Khan K, Saeed IDK. Nanoparticles: Properties, applications and toxicities. Arabian Journal of Chemistry 2017 https://doi.org/10.1016/j.arabjc.2017.05.011.

[18] Jong WHD, Borm PJ. Drug delivery and nanoparticles: Applications and hazards. Int J Nanomedicine 2008;3:133–149.

[19] Ferraro A. Biomaterials and therapeutic applications, IOP Conf. Ser : Mater Sci Eng 2016;108:1-5.

[20] Manivannan R. Nano Technology: A Review, JAPS 2011;2:8-16.

[21] Monteiro N, Martins A, Reis RL, Neves NM. Nanoparticle-based bioactive agent release systems for bone and cartilage tissue engineering, Regenerative Therapy 2015;1:109–118.

[22] Cha C, Shin SR, Annabi N, Dokmeci MR, Khademhosseini A. Carbon-Based Nanomaterials: Multi-Functional Materials for Biomedical Engineering, ACS Nano 2013;6:2891–2897.

[23] Qi LY, Michael G, Feng QZ, Adva C, Si PP. Highly energetic compositions based on functionalized carbon nanomaterials, Nanoscale 2016;9:4799-4851.

[24] Kokorina AA, Prikhozhdenko ES, Sukhorukov GB, Sapelkin AV, Goryacheva IY. Luminescent carbon nanoparticles: synthesis, methods of investigation, applications, Russ Chem Rev 2017;86:1157–1171.

[25] Khan I, Saeed K, Khan I. Nanoparticles: Properties, applications and toxicities, Arabian Journal of Chemistry. 2017. https://doi.org/10.1016/j.arabjc.2017.05.011.

[26] Zhang ZG, Li ZH, Mao ZH, Wang WC. Advances in bone repair with nanobiomaterials: mini-review, Cytotechnology 2011;63:437–443.

[27] Hamilton RF, Xiang C, Li M, Ka I, Yang F, Ma D, et al., Purification and sidewall functionalization of multiwalled carbon nanotubes and resulting bioactivity in two macrophage models, Inhal Toxicol 2013;25:199–210.

[28] Zdenek S, Jaroslav S. Bio-Compatible Ceramics as Mimetic Material for Bone Tissue Substitution, Journal of Thermal Analysis and Calorimetry 2007;88:1-49.

[29] Ozcan M, Hammerle C. Titanium as a Reconstruction and Implant Material in Dentistry: Advantages and Pitfalls, Materials 2012;5:1528–1545.

[30] Li Y, Munir KS, Lin J, Wen C. Titanium-niobium pentoxide composites for biomedical applications, Bioactive Materials 2016;1:127–131.

[31] Brama M, Rhodes N, Hunt J, Ricci A, Teghil R, Migliaccio S, et al., Effect of titanium carbide coating on the osseointegration response in vitro and in vivo, Biomaterials 2007;28:595–608.

[32] Hnin NS, Matthana K, Supaporn S, Jirut M, Rungrote K. TiC-coated carbon particles as bioactive substrates for inducing of mineralization in bone healing, Materials Letters. 2018;229:118–121.

[33] Kim BS, Kang HJ, Lee J. Improvement of the compressive strength of a cuttlefish bone-derived porous hydroxyapatite scaffold via polycaprolactone coating, J Biomed Mater Res B Appl Biomater 2013;101:1302–1309.

[34] Li TT, Ebert K, Vogel J, Groth T. Comparative studies on osteogenic potential of micro- and nanofibre scaffolds prepared by electrospinning of poly(ε-caprolactone), Progress in Biomaterials 2;2013:1–13.

[35] Wang HY, Liu Y, Maye P, Rowe DW. Examination of mineralized nodule formation in living osteoblastic cultures using fluorescent dyes, Biotechnology 2006;22:1697–1701.

[36] H. Ji, Lysis of cultured cells for immunoprecipitation, Cold Spring Harb Lab Protoc 2010 (2010) 1–5.

[37] Hnin NS, Matthana K, Supaporn S, Jirut M, Rungrote K. TiC-coated carbon particles as bioactive substrates for inducing of mineralization in bone healing, Materials Letters. 2018;229:118–121.

[38] Kloprogge JT, Frost RL, Hickey L. FT-Raman and FT-IR spectroscopic study of the local structure of synthetic Mg/Zn/Al-hydrotalcites, Journal of Raman Spectroscopy 2004;35:967-974.

[39] Sergei VB, Myshakina SN, Asher SA. Dependence of Glycine CH2 Stretching Frequencies on Conformation, Ionization State, and Hydrogen Bonding, J Phys Chem B. 2008;112:5803–5812.

[40] Litke A, Su Y, Tranca I, Weber T, Hensen EGH, Hofmann JP. Role of Adsorbed Water on Charge Carrier Dynamics in Photoexcited TiO2, J Phys Chem C. 2017;121:7514–24.

[41] Safwat M, Hoseny El, Pierre B, Gabriel MDO, Costa LMM. Natural ECM-Bacterial Cellulose Wound Healing—Dubai Study, Journal of Biomaterials and Nanobiotechnology 2015;6:237-246.

[42] Qing JS. Chapter 18 - Starch Nanoparticles, Starch in Food (Second Edition) 2017;18:691-745.

[43] Marta K, Mohamed M. FTIR and laser-Raman spectra of oligosaccharides in water: characterization of the glycosidic bond, Carbohydrate Research 284 (1996) 145 – 157.

[44] Khalid EK. Gelation Kinetics of PAM/PEI System: DSC Investigation, Journal of Thermal Analysis and Calorimetry 2014;116:1409–1415.

[45] Barthelat MM. The quest for stiff, strong and tough hybrid materials: an exhaustive exploration, J R Soc Interface 2013;10:1-8.

[46] Tomas J, Madera S, Manjusri M, Lawrence TD, Daniel R. Preparation and Characterization of Biodegradable Agar/Poly(butylene adipate-co-terephatalate) Composites, Polymer Engineering and Science 2009;49:1117 – 1126.

[47] Shang J, Xiaohu G. Nanoparticle Counting: Towards Accurate Determination of the Molar Concentration, Chem Soc Rev 2014;43:7267–7278.

[48] Hnin NS, Matthana K, Supaporn S, Jirut M, Rungrote K. TiC-coated carbon particles as bioactive substrates for inducing of mineralization in bone healing, Materials Letters 2018;229:118–121.

[49] Urrutia AM, Arroiabe PFD, Ramirez M, Agirre MM, Ali MMB. Contact angle measurement for LiBr aqueous solutions on different surface materials used in absorption systems Mesure de l'angle de contact pour les solutions aqueuses de LiBr sur différents matériaux de surface utilises dans les systemes a absorption, International Journal of Refrigeration 2018;95:182-188.

[50] Shah SA, Habib T, Gao H, Gao P, Sun W, Green MJ. Template-free 3D titanium carbide (Ti3C2Tx) MXene particles crumpled by capillary forces, Chem. Commun 2017;53:400-403.

[51] Chiu CC, Moore PB, Shinoda W, Steven ON. Size-dependent hydrophobic to hydrophilic transition for nanoparticles:A molecular dynamics study, J Chem Phys 2009;131:1-8.

[52] Steven RC, Jason AB. A Practical Guide to Hydrogels for Cell Culture, Nat Methods 2016;13:405–414.

[53] Xiaoyuan M, Xia Y, Lili M, Liangjing M, Zhouping W. Preparation of gold nanoparticles–agarose gel composite and its application in SERS detection, Spectrochimica Acta Part A: Molecular and Biomolecular Spectroscopy 2014;121:657–661.

[54] Muthusamy S, Wang S, Chung DDL. Unprecedented vibration damping with high values of loss modulus and loss tangent, exhibited by cement–matrix graphite network composite, CARBON 2010;48:1457 – 1464.

[55] Phaner-Goutorbe M, Iazykov M, Villey R, Sicard D, Robach Y. Energy dissipation effects on imaging of soft materials by dynamic atomic force microscopy: A DNA-chip study, Materials Science and Engineering C 2013;33: 2311–2316.

[56] Murphy WL, McDevitt TC, Engler AJ. Materials as stem cell regulators, Nat Mater 2014;13:547–557.

[57] Ali AZ, Zia HM, Haq UI, Phull AR, Ali JS, Hussain A. Synthesis, characterization, applications, and challenges of iron oxide nanoparticles. Nanotechnol Sci Appl 2016;9:49–67.

[58] Goponenko AV, Dzenis YA. Role of Mechanical Factors in Applications of Stimuli-Responsive Polymer Gels – Status and Prospects, Polymer 2016;101:415–449.

[59] Meid J, Friedrich T, Tieke B, Lindner P, Richtering W. Composite hydrogels with temperature sensitive heterogeneities: influence of gel matrix on the volume phase transition of embedded poly-(N-isopropylacrylamide) microgels, Phys Chem Chem Phys 2011;13:3039–3047.

[60] Cassidy S, Kaylee M, Emil J, Rupak MR. Application of Composite Hydrogels to Control Physical Properties in Tissue Engineering and Regenerative Medicine, Gels 2018;4:1-13.

[61] Ody T, Panth M, Sommers MAD, Eid KF. Controlling the Motion of Ferrofluid Droplets Using Surface Tension Gradients and Magnetoviscous Pinning, Langmuir 2016;32:6967–6976.

[62] Brama M, Rhodes N, Hunt J, Ricci A, Teghil R, Migliaccio S, et al., Effect of titanium carbide coating on the osseointegration response in vitro and in vivo. Biomaterials 2007;28:595–608.

[63] Jemat A, Ghazali MJ, Razali M, Otsuka Y. Surface Modifications and Their Effects on Titanium Dental Implants. Biomed Res Int 2015;2015:1-11.

[64] Liu XQ, Tang RZ. Biological responses to nanomaterials: understanding nano-bio effects on cell behaviors, Drug Delivery 2017;24:1–15.

[65] Kuo TR, Chen CH. Bone biomarker for the clinical assessment of osteoporosis: recent developments and future perspectives. Biomark Res 2017;5:1-9.

[66] Longo G, Ioannidu CA, Scotto AA, Superti F, Misiano C, Zanoni R, et al., Improving Osteoblast Response In Vitro by a Nanostructured Thin Film with Titanium Carbide and Titanium Oxides Clustered around Graphitic Carbon, PLoS One 2016;11:1-22.

[67] Kun M, Cuie W, Elena PI, Christopher CB, Wang J. Sputtered Hydroxyapatite Nanocoatings on Novel Titanium Alloys for Biomedical Applications, 2013. IntechOpen, DOI: 10.5772/54263.

[68] Bobbert FSL, Zadpoor AA. Effects of bone substitute architecture and surface properties on cell response, angiogenesis, and structure of new bone, J. Mater. Chem. B 2017;5:6175-6192.

[69] Gandavarapu NR, Mariner PD, Schwartz MP, Anseth K. Extra-cellular matrix protein adsorption to phosphate-functionalized gels from serum promotes osteogenic differentiation of human mesenchymal stem cells. Acta Biomater 2013;9:4525–4534.

[70] Longo G, Ioannidu CA, Scotto AA, Superti F, Misiano C, Zanoni R, et al., Improving Osteoblast Response In Vitro by a Nanostructured Thin Film with

Titanium Carbide and Titanium Oxides Clustered around Graphitic Carbon. PLoS One 2016;11:1-22.

[71] Torri ER, Brandon DP, Marian HH, David MS, Todd CM, Johnna ST. Microparticle-mediated sequestration of cell-secreted proteins to modulate chondrocytic differentiation, Acta Biomaterialia 2018;68:125-136.

[72] Gurpreet SB, Linda V, Benjamin AA. The Role of the Immune Cells in Fracture Healing. Curr Osteoporos Rep 2018;16:138–145.

Chapter 7

Conclusion and future works

In this research, silk fibroin fabric were improved their performance by coating with silk fibroin solution. The result showed that silk fibroin fabric coated with silk fibroin solution can promote cell proliferation and cell attachment for soft tissue in cleft palate. In addition, to make the mimick anatomical biphasic scaffolds based on silk woven fabric/gelatin layer was supported both fibroblast cell and keratinocyte cell so it promising for mucosa tissue construction in maxillofacial surgery.

The morphology of silk fibroin/gelatin of SF/GT (50:50) showed a heterogeneous morphology of main, porous structure, incorporated within its network structure. Hence, SF/GT (50:50) had suitable physical as well as biological performance, which could be related to irregular bone remodeling. Finally, the results indicated that SF/GT (50:50) is promising as an ex-vivo biomaterial for evaluation of pathogenic structures in osteoporosis.

Chitosan with bicomponent calcium phosphate was fabricated into biomineralized scaffolds, based on bioinspiration of bone remodeling. The results revealed that the morphological formation of calcium phosphate deposition on chitosan fiber is similar to biomineralization in bone remodeling. The physical performance of biomineralized scaffolds demonstrated a dynamic behavior of swelling properties, and degradation, which is related to bone remodeling. Furthermore, the biological performance of biomineralized scaffolds was suitable for the enhancement bone formation. Finally, the results deduced that biomineralized scaffolds, based on bioinspiration of bone remodeling, is promising for maxillofacial tissue engineering, particularly in chitosan with 2 and 4% of bicomponent calcium phosphate.

TCBs were used for inducing the mineralization bone tissue engineering, the result showed that the good cell proliferation and attachment was found in group of agarose that modified with TCBs and the differentiation stage was improved by using TCBs, so is promising for maxillofacial tissue engineering.

This result was successful *in vitro* so it is possible for using this modified silk fibroin fabric and chitosan with BiCP in vivo experiment for evaluate the performance of material before study in human.

Appendix

VITAE

Name Miss Supaporn Sangkert

Student ID 5810330023

Educational Attainment

Degree	Name of Institution	Year of Graduation
Bachelor of Science (Animal Science)	Prince of Songkla University	2009
Master of Science (Biomedical engineering)	Prince of Songkla University	2015

List of publications

1. Supaporn Seangkert, Jirut Meesane, Suttatip Kamonmattayakul, Chai Wen Lin, Modified silk fibroin scaffolds with collagen/decellularized pulp for bone tissue engineering in cleft palate: morphological structures, and biofunctionalities. Materials Science and Engineering C Materials for Biological Applications 2016;58:1138-1149.
2. Supaporn Seangkert, Suttatip Kamonmattayakul, Chai Wen Lin, Jirut Meesane, A biofunctional-modified silk fibroin scaffold with mimic reconstructed extracellular matrix of decellularized pulp/collagen/fibronectin for bone tissue engineering in alveolar bone resorption. Materials Letters 2016:166;30-34.
3. Supaporn Seangkert, Suttatip Kamonmattayakul, Chai Wen Lin, Jirut Meesane, Modified silk and chitosans with collagen assembly for osteopoeosis. Bioinspirated Biomimetic and Nanobiomaterials. 2016;5(1):1-11.
4. Supaporn Sangkert, Suttatip Kamonmattayakul, Wen Lin Chai and Jirut Meesane. Modified porous scaffolds of silk fibroin with mimicked microenvironment based on decellularized pulp/fibronectin for designed

performance biomaterials in maxillofacial bone defect. Journal of Biomedical Materials Research Part A. 2017.

5. Hnin NandarSoe, Matthana Khangkhamano, Supaporn Sangkert, Jirut Meesane, Rungrote Kokoo. TiC-coated carbon particles as bioactive substrates for inducing of mineralization in bone healing. Materials Letters 2018: 229;118-121.
6. Hnin NandarSoe, Matthana Khangkhamano, Supaporn Sangkert, Jirut Meesane, Rungrote Kokoo. TiC-coated carbon particles as bioactive substrates for inducing of mineralization in bone healing. Materials Letters. 2018;229:118-121.

Proceedings and International Conferences

1. Supaporn Sangkert, Suttatip Kamonmattayakul, Chai Wen Lin, Jirut Meesane. Modified silk fibroin scaffolds coated with a reconstructed collagen/fibronectin for bone tissue engineering in alveolar bone resorption: morphological structure and biological functionalities. The 5th National and International Graduate Study Conference 2015 “Creative Education Intellectual Capital toward ASEAN.
2. Supaporn Sangkert, Jirut Meesane, and Suttatip Kamonmattayakul. A modified chitosan film by coating with reconstruction of decellularized pulp/collagen for wound healing. 9th World Congress Biomaterials, May2016, Montreal, Canana.
3. Supaporn Sangkert, Suttatip Kamonmattayakul, Michael Gelinsky, Jirut Meesane. Constructed functional sheet scaffolds of coated silk fabric with silk fibroin solution for soft tissue regeneration in cleft palate surgery. The 7th National and International Graduate Study Conference “Thailand 4.0 Creative Innovation for Sustainable Development”